

Supporting Information for

Main-Chain Scission of Individual Macromolecules Induced by Solvent Swelling

Daniel Messmer^{a),*}, Oscar Bertran^{b)}, Reinhard Kissner^{c)}, Carlos Alemán^{d)}, A. Dieter Schlüter^{a),*}

- a) Polymer Chemistry, Department of Materials, ETH Zürich, Vladimir-Prelog-Weg 5, 8093 Zürich, Switzerland
- b) Department of Physics, EETAC, Universitat Politècnica de Catalunya, c/ Esteve Terrades, 7, 08860, Castelldefels, Spain
- c) Laboratory of Inorganic Chemistry, Department of Chemistry and Applied Biosciences, ETH Zürich, Vladimir-Prelog-Weg 3, 8093 Zürich, Switzerland
- d) Departament d'Enginyeria Química (EEBE) and Barcelona Research Center for Multiscale Science and Engineering, Universitat Politècnica de Catalunya, C/ Eduard Maristany, 10-14, Ed. I2, 08019, Barcelona, Spain.

Contents

1. Methods & Materials	2
1.1 Synthesis	2
1.2 Analytics	3
2. Syntheses of Polymers & Small-Molecules Precursors	5
3. Experiments involving charged DPs	13
3.1 TFA-mediated deprotection of $g > 5$ DPs.....	13
3.2 Base-free deprotection of PG5500NHAlloc	14
3.3 Attempted acid titration of PG5500NH ₂	14
3.4 Deprotection & dendronization of mixed-substitution $g = 5$ DPs	15
3.5 Deprotection & deprotonation of PG5500CO ₂ tBu	17
4. Experiments involving charge-neutral DPs	18
4.1 Initial observations.....	18
4.2 "Hot solvent" mediated scission experiments: General comments	19
4.3 Impact of solvent & temperature	19
4.4 Impact of dendritic generation g	22
4.5 Impact of peripheral chemistry.....	28
4.6 Impact of structural perfection.....	30
4.7 Impact of external shear	31
4.8 Characterization of low molar mass DP scission products	31

5. Molecular dynamics simulation	44
5.1 Methods	45
5.2 Additional results	46
6. EPR spectroscopy	50
7. Discussion of possible backbone scission mechanisms	53
8. NMR Spectra	55
Bibliography	67

1. Methods & Materials

1.1 Synthesis

Chemicals employed for synthetic reactions were purchased from commercial suppliers (ABCR, Acros, Fluorochem, Sigma-Aldrich, TCI, Iris Biochem) and used without further purification unless mentioned otherwise. **1** (DG1^{NHBoc}) was obtained from Synwit Technology Co. Ltd. (Beijing) and used without further purification; AIBN (Fluka, ≥ 98 %) was recrystallized from 35 °C MeOH before use; 1,4-dioxane (analytical reagent grade, stabilized, Fisher) for use in the lyophilization of polymers was distilled by rotary evaporation prior to use; dry solvents were either obtained from commercial sources (Acros AcroSeal bottles containing 4 Å mol sieves: DMF, DMSO, NMP, DMAc, Sigma Aldrich SureSeal bottles containing 4 Å mol sieves: DMPU) or prepared from HPLC grade solvents (methylene chloride, acetonitrile and THF, Fisher) by storing over freshly activated 4 Å mol sieves (Acros, 8 to 12 mesh) for at least 24 h before use.

Solvents used for standard workup procedures (EtOAc, hexane, acetone, methylene chloride, Et₂O; used for extraction, precipitation, column chromatography, and recrystallizations) were usually obtained in technical grade (Thommen Furler AG) and distilled by rotary evaporation, with the exception of Et₂O which was used as received.

Where the exclusion of oxygen and/or moisture is indicated in an experimental procedure, standard Schlenk glassware and handling techniques were employed unless specified otherwise, and the corresponding reactions were conducted under dry N₂. Where removal of solvent is indicated, rotary evaporation (Laborota 4000, Heidolph, equipped with a PC 2001 VARIO vacuum pump, Vacuubrand) at 40–50 °C was used unless otherwise noted. Lyophilization was conducted either using a vacuum manifold and a liquid nitrogen-cooled condenser or using a dedicated freeze dryer (Christ AG).

For purification by flash column chromatography, 230-400 mesh silica gel (SiliFlash P60, SiliCycle or high purity grade, Sigma-Aldrich) was used. For thin-layer chromatography, aluminium plates pre-coated with fluorescent silica gel (TLC Silica gel 60 F₂₅₄, Merck) were used. After development, spots were visualized with the help of a UV lamp (245 or 366 nm, CAMAG) and staining solutions (KMnO₄, vanillin, *p*-anisaldehyde, ninhydrin).

1.2 Analytics

NMR spectra were measured using a 300 MHz magnet (Avance 300, Bruker) equipped with an autosampler (SampleXpress, Bruker). Deuterated solvents for ^1H -NMR (CDCl_3 , $\text{DMSO}-d_6$, D_2O , $\text{TCE}-d_2$, $\text{TFA}-d_4$) were obtained from commercial suppliers (Cambridge Isotopes and ARMAR Chemicals). Spectra were evaluated using the MestreNova software suite (Mestrelab Research). ^{13}C -NMR spectra were assigned with the help of 2D experiments (HSQC, HMBC) where necessary. Chemical shifts are given in ppm relative to tetramethylsilane and were referenced using residual solvent protons. Peak splittings are noted as follows: s = singlet, d = doublet, t = triplet, q = quadruplet, m = multiplet, b = broad.

X-band CW-EPR spectra were measured on an EMX spectrometer (Bruker) equipped with a TM cavity and a thermostat (Eurotherm). Processing and simulation of signal components were conducted in Microsoft Excel.

Mass spectrometry and elemental analyses were conducted by the Molecular and Biomolecular Analysis Service (MoBIAS) at the Laboratory of Organic Chemistry (ETH Zürich). HR-ESI-MS was used for compound identification of small molecules precursors and MALDI-TOF-MS was employed for the analysis of DP chain scission products, using DCTB+Na Mix 1:10:1 as the matrix.

Samples for GPC were dissolved by dissolution in the running solvent containing a small amount of toluene (*ca.* 0.1 % v/v) as a flow marker, resulting in concentrations of *ca.* 1 mg L⁻¹ of polymer. The samples were shaken at 35 °C (CHCl_3) or 45 °C (DMF/LiBr) for at least 1 h on an orbital shaker (PL-SP 260, Polymer Laboratories), then filtered through 0.45 μm pore size Teflon syringe filters into screw-cap vials. Measurements were conducted using two Viscotek GPCMax systems (Malvern/Viscotek) equipped with a triple-detector array (DRI, intrinsic viscosity, right- and low-angle light scattering; Viscotek TDA, Malvern/Viscotek), both fitted with a switching valve to permit the use of two column sets. One system was operated with CHCl_3 as the eluent at 35 °C and was equipped with a column set covering intermediate (2 x PLGel MIXED-B, Polymer Laboratories) and high molar masses (2 x PLGel MIXED -A, Polymer Laboratories), as well as an additional variable-wavelength UV/Vis detector (UV-Detector 2500, Viscotek), the other was operated using DMF containing 1 g L⁻¹ LiBr as the eluent and equipped with column sets covering low (1 x PLGel MIXED-D, Polymer Laboratories) and high molar masses (2x D-5000, Malvern). Typically, 100 μL of sample were injected. Where relevant, molar masses were determined from universal calibration, established using monodisperse polymer standards (CHCl_3 : PS; DMF: PMMA; Polymer Laboratories).

UV/Vis spectra were recorded on a 2-beam UV/Vis/NIR spectrophotometer (V-670, Jasco) using 2 mm or 10 mm fused quartz cuvettes (Hellma); samples were typically prepared using analytical or HPLC grade solvents. Fluorescence spectra were recorded at right angle on a Fluorolog 2 (SPEX) using 1 cm fluorescence cuvettes (Hellma).

Melting points were measured using a melting point determination apparatus (B-540, Büchi).

Samples for atomic force microscopy were prepared by drop-casting solutions of DPs (typically 0.5 – 20 mg L⁻¹ in methylene chloride or MeOH) onto freshly cleaved substrates (mica or HOPG, obtained from Plano GmbH) affixed to 12 mm or 20 mm diameter magnetic specimen disks (Ted Pella Inc.). Microscopy was performed on a Dimension Icon AFM (Bruker), in using silicon cantilevers with a

typical resonance frequency of 300 MHz and a typical spring constant of 26 N m^{-1} (OMCL-160TS-R3, Olympus). Images were processed using NanoScope Analysis (Bruker), FiberApp,¹ and Fiji.²

DLS was measured in analytical grade methanol (Fisher), using a Zetasizer Nano (Malvern) using and disposable polystyrene semimicro-cuvettes (VWR). A uniform refractive index of 1.51 was assumed for all polymers. DP concentrations of *ca.* 0.1 mg mL^{-1} were used for all samples.

2. Syntheses of Polymers & Small-Molecules Precursors

The following compounds were prepared as described in the literature: benzyl 3,5-dihydroxybenzoate (**S4**);³ *tert*-butyl 4-bromobutyrate;⁴ methyl 4-bromobutyrate;⁵ DG1^{NHAlloc} (**S1**);⁶ MG1^{NHBoc}.⁷ Polymers not specified below were likewise prepared by literature procedures: PG g_{500}^{NHBoc} ($g = 1 - 8$; low structural perfection⁸/high structural perfection⁶), PG5 $_{500}^{\text{NHAlloc}}$.⁶

General procedure A: Deprotection of DPs of the type PG g_n^{NHBoc}

For NHBoc-deprotection, the polymer in question (PG g_n^{NHBoc}) was cooled to 0 °C in a suitably sized round-bottom flask or vial. While stirring, cold, neat TFA (*ca.* 2 mL per 100 mg DP, approx. 50 equiv. TFA per amine) was added slowly. In this process, care was taken that all polymer adhering to the glass walls was flushed down. The resulting mixture (usually a white suspension) was then warmed to RT and MeOH is added dropwise until the mixture was permanently clear (usually < 50 μL per 100 mg DP). The polymer was stirred at RT overnight, then cooled to 0 °C in an ice bath and treated with MeOH (*ca.* 5 mL per 100 mg DP). The mixture was stirred at RT for 5 min, then solvents were removed by rotary evaporation at ≤ 35 °C. The addition of MeOH and removal of solvents was repeated twice, then the resulting glassy polymer was lyophilized from deionized water.

General procedure B: Dendronization of DPs of the type PG $g_n^{\text{NH}_3\text{TFA}}$

The lyophilizate of PG $g_n^{\text{NH}_3\text{TFA}}$ (typically a colourless or off-white foam) was dissolved in DMF (*ca.* 1.5 mL per 100 mg DP) and the solution was cooled to 0 °C in an ice bath. NEt₃ (2 equiv./amine) and DMAP (catalytic amount, *ca.* 0.1 – 0.3 equiv./amine) were added, followed by addition of a suitable *N*-hydroxysuccinimide ester (3 equiv./amine). The reaction mixture was then warmed to RT and stirred for a total of g weeks (*e.g.* 3 weeks for PG3 $_{n}^{\text{NHBoc}}$ as the starting material). During this time, after *ca.* one third and two thirds of the total reaction time had elapsed, the reaction mixture was cooled back to 0 °C and further portions of the dendronization agent were added (1 equiv./amine on both occasions). After the indicated amount of stirring time, the reaction mixture was either concentrated in vacuum or precipitated into Et₂O (*ca.* 200 mL per 100 mg initial DP). In either case, the polymer (PG $(g+1)_n^{\text{NHBoc}}$) was then purified by column chromatography (methylene chloride, $R_f \approx 1.0$) and lyophilized from freshly distilled 1,4-dioxane.

General Procedure C: Labelling of unreacted amines with Sanger's reagent

For the determination of functional group conversion after dendronization, a modification of the previously published method⁹ was used. A sample of the polymer (20 – 30 mg) was dissolved in 1,1,2,2-tetrachloroethane (2 mL). 2 mL of a solution of 2,4-dinitrofluorobenzene (25 mg mL⁻¹) in 1,1,2,2-tetrachloroethane and 5 % aq. NaHCO₃ (4 mL) were added and the mixture was stirred vigorously at 50 °C overnight. The resulting biphasic yellow mixture was then diluted with methylene chloride (30 mL), washed with 5 % aq. NaHCO₃ (5 x 30 mL), then brine (30 mL), dried over Na₂SO₄ and concentrated to a volume of *ca.* 1 mL. The solution was transferred to a 15 mL centrifuge tube and precipitated with Et₂O (*ca.* 12 mL). The precipitate was sedimented by centrifugation (5 min at 4000 RPM). The polymer was precipitated twice more from little methylene chloride, then lyophilized from freshly distilled dioxane. The concentration of labelled amines (see below for details) was determined by measuring the absorption of the polymers at 360 nm in 1,1,2,2-tetrachloroethane ($\epsilon_{360} = 16400 \text{ L mol}^{-1} \text{ cm}^{-1}$). Values of structure perfection given in this publication were calculated by the recursive method,¹⁰

taking into account defects detected in the precursor polymers by labelling with Sanger's reagent. The functional group conversion X is then calculated recursively according to the following relation :

$$X(g)_{(n_{g+1})} = \frac{n_g + 1}{2(n_{g-1} + 1)}$$

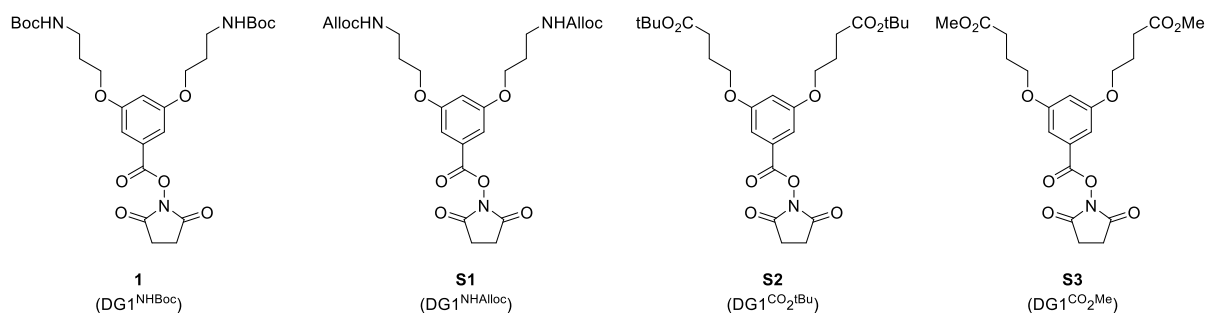
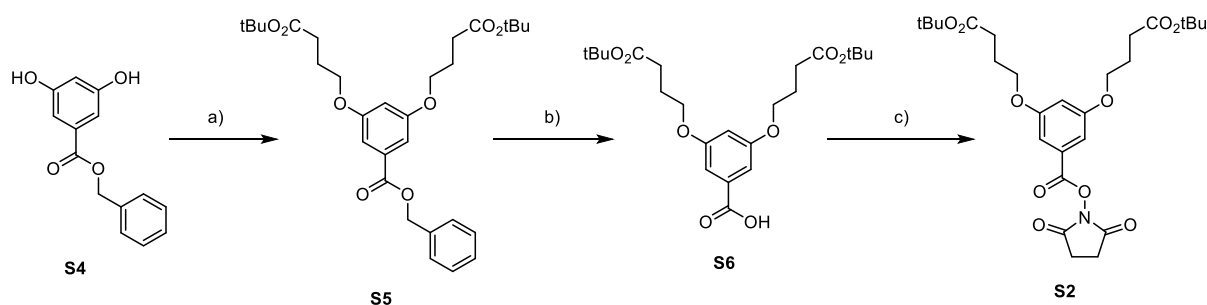
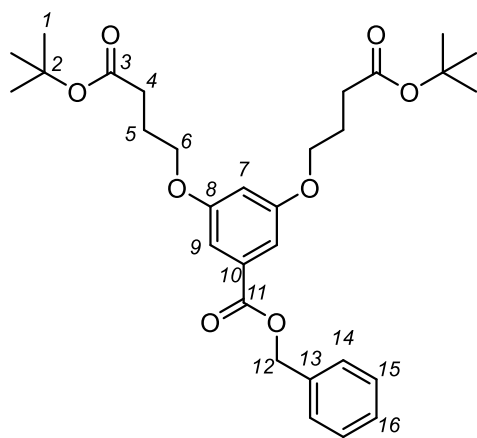


Figure S 1: Chemical structures of dendronization agents $DG1^X$ used e.g. in General Procedure B.



Scheme S 1: Synthesis of $S2$ ($DG1^{CO_2Me}$) Conditions: a) tert-butyl-4-bromobutyrate, K_2CO_3 , DMF, 60 °C; b) H_2 , Pd/C, MeOH; c) HOSu, DCC, methylene chloride, 0 °C to RT.

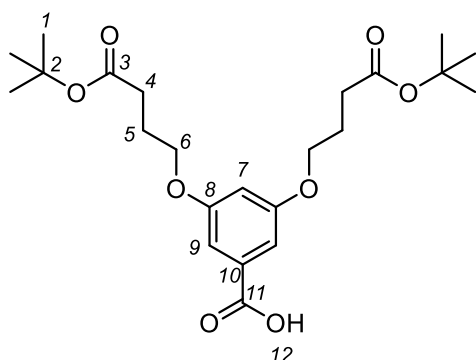
Synthesis of benzyl 3,5-Bis(3-(tert-butyloxycarbonyl)propoxy)benzoate (**S5**)



To a solution of **S4** (21.87 g, 87 mmol) in DMF (180 mL), K_2CO_3 (49.78 g, 360 mmol, 4 equiv.) was added and the mixture was stirred at RT for 30 min. Then, tert-butyl-4-bromobutyrate (41.69 g, 188 mmol, 2.1 equiv.) was added as a solution in DMF (70 mL) and the mixture was stirred at 60 °C for 18 h. The resulting suspension was diluted with EtOAc (500 mL) and washed with water (2 x 800 mL) and brine (800 mL), then dried over $MgSO_4$ and concentrated in vacuum. Column chromatography (EA/Hex 10:1) afforded **S5** as a slightly yellow-tinged oil (41.5 g, 88 %). 1H -NMR (300 MHz, $CDCl_3$, 298 K): 7.42 – 7.21 (m, 5H, 14 – 16), 7.11 (d, $J = 2.3$ Hz, 2H, 9), 6.56 (t, $J = 2.4$ Hz, 1H, 7), 5.27 (s, 2H, 12), 3.92 (t, $J = 6.1$ Hz, 4H, 6), 2.34 (t, $J = 7.3$ Hz, 4H, 4), 1.98 (m, 4H, 5), 1.37 (s, 18H, 1). ^{13}C -NMR (76 MHz, $CDCl_3$, 298 K): 172.56 (3), 166.33 (11), 160.06 (8), 136.13 (13), 132.07 (10), 128.73 (15), 128.37 (16), 128.34 (14), 108.17 (9), 106.58 (7), 80.55 (2),

67.37 (6), 66.97 (12), 32.12 (4), 28.27 (1), 24.82 (5). HR-MS: Calc. For $C_{30}H_{44}NO_8$ ($M+NH_4^+$): $m/z = 546.3061$; found: $m/z = 546.3064$. Elemental analysis; Calc. 68.16 % C, 7.63 % H; found 68.19 % C, 7.7 % H.

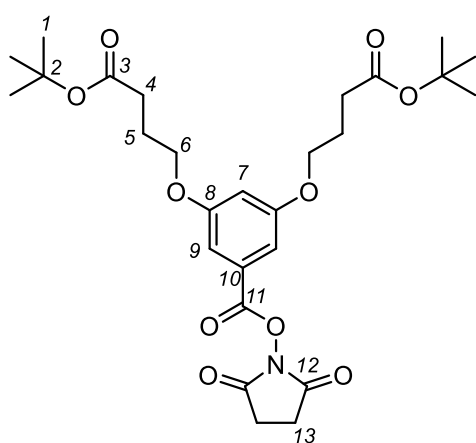
Synthesis of 3,5-bis(3-(*tert*-butyloxycarbonyl)propyloxy)benzoic acid (**S6**)



S5 (41.26 g, 52 mmol) was dissolved in MeOH (250 mL) and Pd/C (500 mg, 10 % Pd) was added. The mixture was stirred vigorously under 1 atm H_2 supplied from a balloon for 15 h. The solution was then filtered through celite and concentrated in vacuum, affording **S6** (34.07 g, 99.5 %) as a colorless solid. 1H -NMR (300 MHz, $CDCl_3$, 298 K): 7.22 (d, $J = 2.3$ Hz, 2H, 9), 6.68 (t, $J = 2.3$ Hz, 1H, 7), 4.02 (t, $J = 6.1$ Hz, 4H, 6), 2.43 (t, $J = 7.3$ Hz, 4H, 4), 2.07 (m, 4H, 5), 1.45 (s, 18H, 1). ^{13}C -NMR (76 MHz, $CDCl_3$, 298 K): 172.63 (3), 171.46 (11), 160.12 (8), 131.17 (10), 108.50 (9), 107.56 (7), 80.63

(2), 67.41 (6), 32.13 (4), 28.28 (1), 24.83 (5). Melting point: 98-99 °C. HR-MS: Calc. for $C_{23}H_{34}NaO_8$ ($M+Na^+$) $m/z = 461.2146$, found $m/z = 461.2154$. Elemental analysis: Calc. 63 % C, 7.81 % H, found 62.72 % C, 7.72 % H.

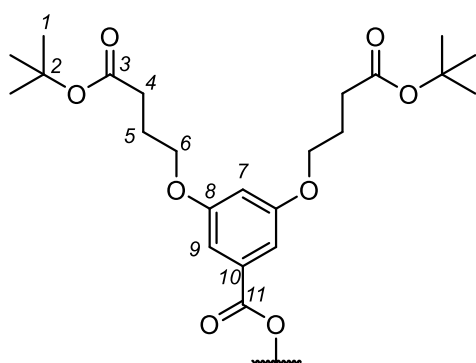
Synthesis of 2,5-Dioxopyrrolidin-1-yl 3,5-Bis(3-(*tert*-butyloxycarbonyl)propyloxy)benzoate (**S2**)



A solution of **S6** (15.09 g, 34 mmol) and *N*-hydroxysuccinimide (4.16 g, 36 mmol, 1.05 equiv.) in dry methylene chloride (250 mL) was cooled to 0 °C in an ice bath. DCC (12.28 g, 38 mmol, 1.1 equiv) was added and the resulting mixture was stirred at RT under nitrogen for 16 h. The resulting slurry was filtered and the filtrate was concentrated in vacuum. The resulting oil was redissolved in little acetonitrile and cooled to 0 °C for 3 h. Solids were removed by filtration. After purification by flash chromatography (EtOAc/Hex 1:1), **S2** (22.22 g, 95 %) was obtained as a colorless solid. 1H -NMR (300 MHz, $CDCl_3$, 298 K): 7.22 (d, $J = 2.3$ Hz, 2H, 9), 6.72 (t, $J = 2.4$ Hz, 1H, 7), 4.01

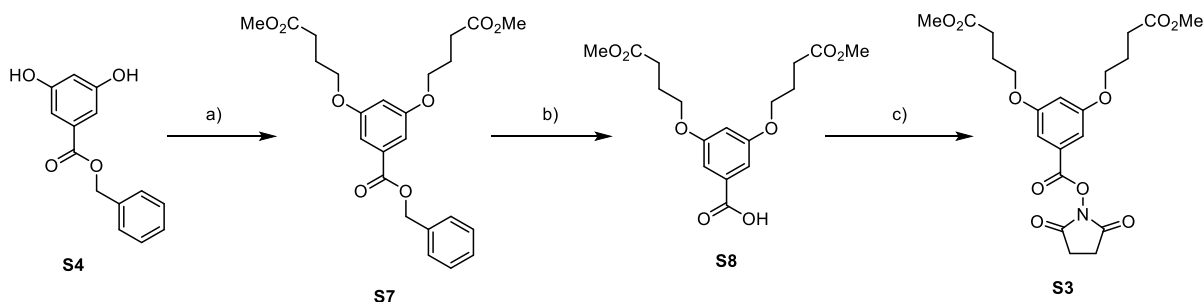
(t, $J = 6.1$ Hz, 4H, 6), 2.9 (s, 4H, 12), 2.41 (t, $J = 7.3$ Hz, 4H, 4), 2.06 (m, 4H, 5), 1.45 (s, 18H, 1). ^{13}C -NMR (76 MHz, $CDCl_3$, 298 K): 172.49 (3), 169.25 (12), 161.85 (11), 160.28 (8), 126.75 (10), 108.87 (7), 108.60 (9), 80.62 (2), 67.52 (6), 32.02 (4), 28.27 (1), 25.82 (13), 24.74 (5). Melting point: 78-79 °C. HR-MS: Calc. for $C_{27}H_{37}NNaO_{10}$ ($M+Na^+$): $m/z = 558.231$; found: $m/z = 558.2309$. Elemental analysis: Calc 60.55 % C, 6.96 % H, 2.62 % N; found 60.38 % C, 6.97 % H, 2.67% N.

Synthesis of PG5₅₀₀^{CO₂tBu} (**9**)



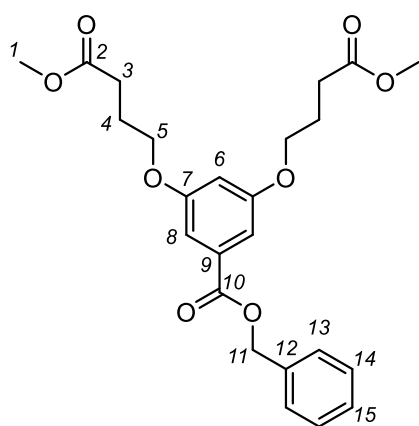
To a solution of PG4₅₀₀^{NH₃TFA} (513.2 mg, 91 μmol, 1.45 mmol amines), DMAP (30.1 mg, 0.2 mmol, 0.17 equiv./amine) and NEt₃ (0.45 mL, 3.2 mmol, 2.2 equiv./amine) in DMF (5 mL), **S2** was added (2.3 g, 4.3 mmol, 3 equiv./amine) as a solution in DMF (*ca.* 5 mL) at 0 °C. The mixture was warmed to RT and monitored by visual inspection. CHCl₃ was added to the mixture as necessary (*ca.* 10 mL in portions of 1 – 2 mL, added over the course of 7 d) in order to maintain a clear solution, after which no turbidity arose, anymore. The solution was stirred for an additional 2 weeks, then

precipitated into hexane. The resulting polymer was isolated by column chromatography (methylene chloride) and lyophilized from freshly distilled dioxane, affording PG5₅₀₀^{CO₂tBu} (**9**) as a colorless powder (816 mg, 85 %). ¹H-NMR (300 MHz, TCE-d₂, 343 K): 6.94 (app. s(b), 9), 6.47 (app. s(b), 7), 3.88 (app. s(b), 6), 2.29 (s(b), 4), 1.81 (app. s(b), 5), 1.36 (s, 1).



Scheme S 2: Synthesis of **S3** (DG1^{CO₂Me}) Conditions: a) methyl-4-bromobutyrate, K₂CO₃, DMF, 60 °C; b) H₂, Pd/C, MeOH; c) HOSu, DCC, methylene chloride, 0 °C to RT.

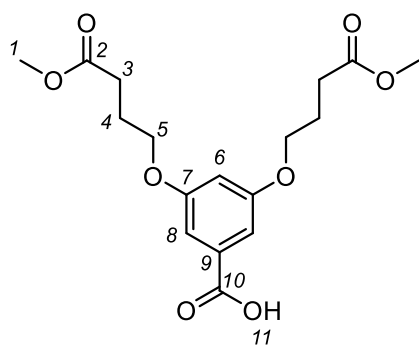
Synthesis of benzyl 3,5-Bis(3-(methoxycarbonyl)propyloxy)benzoate (**S7**)



To a solution of **S4** (13.441 g, 55 mmol) in DMF (230 mL), K₂CO₃ (30.87 g, 223 mmol, 4.1 equiv.) was added and the mixture was stirred at RT for 20 min. Then, methyl-4-bromobutyrate (24.16 g, 133 mmol, 2.4 equiv.) was added as a solution in DMF (70 mL) and the mixture was stirred at 60 °C for 16 h. The resulting suspension was diluted with EtOAc (500 mL) and washed with water (2 x 1 L) and brine (800 mL), then dried over MgSO₄ and concentrated in vacuum. Column chromatography (EA/Hex 1:1) afforded **S7** as a colourless oil (23.5 g, 96 %). ¹H-NMR (300 MHz, CDCl₃, 298 K): 7.45 – 7.23 (m, 5H, 13 – 14), 7.18 (d, *J* = 2.3 Hz, 2H, 8), 6.61 (t, *J* = 2.4 Hz, 1H, 6), 5.34 (s, 2H, 11), 4.10 (t, *J* = 6.1

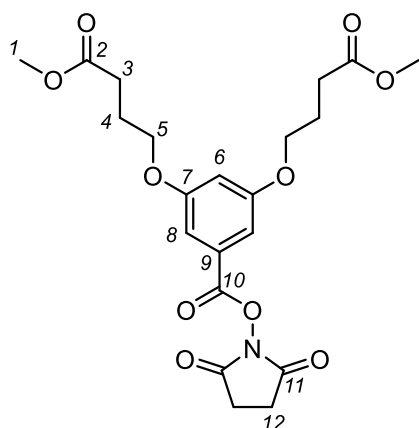
Hz, 4H, 5), 3.68 (s, 6H, 1), 2.52 (t, *J* = 7.3 Hz, 4H, 3), 2.1 (m, 4H, 4). ¹³C-NMR (76 MHz, CDCl₃, 298 K): 173.68 (2), 166.30 (10), 159.98 (7), 136.12 (12), 132.12 (9), 128.74 (13 or 14), 128.40 (15), 128.36 (13 or 14), 108.17 (7), 106.62 (7), 67.18 (5), 67.01 (11), 51.81 (1), 30.63 (3), 24.68 (4). HR-MS: Calc. for C₂₄H₂₈NaO₈ (M+Na⁺): *m/z* = 467.1676, found: *m/z* = 467.1682. Elemental analysis: Calc. 64.85 % C, 6.35 % H, 28.8% O, found 64.79 % C, 6.35 % H, 28.97 % O.

Synthesis of 3,5-Bis(3-(methyloxycarbonyl)propyloxy)benzoic acid (**S8**)



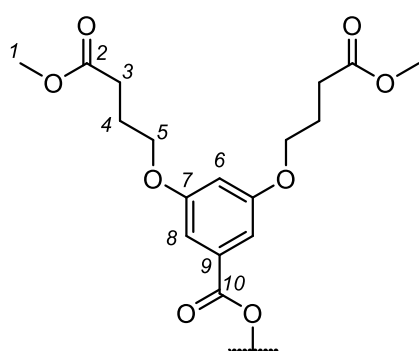
S7 (23.2 g, 52 mmol) was dissolved in MeOH (250 mL) and Pd/C (500 mg, 10 % Pd) was added. The mixture was stirred vigorously under 1 atm H₂ supplied from a balloon for 15 h. The solution was then filtered through celite and concentrated in vacuum, affording **S8** (19 g, quantitative) as a colorless solid. ¹H-NMR (300 MHz, CDCl₃, 298 K): 7.22 (d, *J* = 2.3 Hz, 2H, 8), 6.66 (t, *J* = 2.3 Hz, 1H, 6), 4.04 (t, *J* = 6.1 Hz, 4H, 5), 3.70 (s, 6H, 1), 2.53 (t, *J* = 7.3 Hz, 4H, 3), 2.12 (m, 4H, 4). ¹³C-NMR (76 MHz, CDCl₃, 298 K): 173.72 (2), 171.35 (10), 160.03 (7), 131.19 (9), 108.49 (8), 107.56 (6), 67.22 (5), 51.84 (1), 30.64 (3), 24.67 (4). Melting point: 89 °C. HR-MS: calc. for C₁₇H₂₃O₈ (M+H⁺): *m/z* = 355.1387; found: *m/z* = 355.1389. Elemental analysis: Calc. 57.62 % C, 6.26 % H, 36.12 % O; found 57.68 % C, 6.26 % H, 36.24 % O.

Synthesis of 2,5-Dioxopyrrolidin-1-yl 3,5-Bis(3-(methyloxycarbonyl)propyloxy)benzoate (**S3**)



A solution of **S8** (18.14 g, 51 mmol) and *N*-hydroxysuccinimide (6.49 g, 56 mmol, 1.1 equiv.) in dry acetonitrile (250 mL) was cooled to 0 °C in an ice bath. DCC (12.28 g, 60 mmol, 1.2 equiv) was added and the resulting mixture was stirred under nitrogen for 14 h. The resulting slurry was filtered and the filtrate was concentrated in vacuum. The resulting oil was redissolved in little acetonitrile and cooled to 0 °C for 3 h. Solids were removed by filtration. After purification by flash chromatography (EtOAc/Hex 1:1), **S3** (22.22 g, 95 %) was obtained as a colorless oil. ¹H-NMR (300 MHz, CDCl₃, 298 K): 7.21 (d, *J* = 2.3 Hz, 2H, 8), 6.7 (t, *J* = 2.3 Hz, 1H, 6), 4.01 (t, *J* = 6.1 Hz, 4H, 5), 3.68 (s, 6H, 1), 2.89 (s, 4H, 12), 2.51 (t, *J* = 7.2 Hz, 4H, 3), 2.1 (m, 4H, 4). ¹³C-NMR (76 MHz, CDCl₃, 298 K): 173.58 (2), 169.27 (11), 161.79 (10), 160.17 (7), 126.7 (9), 108.81 (8), 108.61 (6), 67.31 (5), 51.81 (1), 30.52 (3), 25.80 (12), 24.57 (4). HR-MS: calc. for C₂₁H₂₉N₂O₁₀ (M+NH₄⁺): *m/z* = 469.1817; found: *m/z* = 469.1815. Elemental analysis: Calc. 55.87 % C, 5.58 % H, 3.1 % N; found 55.61 % C, 5.8 % H, 3.28 % N.

Synthesis of PG5₅₀₀^{CO₂Me} (**8**)



Prepared from PG4₅₀₀^{NH₃TFA} (115 mg, 20 μmol, 0.32 mmol amines), Prepared according to General Procedure B using **S3**, affording PG5₅₀₀^{CO₂Me} (**8**) as a colorless powder (104 mg, 56 %). ¹H-NMR (300 MHz, DMSO-d₆, 343 K): 8.14 (app. s(b), amide H of underlying structure), 6.85 (app. s(b), 8), 6.39 (app. s(b), 6), 3.82 (app. s(b), 5), 3.41 (s(b), 1), 2.23 (app. s(b), 3), 1.76 (app. s(b), 4).

Synthesis of PG5₅₀₀^{NHAlloc36} (S9)

PG4₅₀₀^{NH₃TFA} (prepared according to General Procedure A from PG4₅₀₀^{NHBoc}, 100.5 mg, 19 μmol RUs) was dissolved in DMF (3 mL); at 0 °C, DMAP (9.3 mg, 80 μmol, 0.25 equiv./amine) and NEt₃ (0.1 mL, 0.7 mmol, 2.3 equiv./amine) were added, followed by a 54.5 mg mL⁻¹ solution of DG1^{NHAlloc} (**1**, 0.73 mL, 75 μmol 0.25 equiv./amine) in DMF. The resulting solution was stirred at RT for 5 d, then DG1^{NHBoc} (**1**, 400 mg, 0.7 mmol, 2.3 equiv./amine) was added. After 10 more days of stirring, another portion of DG1^{NHBoc} (**1**, 417 mg, 0.7 mmol, 2.3 equiv./amine) was added. After a total of 35 d of stirring, the reaction mixture was concentrated in vacuum and precipitated into Et₂O (80 mL). Purification of the polymer by flash chromatography (DCM, *R_f* ≈ 1), followed by lyophilization from freshly distilled 1,4-dioxane afforded a white powder (**S9**, 78 mg, 39 %). ¹H-NMR (300 MHz, DMSO-*d*₆, 343 K): 8.21 (s (b)), 6.89-6.73 (m (b)), 6.45-6.3 (m (b)), 5.75 (app. s (b)), 5.1-5.01 (m (b)), 4.36 (app. s (b)), 3.02 (app. s(b)), 1.75 (app. s (b)), 1.25 (s (b)). Integration of NMR signals indicates *ca.* 36 % NHAlloc.

Synthesis of PG5₅₀₀^{NHAlloc57} (S10)

PG4₅₀₀^{NH₃TFA} (prepared according to General Procedure A from PG4₅₀₀^{NHBoc}, 108.1 mg, 20 μmol RUs) was dissolved in DMF (3 mL); at 0 °C, DMAP (6.5 mg, 53 μmol, 0.16 equiv./amine) and NEt₃ (0.1 mL, 0.7 mmol, 2.2 equiv./amine) were added, followed by a 54.5 mg mL⁻¹ solution of DG1^{NHAlloc} (**1**, 2.45 mL, 0.25 mmol, 0.75 equiv./amine). The resulting solution was stirred at RT for 5 d, then DG1^{NHBoc} (**1**, 404.9 mg, 0.7 mmol, 2.1 equiv./amine) was added. After 10 more days of stirring, another portion of DG1^{NHBoc} (**1**, 404.5 mg, 0.7 mmol, 2.1 equiv./amine) was added. After a total of 35 d of stirring, the reaction mixture was concentrated in vacuum and precipitated into Et₂O (80 mL). Purification of the polymer by flash chromatography (DCM, *R_f* ≈ 1), followed by lyophilization from freshly distilled 1,4-dioxane afforded a white powder (**S10**, 91 mg, 43 %). ¹H-NMR (300 MHz, DMSO-*d*₆, 343 K): 8.15 (s (b)), 6.88-6.73 (m (b)), 6.45-6.3 (m (b)), 5.75 (app. s (b)), 5.1-5.01 (m (b)), 4.36 (app. s (b)), 3.06 (app. s(b)), 1.75 (app. s (b)), 1.24 (s (b)). Integration of NMR signals indicates *ca.* 57 % NHAlloc.

Synthesis of PG5₅₀₀^{NHAlloc80} (S11)

PG4₅₀₀^{NH₃TFA} (prepared according to General Procedure A from PG4₅₀₀^{NHBoc}, 113.3 mg, 21 μmol RUs) was dissolved in DMF (3 mL); at 0 °C, DMAP (9.3 mg, 0.25 equiv./amine) and NEt₃ (0.1 mL, 0.7 mmol, 2.4 equiv./amine) were added, followed by a 54.5 mg mL⁻¹ solution of DG1^{NHAlloc} (**S1**, 0.73 mL, 0.25 equiv./amine). The resulting solution was stirred at RT for 5 d, then DG1^{NHBoc} (**1**, 400 mg, 0.7 mmol, 2.4 equiv./amine) was added. After 10 more days of stirring, another portion of DG1^{NHBoc} (**1**, 417 mg, 0.7 mmol, 2.4 equiv./amine) was added. After a total of 35 d of stirring, the reaction mixture was concentrated in vacuum and precipitated into Et₂O (80 mL). Purification of the polymer by flash chromatography (DCM, *R_f* ≈ 1), followed by lyophilization from freshly distilled 1,4-dioxane afforded a white powder (**S11**, 97 mg, 44 %). ¹H-NMR (300 MHz, DMSO-*d*₆, 343 K): 8.15 (s (b)), 6.76 (m (b)), 6.44 (app. s (b)), 5.74 (app. s (b)), 5.14-5.0 (m (b)), 4.34 (app. s (b)), 3.12 (app. s(b)), 1.73 (app. s (b)), 1.25 (s (b)). Integration of NMR signals indicates *ca.* 80 % NHAlloc.

Synthesis of PG1_{10'000}^{NHBoc} (S12)

A solution of MG1^{NHBoc} (15.24 g, 29.1 mmol) and AIBN (41 mg, 25 μmol, 0.8 mol%) in dry DMF (15 mL) was degassed by freeze-pump-thaw cycles and then stirred at 65 °C overnight. The resulting highly viscous substance was dissolved in methylene chloride and purified by column chromatography (methylene chloride, *R_f* ≈ 1.0). The product was lyophilized from freshly distilled 1,4-dioxane, affording PG1_{10'000}^{NHBoc} as a glassy, colorless solid (**S12**, 14.5 g, 95 %). GPC (DMF, 0.1 % LiBr): *M_n* > 3 MDa (partially in column cutoff; peak almost entirely out of calibration range), Đ ≈ 1.5.

Synthesis of PG2^{NHBoc}_{10'000} (S13)

Prepared according to General Procedures A, then B, starting from PG1^{NHBoc}_{10'000} (S12, 3.987 g, 7.6 mmol RUs), resulting in a colorless foam (S13, PG2^{NHBoc}_{10'000}, 7.75 g, 83 %). Functional group conversion (General Procedure C): $X = 99.9\%$. ¹H-NMR (300 MHz, DMSO-*d*₆, 343 K): 8.15 (s (b)), 6.9 (app. s (b)), 6.48 (s), 6.39 (app. s(b)), 3.87 (app. s(b)), 3.31 (app. s(b)), 3.02 (m (b)), 1.75 (m (b)), 1.3 (s).

Synthesis of PG3^{NHBoc}_{10'000} (S14)

Prepared according to General Procedures A, then B, starting from PG2^{NHBoc}_{10'000} (S13, 4.6 g, 3.7 mmol RUs), resulting in a colorless foam (S14, PG3^{NHBoc}_{10'000}, 7.31 g, 74 %). Functional group conversion (General Procedure C): $X = 99.9\%$. ¹H-NMR (300 MHz, DMSO-*d*₆, 343 K): 8.13 (s (b)), 6.88 (app. s (b)), 6.45 (s), 6.33 (app. s(b)), 3.85 (app. s(b)), 3.28 (app. s(b)), 3.0 (m (b)), 1.73 (m (b)), 1.27 (s).

Synthesis of PG4^{NHBoc}_{10'000} (S15)

Prepared according to General Procedures A, then B, starting from PG3^{NHBoc}_{10'000} (S14, 3.6 g, 1.4 mmol RUs), resulting in a colorless foam (S15, PG4^{NHBoc}_{10'000}, 7.31 g, 76 %). Functional group conversion (General Procedure C): $X = 99.8\%$. ¹H-NMR (300 MHz, DMSO-*d*₆, 343 K): 8.16 (s (b)), 6.87 (app. s (b)), 6.3 (app. s(b)), 3.0 (m (b)), 1.7 (app. s (b)), 1.24 (s).

Synthesis of PG5^{NHBoc}_{5'000} (2)

Prepared according to General Procedures A, then B, starting from PG4^{NHBoc}_{10'000} (S15, 1.75 g, 0.3 mmol RUs), resulting in a colorless foam (2, 2.15 g, 60 %). Functional group conversion (General Procedure C): $X = 99.6\%$. ¹H-NMR (300 MHz, DMSO-*d*₆, 343 K): 8.21 (s (b)), 6.89 (app. s (b)), 6.43 (app. s (b)), 3.87 (app. s(b)), 3.0 (app. s (b)), 1.72 (app. s (b)), 1.24 (s). The reduced degree of polymerization obtained in this synthesis is likely the result of inadvertent heating during workup of the reaction.

Synthesis of PG5^{NHAlloc}_{10'000} (4)

Prepared according to General Procedures A, then B (with the sole modification that DG1^{NHAlloc} (S1) was used instead of DG1^{NHBoc} (1), starting from PG4^{NHBoc}_{10'000} (S15, 1.71 g, 0.3 mmol RUs), resulting in a colorless foam (4, 1.71 g, 52 %). Functional group conversion (General Procedure A): $X = 99.3\%$. ¹H-NMR (300 MHz, DMSO-*d*₆, 343 K): 8.2 (s (b)), 6.82 (app. s (b)), 6.43 (app. s(b)), 4.95 – 5.1 (m (b)), 4.33 (s (b)), 3.87 (app. s(b)), 3.05 (app. s (b)), 1.73 (app. s (b)).

The DP of $g = 5$ in this series of long-chain polymers was notably shorter than the previous members of the series (see GPC in Figure S 2). Likely, this is a consequence of swelling-induced main-chain scission as discussed in the main text: Though not intended, it is possible that accidentally the DMF reaction mixture resulting from dendronization was briefly heated to $> 60\text{ }^{\circ}\text{C}$, *e.g.* in the removal of excess solvent before precipitation and purification of the polymer.

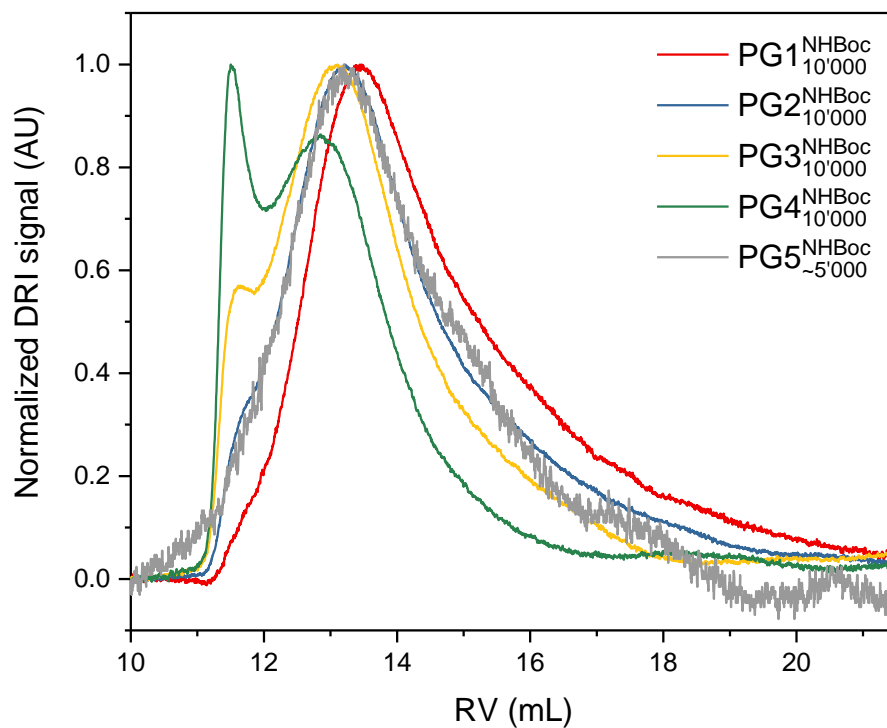


Figure S 2: GPC retention curves of the homologous series of long-chain DPs. Note that the peak RV increases up to $g = 4$, but then drops significantly for $g = 5$. For all DPs, the high molar mass lead of the peak is in the exclusion volume of the column set of $RV \approx 11.2$ mL.

3. Experiments involving charged DPs

3.1 TFA-mediated deprotection of $g > 5$ DPs

Under standard synthetic conditions (neat TFA at RT or below; see General Procedure A) the DPs $\text{PG6}_{500}^{\text{NHBoc}}$, $\text{PG7}_{500}^{\text{NHBoc}}$ and $\text{PG8}_{500}^{\text{NHBoc}}$ do not undergo detectable degradation.⁶ Harsher conditions are necessary in order to provoke main-chain scission. It had previously been found that $\text{PG4}_{500}^{\text{NHBoc}}$ undergoes degradation upon prolonged refluxing in neat TFA.¹¹ The same is true for $\text{PG6}_{500}^{\text{NHBoc}}$ (Figure S 3a), however $\text{PG7}_{500}^{\text{NHBoc}}$ and $\text{PG8}_{500}^{\text{NHBoc}}$ appear to remain intact (Figure S 3b,c).

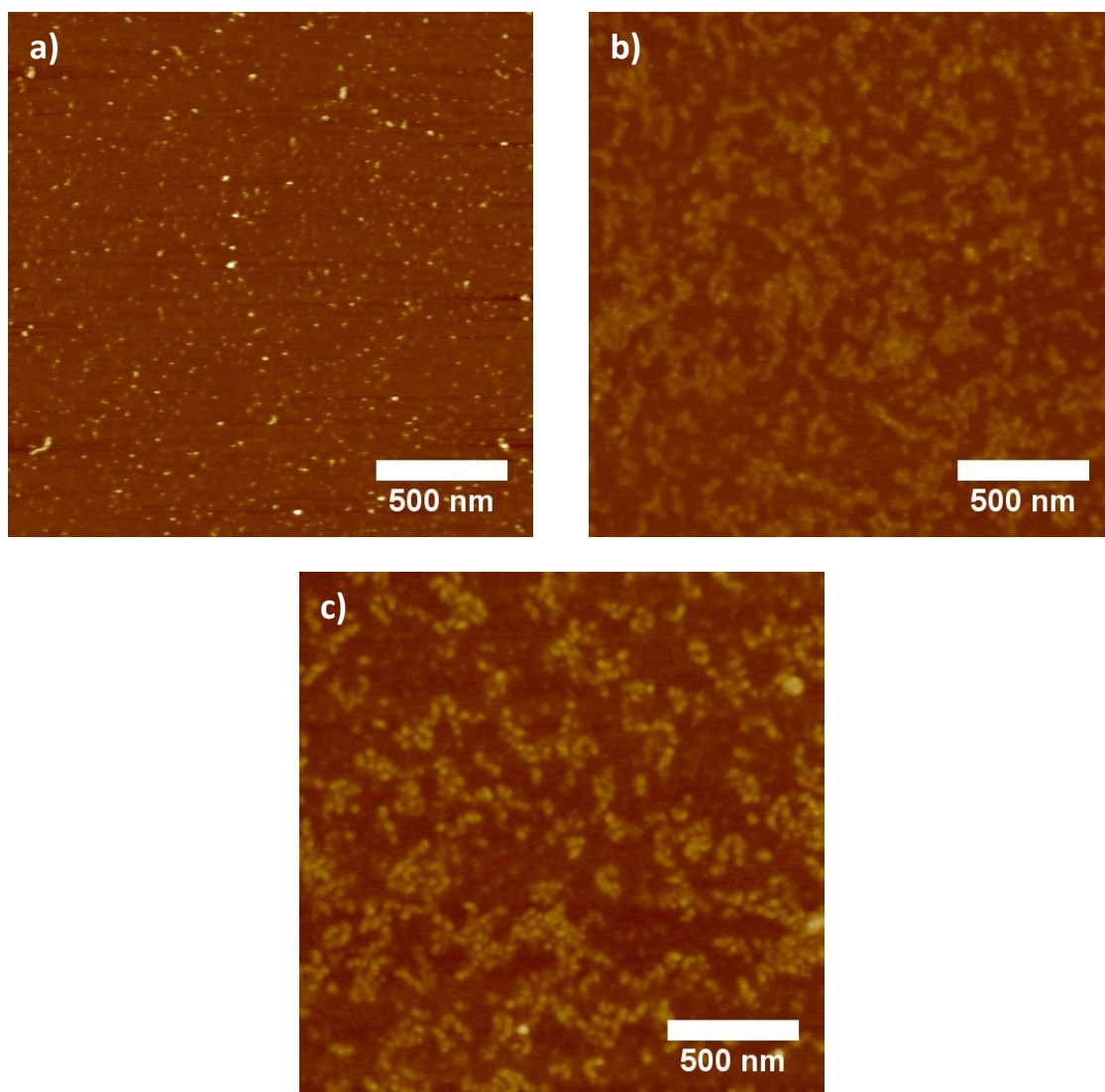
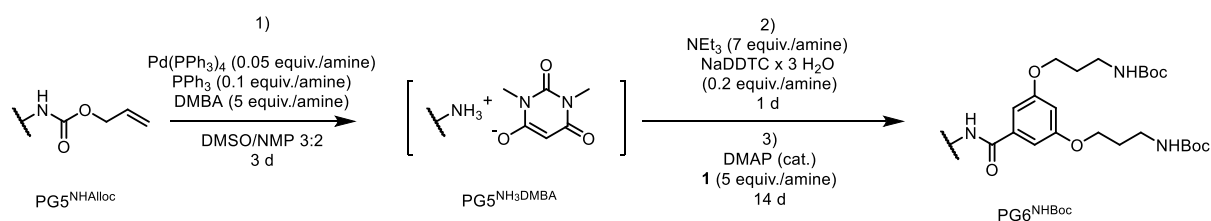


Figure S 3: AFM (tapping mode, mica) of the products obtained after exposure of a) $\text{PG6}_{500}^{\text{NHBoc}}$, b) $\text{PG7}_{500}^{\text{NHBoc}}$ and c) $\text{PG8}_{500}^{\text{NHBoc}}$ to refluxing (80 °C) TFA for 72 h. The DPs were prepared according to the methods described in Ref. 6.

3.2 Base-free deprotection of PG5^{NHAlloc}₅₀₀



Scheme 3: Base-free deprotection of PG5^{NHAlloc}₅₀₀, followed by dendronization to PG6^{NHBOC}_n.

To a solution of PG5^{NHAlloc}₅₀₀ (50.5 mg, 4.8 μmol RU / 0.15 mmol amines) and PPh₃ (4 mg, 15 μmol , 0.1 equiv./amine) in a mixture of dry DMSO (1 mL) and dry NMP (1 mL), DMBA (119 mg, 0.8 mmol, 5 equiv./amine) was added. The resulting solution was degassed by purging with argon supplied from a balloon. Then an argon-purged solution of Pd(PPh₃)₄ (18.9 mg ml⁻¹ in NMP; 0.46 mL, 7.5 μmol , 0.05 equiv./amine) was added. The resulting solution was purged with argon, then the reaction was stirred in the dark for 3 d. To the resulting clear, orange solution, sodium *N,N*-diethyldithiocarbamate trihydrate (9.3 mg, 41 μmol , 0.27 equiv./amine) was added. After purging with argon, the reaction was stirred in the dark overnight, whereupon NEt₃ (0.5 mL, 3.6 mmol, 24 equiv./amine), DMAP (5 mg, 41 μmol , 0.27 equiv./amine) and **1** (260.5 mg, 0.5 mmol, 3.3 equiv./amine) were added, followed by purging with argon. After 16 d of stirring in the dark, the resulting solution was precipitated into Et₂O and further purified by twofold reprecipitation from little methylene chloride, then redissolved in little methylene chloride, which was removed in vacuum to afford a glassy, yellow-orange solid.

3.3 Attempted acid titration of PG5^{NH₂}₅₀₀

To a solution of PG5^{NHAlloc}₅₀₀ (218.7 mg, 20.8 μmol RU / 0.67 mmol amines), NEt₃ (0.74 mL, 5.3 mmol, 8 equiv./amine), and PPh₃ (17.8 mg, 79 μmol , 0.1 equiv./amine) in a mixture of dry DMSO (6 mL) and dry NMP (4 mL) at 0 °C, DMBA (520.7 mg, 3.4 mmol, 5 equiv./amine) was added. The resulting solution was then warmed to RT and degassed by purging with argon supplied from a balloon. To this was added an argon-purged solution of Pd(PPh₃)₄ (18.9 mg ml⁻¹ in NMP; 2.1 mL, 35 μmol , 0.05 equiv./amine). The resulting solution was purged with argon, then the reaction was stirred in the dark for 3 d. From the orange solution, 4 aliquots of 3 mL were removed, each transferred under argon into a separate argon-filled vessel. To each solution, a different amount of TFA was added (as a 195.25 mg/mL solution in dry DMSO; 0.765 mL/0.8 equiv. excess per amine; 0.805 mL/1.2 equiv. excess per amine; 0.875 mL/2 equiv. excess per amine; 1.045 mL/4 equiv. excess per amine). Each sample was then topped up with additional dry DMSO such that 1.5 mL total added volume was achieved.

From each of these solutions, aliquots of 1.5 mL were taken after 15 min, 1 h and 3 h and added to a vial containing a portion of a premade solution (0.6 mL) of **1** (*ca.* 0.3 mmol per sample), DMAP (*ca.* 30 μmol per sample) and NEt₃ (*ca.* 0.5 mmol per sample) in dry NMP. The samples were stirred under argon for 3 d, then each was precipitated into Et₂O, reprecipitated from little methylene chloride, then taken up in little methylene chloride and dried in vacuum, resulting in glassy solids, ranging in color from orange to brown.

3.4 Deprotection & dendronization of mixed-substitution $g = 5$ DPs

To ascertain a lower threshold for the degree of peripheral protonation necessary to induce DP scission (at least for the given solvents composition, *i.e.* a mixture of DMSO and NMP), DPs with mixed peripheral substitution ($\text{PG5}_{500}^{\text{NHAlloc36}}$ **S9**, $\text{PG5}_{500}^{\text{NHAlloc57}}$ **S10**, and $\text{PG5}_{500}^{\text{NHAlloc80}}$ **S11**) were prepared as described in Section 2 of the SI. The conditions for deprotection and dendronization of these mixed-substitution DPs were analogous to those described in subsection 3.2 of the SI, *i.e.* it proceeded in the absence of base, and liberated amines were protonated by DMBA. Figure S 4 shows the GPC traces of the resulting DPs (which are partially of $g = 5$ and partially of $g = 6$), and Figure S 5b,d,f show AFM images of the same three products. As the comparisons with the respective starting materials (Figure S 4, Figure S 5a,c,e) and with the base-free deprotection of $\text{PG5}_{500}^{\text{NHAlloc}}$ conducted as a control experiment (Figure S 4, Figure S 5g,h) show, the three mixed-substitution DPs did not undergo degradation under these mildly acidic conditions. This suggests that main-chain scission only occurs if $> 80\%$ of peripheral groups are charged.

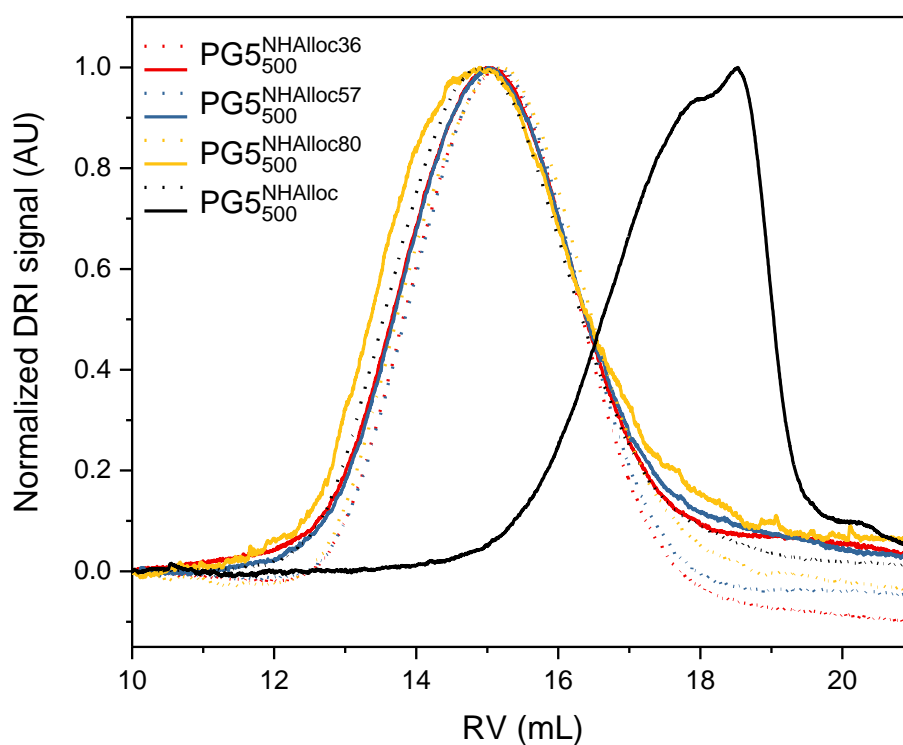


Figure S 4: GPC of starting materials (dashed lines) and reaction products (solid lines) in the base-free deprotection of mixed protecting group DPs.

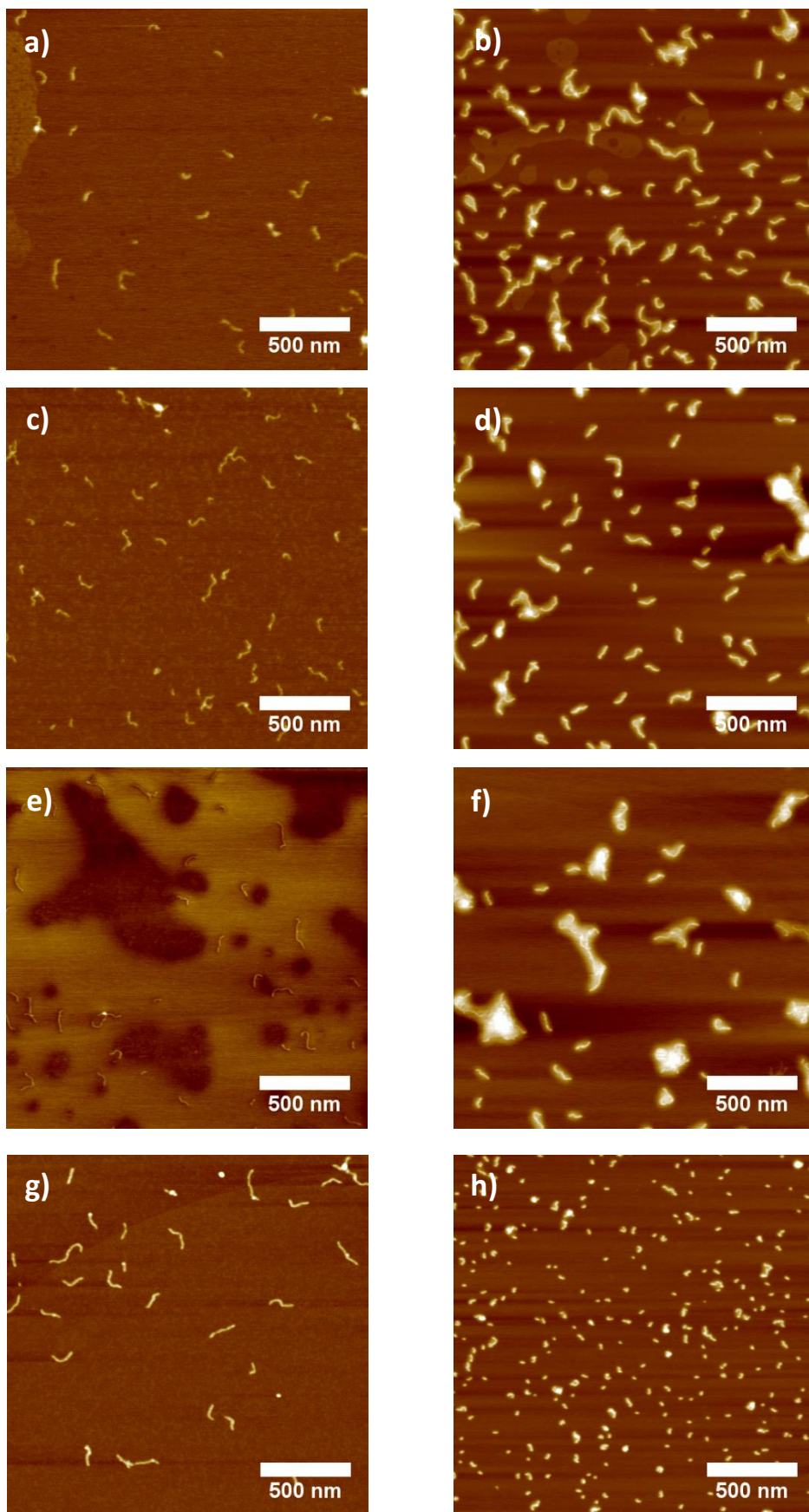
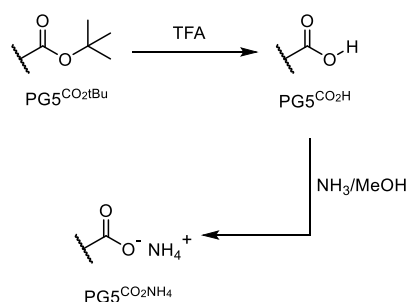


Figure S 5: AFM height images of (left-hand column) starting polymers and (right-hand column) the products of deprotection/dendronization: a)/b) $PG5_{500}^{Alloc36}$, c)/d) $PG5_{500}^{Alloc57}$, e)/f) $PG5_{500}^{Alloc80}$, g)/h) $PG5_{500}^{NHAlloc}$.

3.5 Deprotection & deprotonation of PG5^{CO₂tBu}₅₀₀



Scheme S 4: Transformations starting from the ^tBu-ester protected DP PG5^{CO₂tBu}₅₀₀.

To an ice-cooled vial containing a PTFE-coated stir bar and PG5^{CO₂tBu}₅₀₀ (ca. 20 mg), ice-cold TFA (2 mL) was added. The resulting solution was stirred at RT for 24 h, then the polymer was precipitated into deionized water (20 mL). The colorless solid (PG5^{CO₂H}₅₀₀) was dissolved in MeOH for DLS measurements and AFM. For deprotonation, PG5^{CO₂H}₅₀₀ was dissolved in MeOH saturated with ammonia (prepared by bubbling ammonia produced in the reaction of solid NH₄Cl and 8 M aq. NaOH through MeOH), forming PG5^{CO₂NH₄}₅₀₀. For ¹H-NMR (Figure S 6), deprotection was conducted using TFA-*d* as the acid, directly.

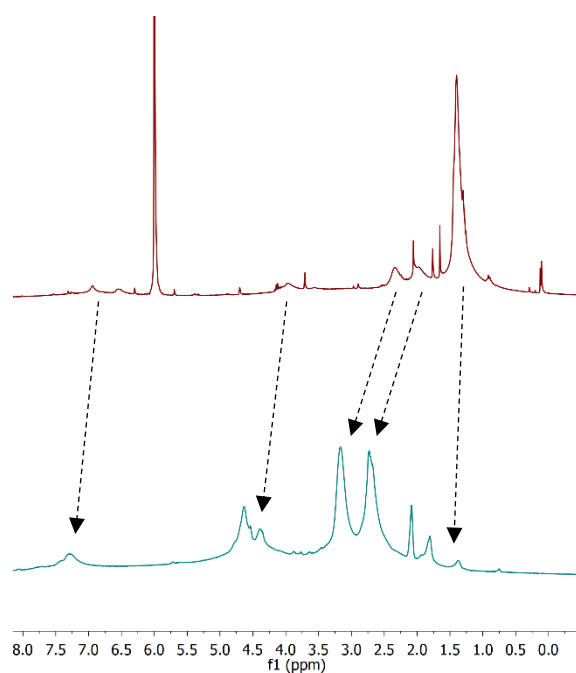


Figure S 6: a) ¹H-NMR spectra of PG5^{CO₂tBu}₅₀₀ (in TCE-*d*₂, red) and PG5^{CO₂H}₅₀₀ (in TFA-*d*, turquoise).

4. Experiments involving charge-neutral DPs

4.1 Initial observations

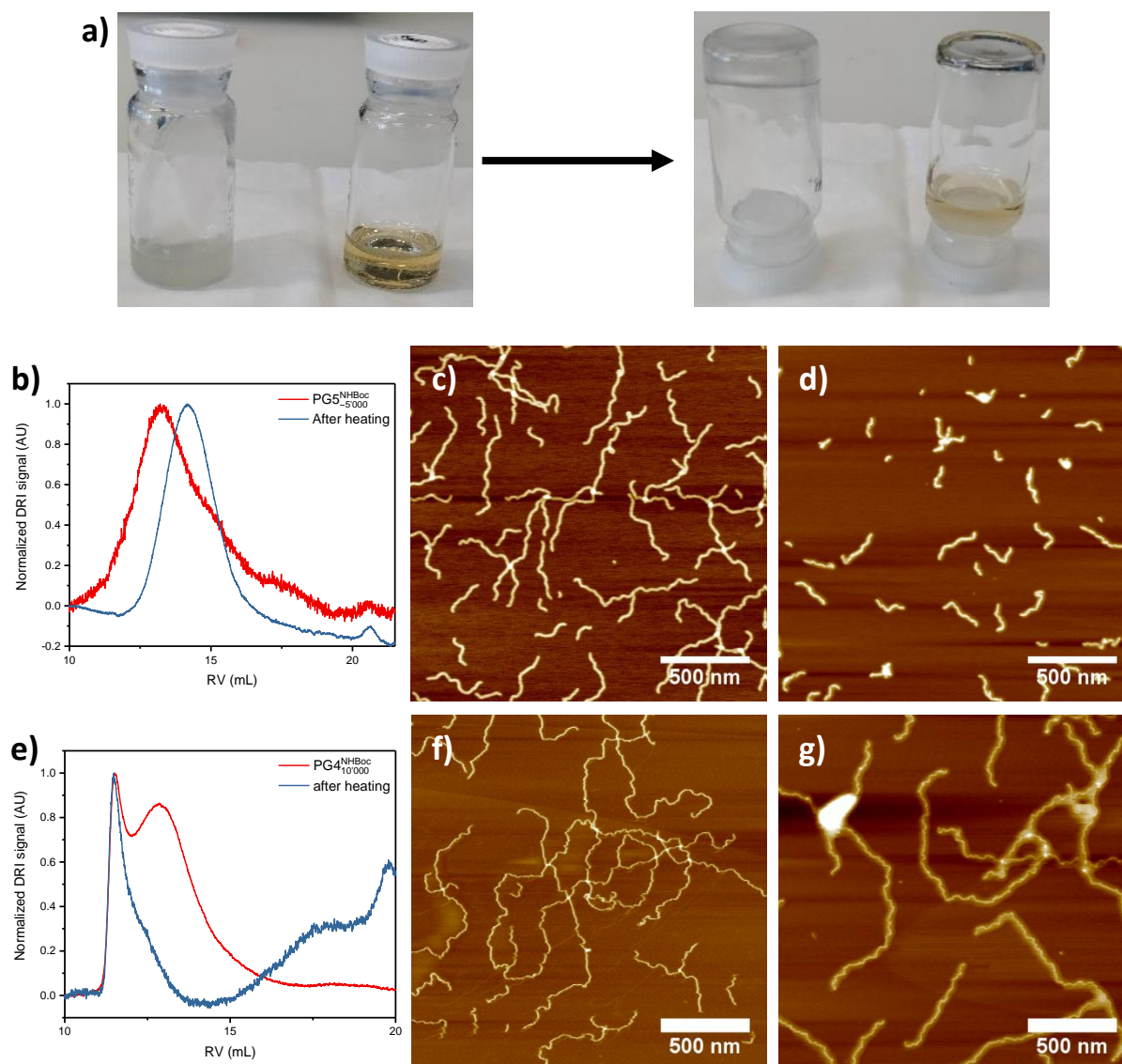


Figure S 7: a) Illustration of viscosity change upon heating by overturning vials with DP solutions (right-hand photograph taken immediately after overturning the vials): The left-hand vial contains a solution of PG5^{NHBoc}_{~5'000} (~10 % w/w in DMF) prepared at RT, the right-hand vial contains the product obtained after heating a similar mixture at 80 °C for 1 h. b) GPC retention curves (DMF + 0.1 % LiBr, 45 °C) of PG5^{NHBoc}_{~5'000} and the product obtained after heating a solution of the DP in DMF to 80 °C for 1 h. c) AFM height images (mica, tapping mode) of c) PG5^{NHBoc}_{~5'000} and d) the product of heating. e) GPC retention curves (DMF + 0.1 % LiBr, 45 °C) of PG4^{NHBoc}_{10'000} and the product obtained after heating a solution of the DP in DMF to 80 °C for 1 h. AFM height images (mica, tapping mode) of f) PG4^{NHBoc}_{10'000} and g) the product of heating.

Initial experiments leading to the discovery of “hot solvent”-induced scission consisted of the heating of (initially heterogenous) mixtures of PG5^{NHBoc}_{~5'000} and DMF at DP concentrations of 10 – 20 % w/w, with the aim of preparing highly concentrated solutions of this high P_n DP for rheological investigations. The samples were shaken on a pre-heated orbital shaker (PL-SP 260, Polymer Laboratories Inc.) in 5 mL glass scintillation vials at 60 °C – 80 °C. Alarmingly, it was found that this led

to a significant reduction in viscosity in the heated samples (Figure S 7a). GPC and AFM imaging (Figure S 7b-d) of polymers isolated by precipitation into Et₂O revealed that this is due to a significant reduction in chain length. Analogous experiments conducted with PG4^{NHBoc}_{~10'000} indicated no such decomposition (Figure S 7e-g; The apparent increase in molar mass in Figure S 7e after heating of PG4^{NHBoc}_{~10'000} may be the result of aggregation by interdigitation at elevated temperatures.

4.2 “Hot solvent” mediated scission experiments: General comments

Experiments probing various factors in “hot solvent” mediated scission were conducted as follows: Samples were prepared by mixing the DPs (1 – 20 % w/V, typically 5 – 100 mg DP) with solvent in 1.5 mL screw-cap HPLC vials equipped with PTFE-lined septa or 5 mL scintillation vials with PP stoppers. In most cases, these samples were first shaken overnight at RT, using an orbital shaker (IKA-VIBRAX-VXR, IKA Werke) set to *ca.* 400 RPM. When heating was indicated, samples were set into a pre-heated aluminium heating block with wells suited for the 1.5 mL screw-cap vials set on a magnetic hotplate (MR3004 safety, Heidolph), or into a pre-heated aluminium block with wells suited for 5 mL scintillation vials on a temperature-controlled orbital shaker (PL-SP 260, Polymer Laboratories).

Samples for GPC were removed from the scission experiments at the indicated times prepared by diluting the sample to ~1 mg mL⁻¹ in the appropriate eluent (DMF/1 g L⁻¹ LiBr/ 1 mL L⁻¹ toluene or CHCl₃/1 mL L⁻¹ toluene), shaking gently at 45 °C (DMF or 35 °C (CHCl₃) for 30 min, then filtering through a 0.45 µm pore size PTFE syringe filter (Chromafil X-Tra PTFE-45/25, Macherey Nagel).

In some cases, *e.g.* to obtain samples for MALDI-TOF-MS analysis, the solutions of scission products were precipitated into Et₂O/hexane 1:1 (for PG5^{CO₂tBu}₅₀₀: 1:10). The resulting polymers were isolated by centrifugation, taken up in little methylene chloride. Solvent removal usually afforded colorless or off-white solids from which GPC samples were prepared in analogy to the procedure in the previous paragraph.

4.3 Impact of solvent & temperature

The reductions in molar mass evident in GPC retention curves of DPs heated in polar-aprotic solvents (Fig. 2a) may also be observed by AFM height images (see Figure S 7c,d and Figure S 8). As is the case for GPC curves, AFM suggests differences in the severity of main-chain scission depending on the solvent: DMF causes the least severe degradation, (Figure S 7d) DMAc (Figure S 8a) and DMPU (Figure S 8b) afford shorter products under otherwise identical conditions.

Another finding of note in the context of solvent effects is that the severity of scission for the “harshest” solvent among those attempted (DMPU) at RT surpasses that of the “mildest” solvent which still does lead to scission (DMF) at much higher temperatures, *e.g.* 80 °C (Figure S 9).

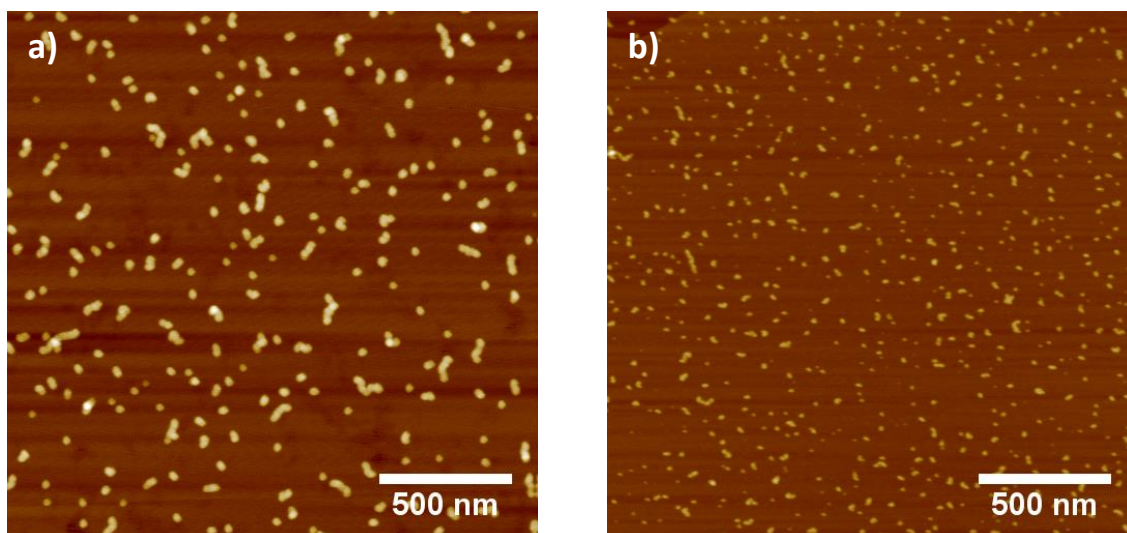


Figure S 8: AFM height images (mica, tapping mode) of the products obtained after heating $PG5_{500}^{NH_{Boc}}$ (see Figure S 7d) to 80 °C for 1 h in a) DMAc, b) DMPU.

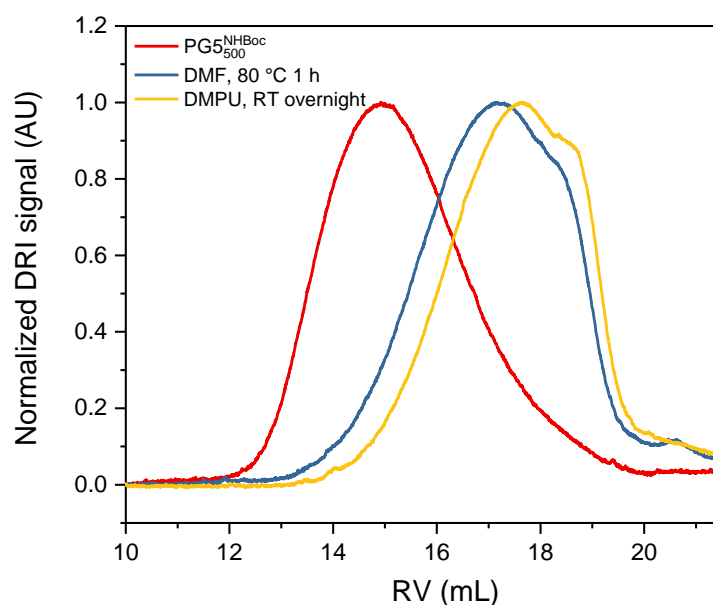


Figure S 9: GPC retention curves of $PG5_{500}^{NH_{Boc}}$ and the scission products obtained from heating to 80 °C for 1 h in DMF or merely shaking gently at RT in DMPU overnight.

To pinpoint the onset temperature of main-chain scission in DMF (the synthetically most relevant solvent among those tested), temperature-controlled rheological tests were performed. A highly concentrated solution (*ca.* 20 % w/w) of $PG5_{500}^{NH_{Boc}}$ in DMF was heated from 20 °C to 80 °C in steps of 5 °C while monitoring rheological properties using a cone-plate geometry (CP50-1) in a MCR502 rheometer (Figure S 10, Aton Paar GmbH). To that end, a frequency sweep ($\omega = 400 - 0.1 \text{ rad s}^{-1}$ at $\gamma_0 = 0.02 \%$) was performed after equilibrating at every multiple of 5 °C. During heating between frequency sweeps (0.1 °C min^{-1}), dynamic testing at $\omega = 10 \text{ rad s}^{-1}$ and $\gamma_0 = 0.02 \%$ was performed.

While a solvent-filled guard ring (a) was used to reduce solvent evaporation in the hood oven, the apparatus could not be closed completely, and above *ca.* 40 °C the onset of evaporation was

observed, indicated by a thickening of the solution after the expected initial decrease of viscosity with increasing temperature. This complicates the interpretation of the data: The absolute values of G' and G'' (Figure S 11a) cannot be interpreted directly due the changes in sample geometry caused by evaporation. However, in the geometry-independent phase-shift angle (Figure S 11b), an inflection point is visible at *ca.* 60 – 65 °C, indicating a thinning of the solution which cannot be explained with evaporating solvent only. This decrease in viscosity is a clear sign of main-chain scission.

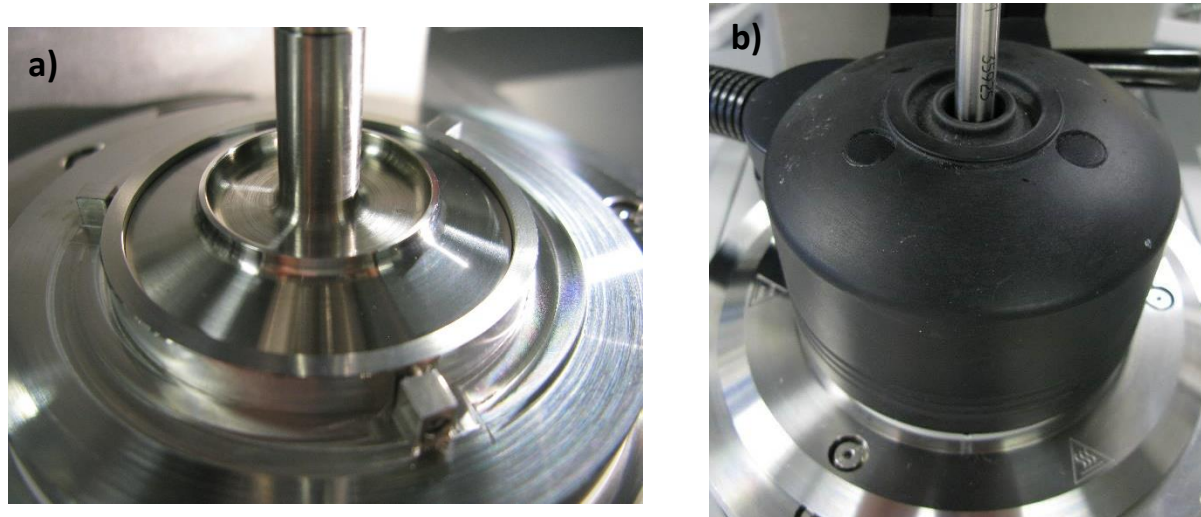


Figure S 10: a) Cone-plate measurement geometry (CP50-1) with a guard ring (*ca.* 0.1 mm gap); during measurement, the solvent reservoir on top was filled with DMF; b) apparatus with the closed hood over, which has no gap at the bottom.

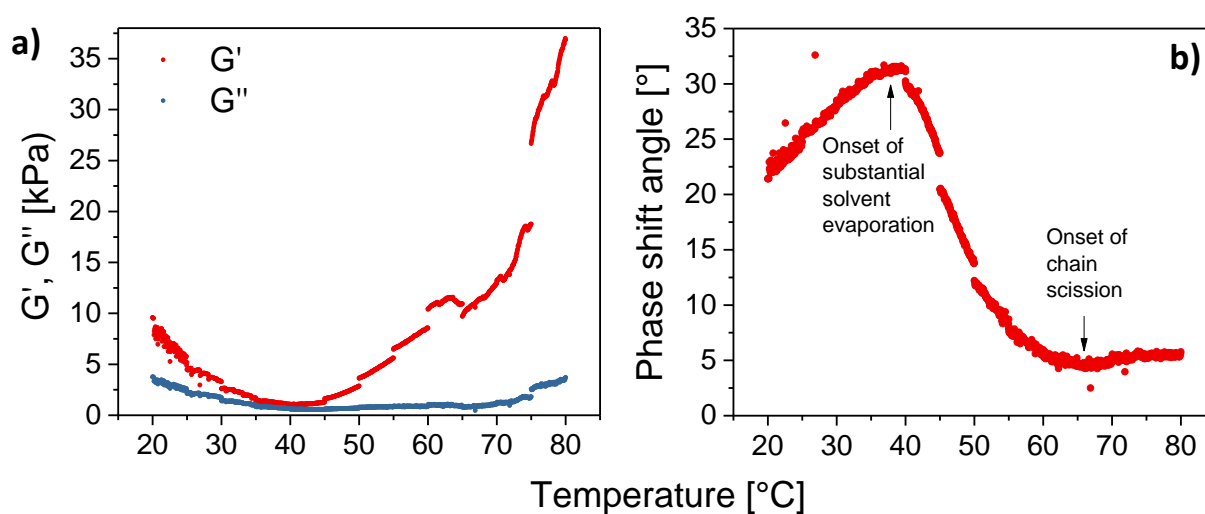


Figure S 11: T-dependent rheological testing of a 20 % w/w solution of $PG5^{NHBoc}_{5000}$ in DMF; a) dynamic moduli (G' , G''), b) geometry-independent phase shift angle.

4.4 Impact of dendritic generation g

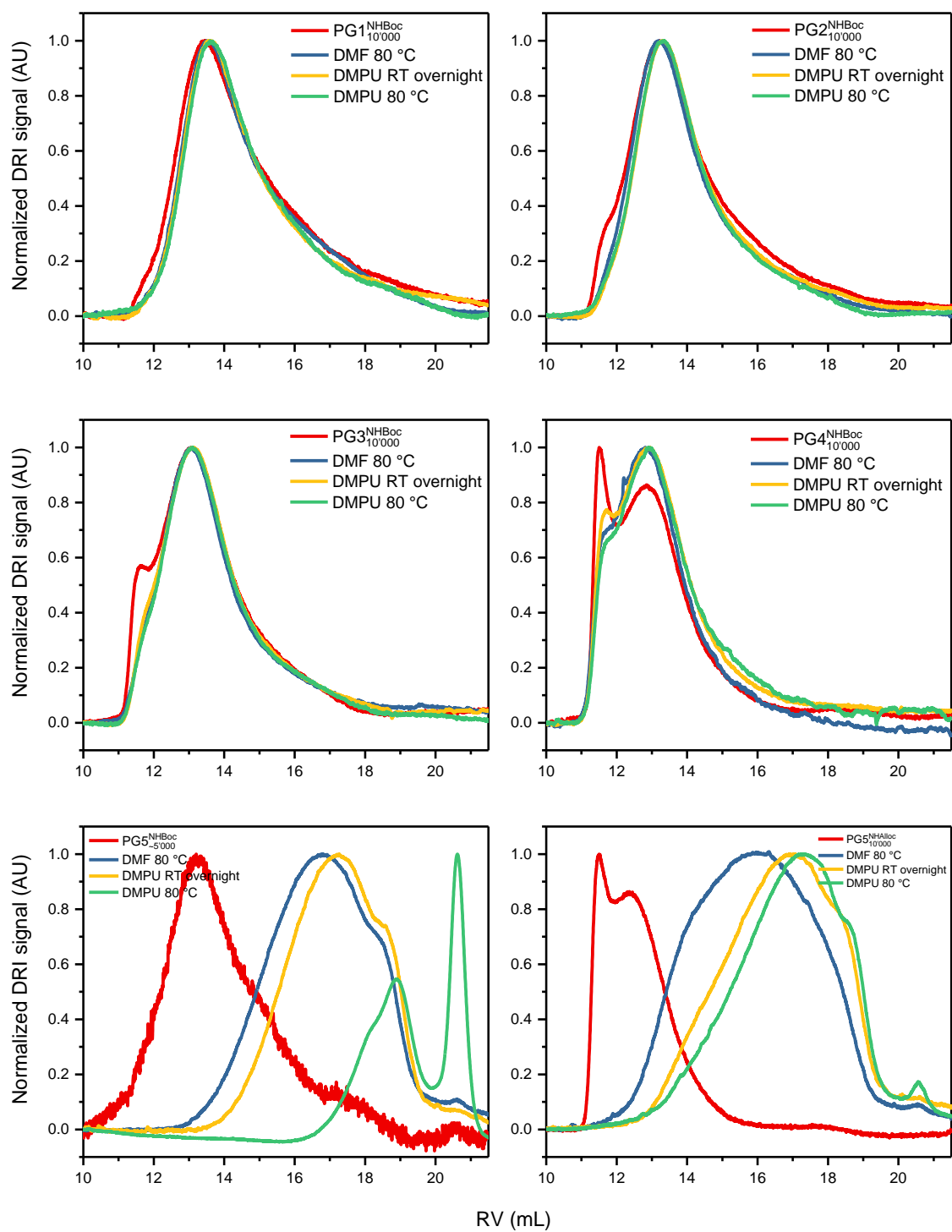


Figure S 12: “Hot solvent” mediated scission experiments for long-chain DPs. GPC was measured in DMF (0.1 % LiBr, 45 °C).

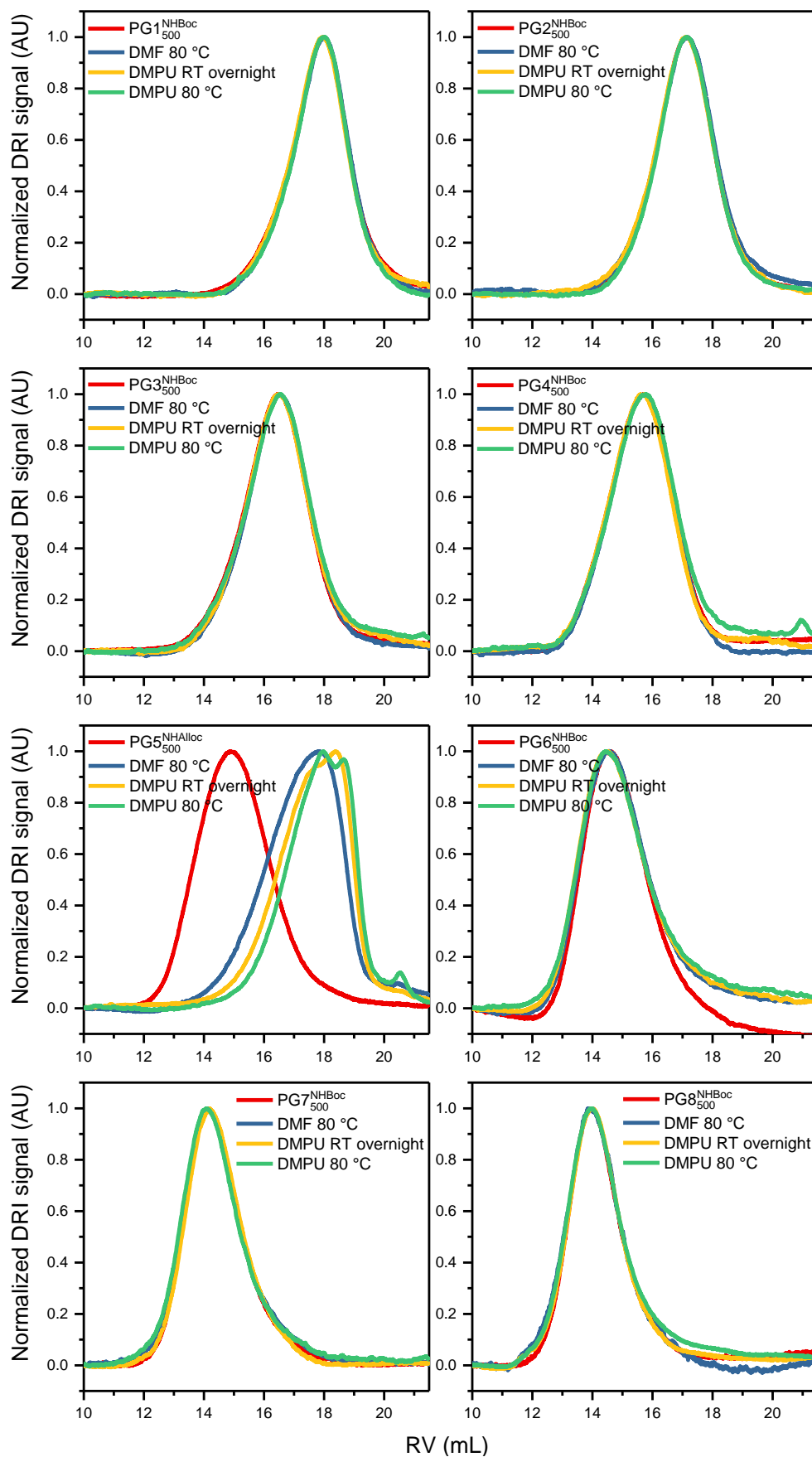


Figure S 13: “Hot solvent” mediated scission experiments of short-chain DPs of $g = 1 - 8$ (series with high structural perfection).⁶ GPC was measured in DMF (0.1 % LiBr, 45 °C).

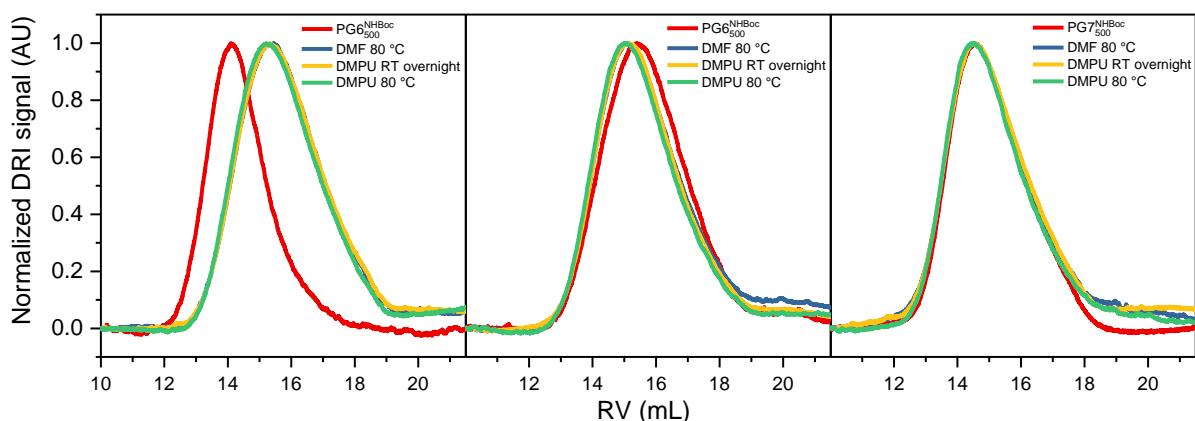


Figure S 14: GPC elution curves for solvent treatment (heating to 80 °C in DMPU & DMF, RT treatment in DMPU) of additional DP batches accessed by strictly “ $g + 1$ ” routes.⁶ GPC was measured in DMF (0.1 % LiBr, 45 °C).

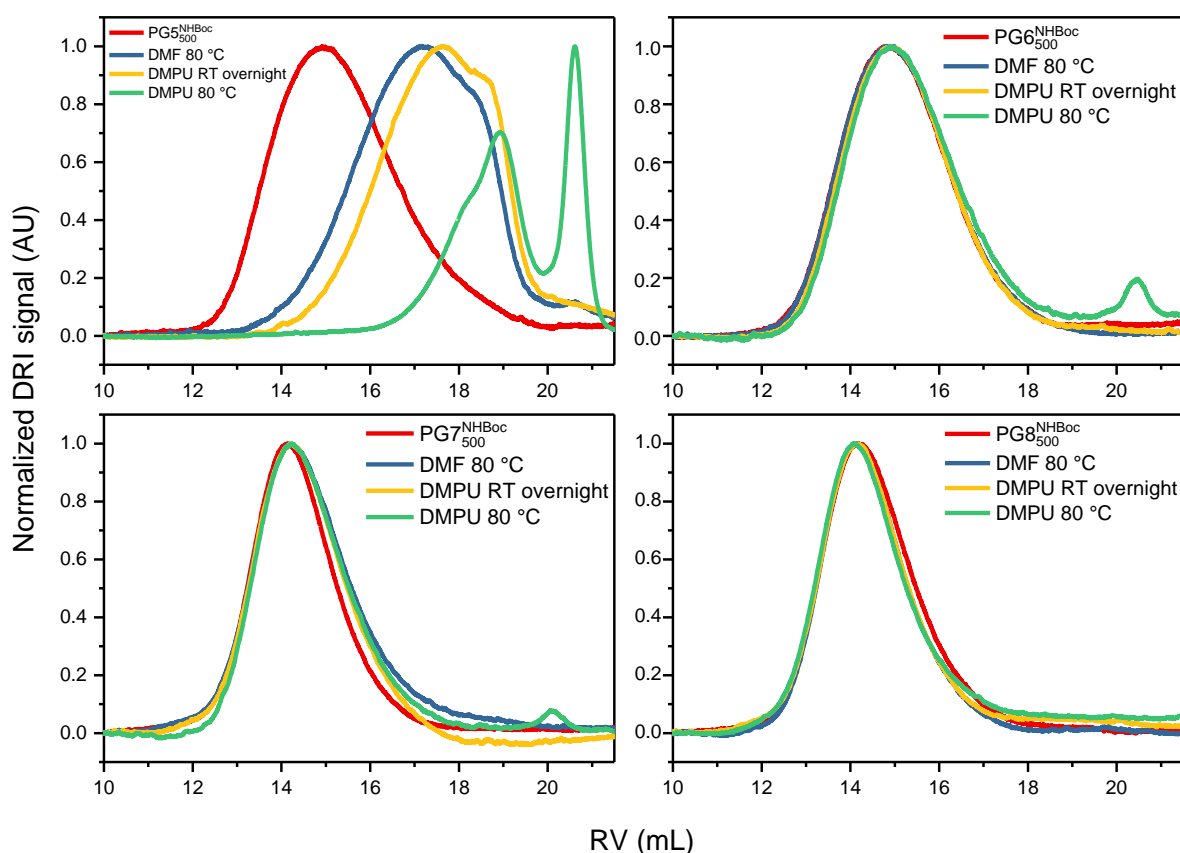


Figure S 15: “Hot solvent” mediated scission experiments of short-chain DPs of $g = 5 - 8$ (series with low structural perfection).⁸ GPC was measured in DMF (0.1 % LiBr, 45 °C).

As is the case for all DPs of $g \neq 5$, significant peak RV shifts were not observed for $\text{PG6}_{500}^{\text{NHBoc}}$ under the moderately harsh conditions used for the generation of Fig. 4a (see main text). The sole exception to this was one specific sample of $\text{PG6}_{500}^{\text{NHBoc}}$ of high structural perfection.⁶ While the sample degraded according to GPC, the result was atypical for three reasons: First, no peak corresponding to macromonomer was observed, as had been the case in all other instances of DP chain scission (Fig. 6a,b). Second, the peak shift is largely independent of temperature and solvent applied (compare *e.g.* Fig. 3c,d or Figure S 9). Third, the peak shape did not change significantly (Figure S 16; compare *e.g.* Figure 5a, main text). The reasons for this particular batch showing such outlier behavior remain unclear.

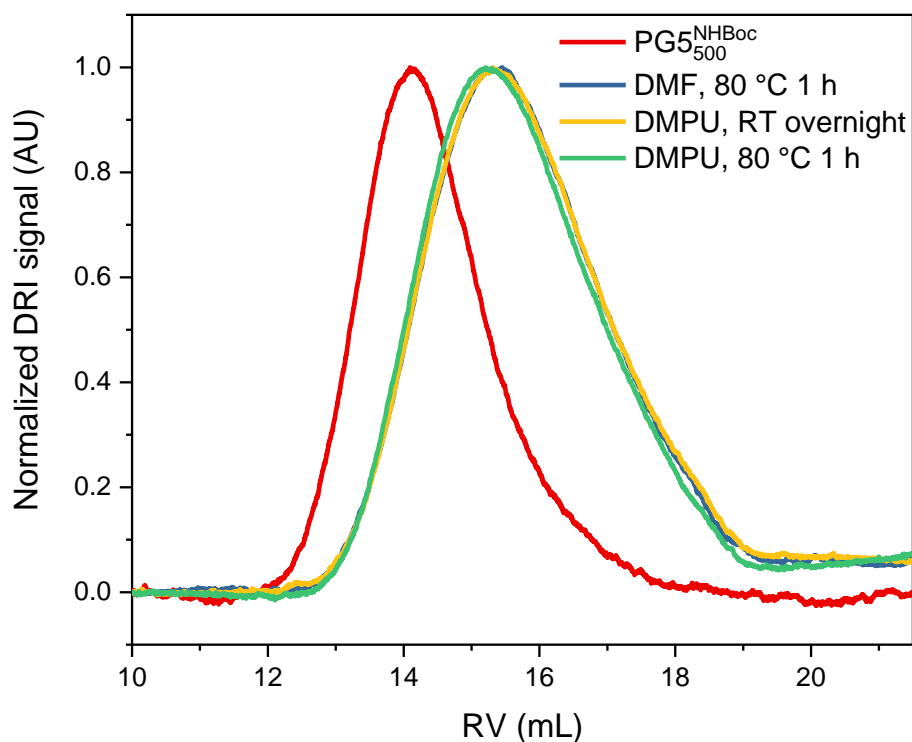


Figure S 16: GPC traces of the single “outlier” $PG5_{500}^{NHBoc}$ batch which had a significant peak shift ΔRV under the conditions employed for the generation of Fig. 5e (see main text). Compare e.g. Figure S 13 for a batch of $PG5_{500}^{NHBoc}$ prepared by the exact same methods⁶ showing no such behavior.

The data shown in the main text, Fig. 6a, can also be plotted in terms of relative molar mass differences ΔM_n , defined as the relative deviation of scission product number average molar mass (main polymeric peak) from the molar mass of the starting material as determined by GPC:

$$\Delta M_n = \frac{M_n^{\text{product}} - M_n^0}{M_n^0} \cdot 100 \%$$

We elected to use ΔRV instead of ΔM_n in the main text even though changes in molar mass are perhaps a more conventional choice often employed to track scission in the sonochemical literature.^{12–14} However, due to the at times minuscule sample amounts employed in scission experiments, and to avoid product fractionation e.g. by intermediate precipitation, we elected to prepare GPC samples ($c \approx 1 \text{ mg mL}^{-1}$) directly by dilution of scission experiment solutions ($c \geq 10 \text{ mg mL}^{-1}$). In many cases, this introduced substantial concentrations (up to 10% V/V of solvent into the GPC samples, thereby making accurate molar mass determination impossible - the Malvern GPC software relies on the presence of a flow marker (toluene), which is masked by the presence of large concentrations of other solvents. We found the molar masses resulting from such unreferenced evaluations to fluctuate by $\sim 10\text{-}20 \%$ (see Figure S 17), a comparatively large margin confounded by other factors (manual setting/adjustment of peak boundaries; poor separation between product peaks in the case of scission; complete polymer exclusion from pores for very high M samples). In view of these uncertainties, and considering that peaks are superimposable in practically all cases where no substantial scission occurred (see Figure S 12 - Figure S 15), ΔRV is a more suitable measure to answer the rather binary question whether scission has occurred or not.

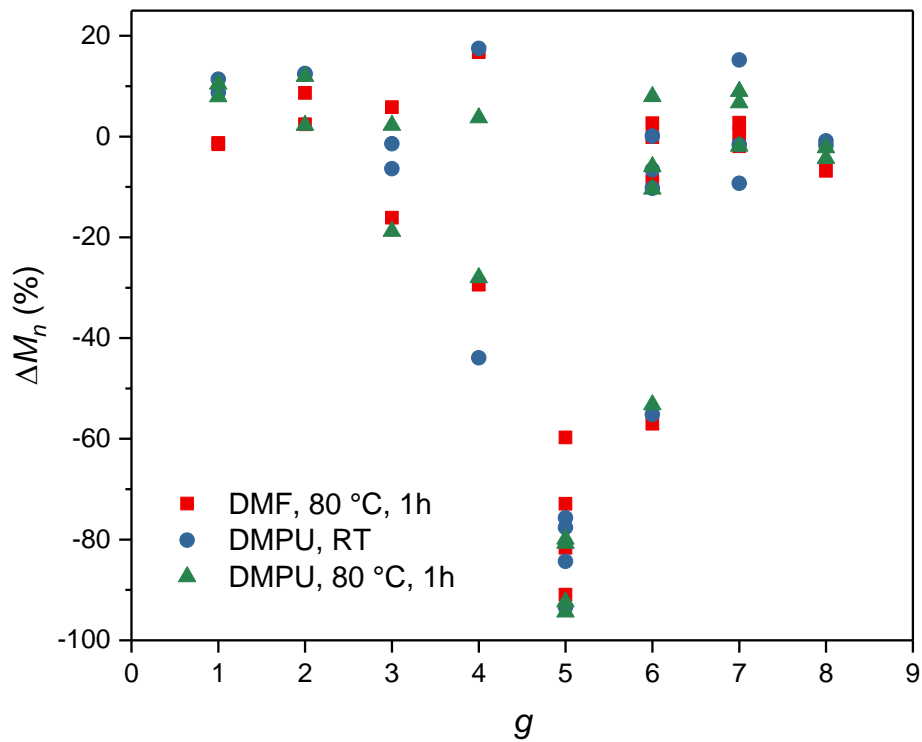


Figure S 17: ΔM_n data corresponding to Fig. 4a in the main text; the large spread for $g = 4$ DPs is owed largely to a significant proportion of the sample being subject to total exclusion effects (see Figure S 12); the set of outliers of $g = 6$ at $\Delta M_n \approx -55\%$ correspond to the curves represented in Figure S 16.

Table S 1: : ΔM_n data derived from GPC retention curves used in Figure S 17; note that GPC data could not be evaluated consistently (see accompanying text).

g	P_n	Synthetic method	ΔM_n [%]		
			DMF, 80 °C, 1 h	DMPU, RT	DMPU, 80 °C, 1 h
1	500	"g+1"	-1	9	8
2	500	"g+1"	9	13	12
3	500	"g+1"	6	-1	2
4	500	"g+1"	17	17	4
5	500	"g+1"	-60	-76	-81
6	500	"g+2"	-9	-10	-10
7	500	"g+2"	-2	15	9
8	500	"g+2"	-7	-1	-2
5	500	"g+1"	-73	-78	-80
6	500	"g+1"	0	-7	-6
7	500	"g+1"	3	-2	-2
8	500	"g+1"	-2	-2	-4
6	500	"g+1"	-57	-55	-53
6	500	"g+1"	3	0	8
7	500	"g+1"	1	-9	7
1	10000	"g+1"	-2	11	10
2	10000	"g+1"	2	12	2
3	10000	"g+1"	-16	-6	-19
4	10000	"g+1"	-29	-44	-28
5	5000	"g+1"	-82	-84	-92
5	10000	"g+1"	-91	-93	-94

4.5 Impact of peripheral chemistry

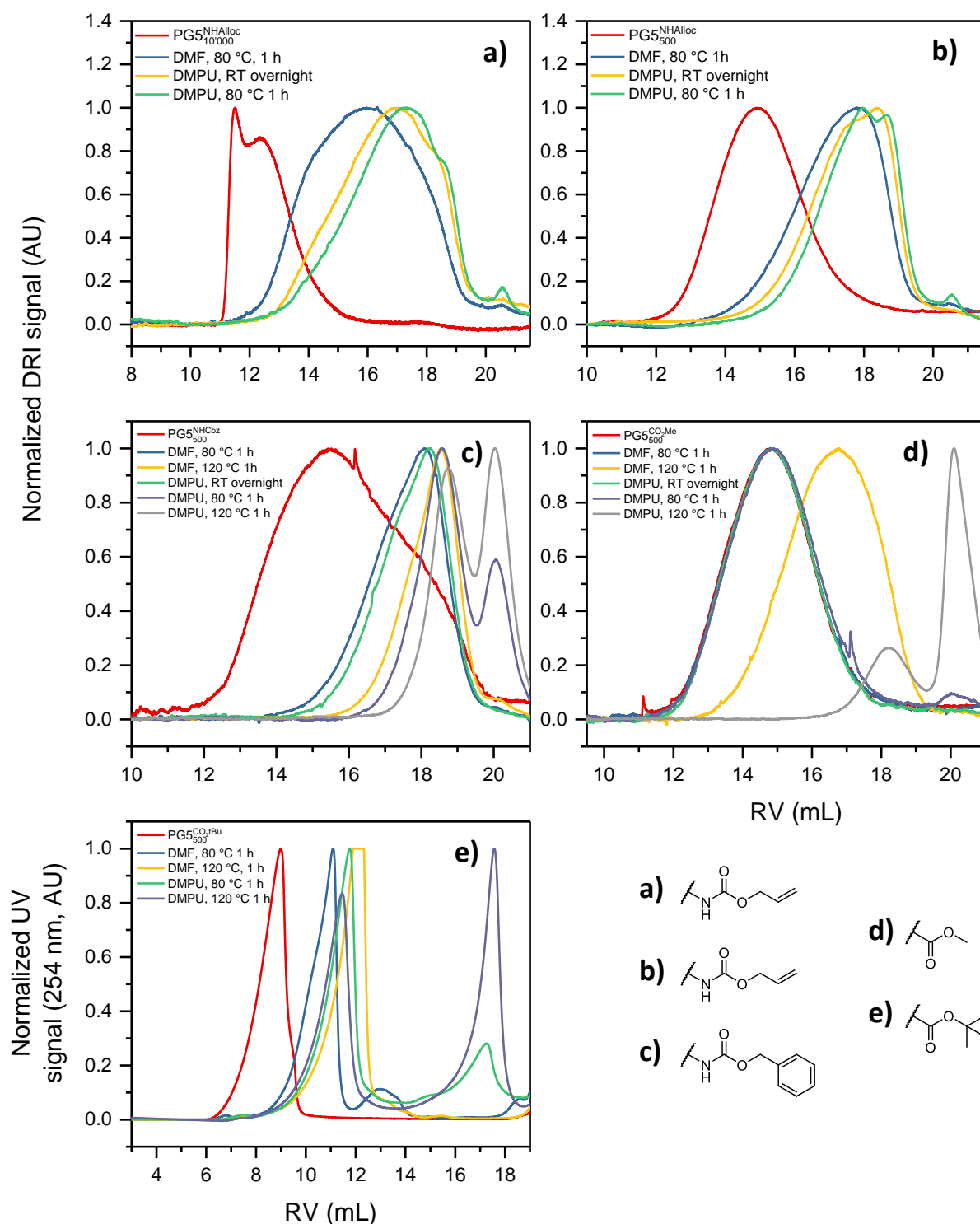


Figure S 18: GPC elution curves representing the “hot solvent” treatment of variously substituted DPs of $g = 5$ (concentration ca. 1 % w/V for all experiments): a) $PG5^{NHAlloc}_{10000}$, b) $PG5^{NHAlloc}_{500}$, c) $PG5^{NHCbz}_{500}$, d) $PG5^{CO_2Me}_{500}$, e) $PG5^{CO_2tBu}_{500}$. The results in Figure S 22e for $PG5^{CO_2tBu}_{500}$ were obtained by GPC in $CHCl_3$; $PG5^{CO_2tBu}_{500}$ is the only DP presented in this thesis which is not well soluble in DMF. The peripheral groups in which these DPs differ are displayed on the bottom right.

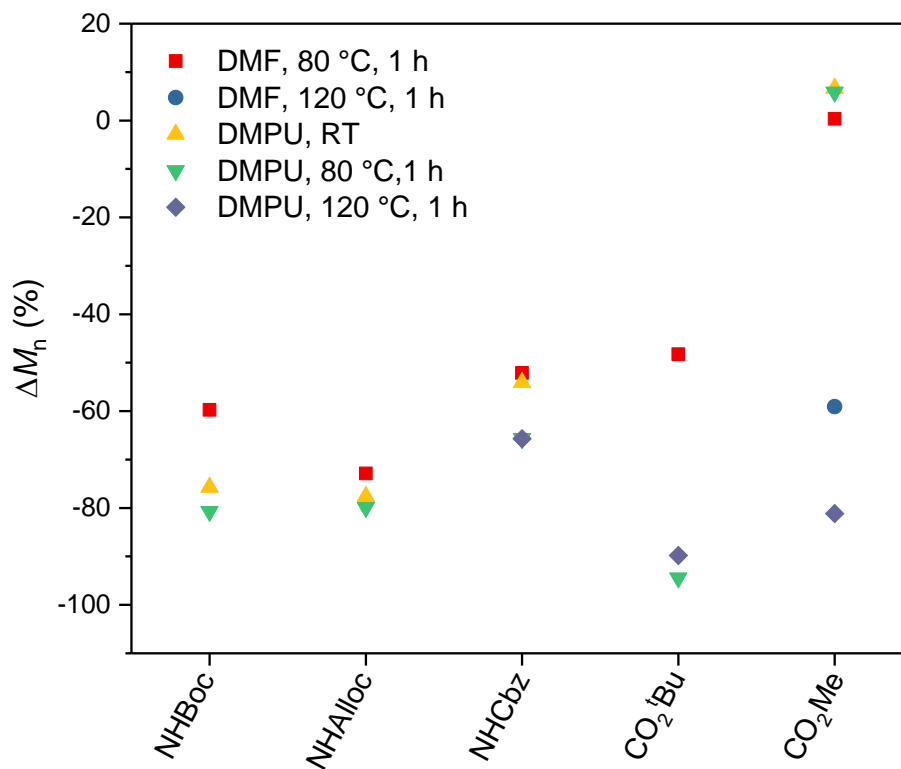


Figure S 19: ΔM_n data corresponding to Fig. 4b in the main text. See subsection 4.4 for relevant comments.

Table S 2: ΔM_n data derived from GPC data corresponding to Figure S 19. See subsection 4.4 for relevant comments. a) GPC evaluation for $PG5_{500}^{CO_2tBu}$ is approximate at the very best, as the SM was far outside the calibrated range for the given column set.

Chemistry	P_n	ΔM_n [%]				
		DMF, 80 °C	DMF, 120 °C	DMPU, RT	DMPU, 80 °C	DMPU, 120 °C
NHBoc	500	-60	N/A	-76	-81	N/A
NHAlloc	500	-73	N/A	-78	-80	N/A
NHCbz	500	-52	N/A	-54	-66	-66
CO ₂ Me	500	0	-59	-7	6	-81
CO ₂ tBu ^{a)}	500	-48	N/A	-100	-94	-90

4.6 Impact of structural perfection

As noted in the main text, DPs of $g > 5$ do not readily undergo scission as indicated by ΔRV (Fig. 4a). A closer look at GPC curves reveals stark differences between batches of $PG6_{500}^{NHBoc}$ and $PG7_{500}^{NHBoc}$ with different degrees of structural perfection:^{6,8} Samples of low structural perfection (Figure S 20a,b) did undergo limited degradation, as indicated by the appearance of an additional peak at low RV in GPC, whereas the corresponding DPs of higher structural perfection (Figure S 20d,e) remained intact. In samples derived from $PG8_{500}^{NHBoc}$, no clear signs of scission were apparent in DPs from either synthetic series (Figure S 20c,f).

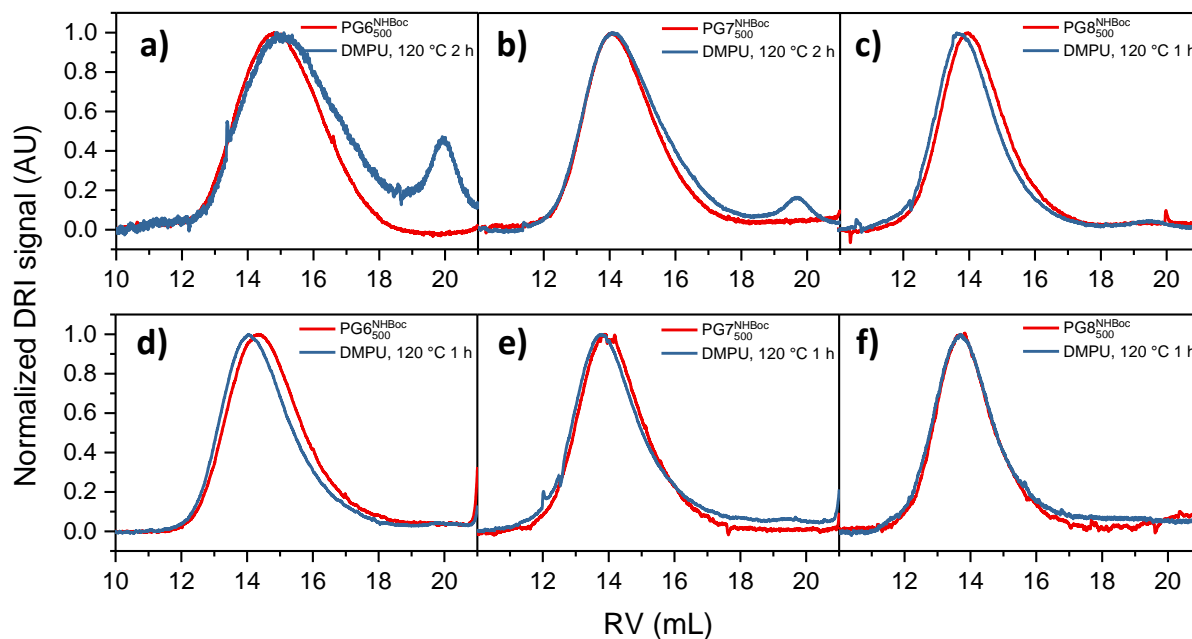


Figure S 20: GPC retention curves of “hot solvent” treatment (1% w/v in DMPU, 120 °C for 1 – 2 h) for a) $PG6_{500}^{NHBoc}$, b) $PG7_{500}^{NHBoc}$, c) $PG8_{500}^{NHBoc}$ (low structural perfection),⁸ d) $PG6_{500}^{NHBoc}$, e) $PG7_{500}^{NHBoc}$, and f) $PG8_{500}^{NHBoc}$ (high structural perfection).⁶ The polymers in the top row are of lower structural perfection⁸ than those in the bottom row.⁶

4.7 Impact of external shear

To test for the influence of externally applied shear (Fig. 5b), samples of $\text{PG5}_{500}^{\text{NHBoc}}$ were suspended in DMPU and then immediately shaken at various speeds on an orbital shaker, then treated as indicated in Section 4.2 of the SI.

4.8 Characterization of low molar mass DP scission products

For the identification of scission products, DPs of $g = 3 - 7$ were subjected to the harshest set of scission conditions employed in this work (DMPU, 120 °C for 1 – 2 h, a). The scission products were isolated by precipitation and investigated by GPC and MALDI-TOF-MS. As DPs of the type $\text{PG5}_n^{\text{CO}_2\text{tBu}}$ are not soluble in DMF at RT, GPC was performed in CHCl_3 instead (see Figure S 18). Samples of $\text{PG6}_{500}^{\text{NHBoc}}$ and $\text{PG7}_{500}^{\text{NHBoc}}$ were of low structural perfection, as only these DPs generated significant low molar mass fractions upon “hot solvent” treatment (see Figure S 20).

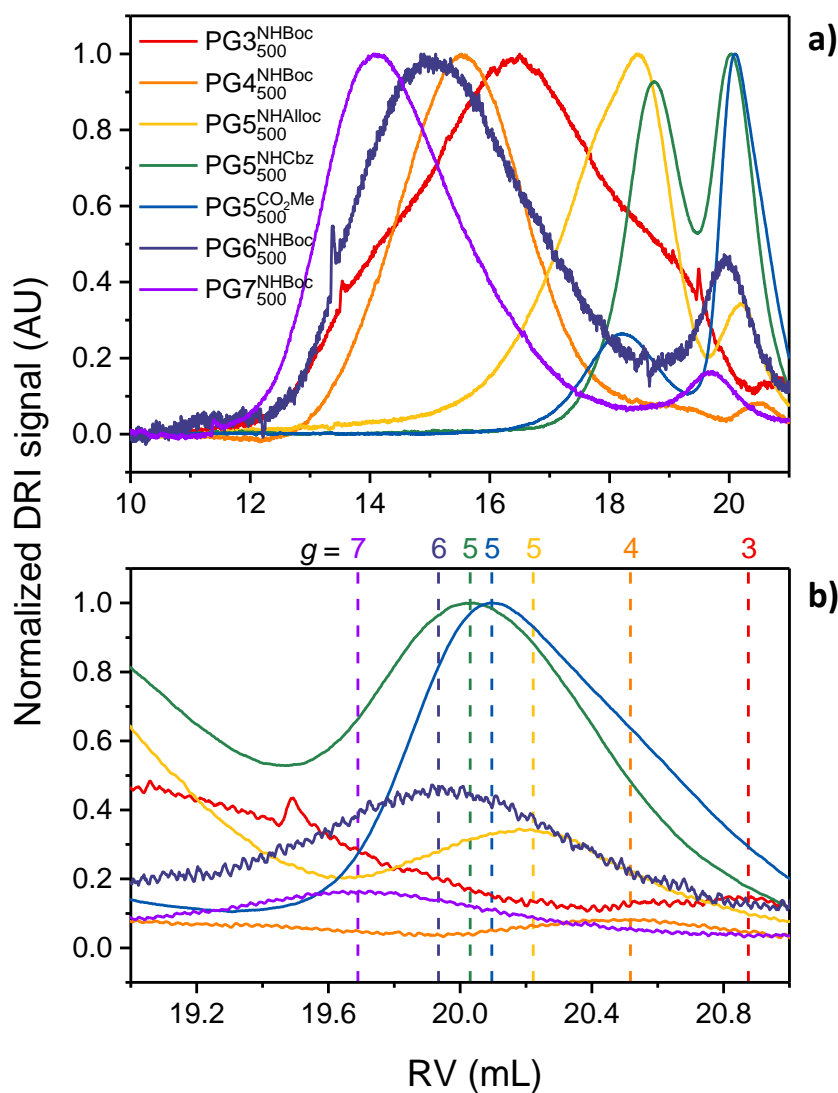


Figure S 21: a) GPC curves of DPs other than $\text{PG5}_{500}^{\text{NHBoc}}$ the scission products of which were investigated after “hot solvent” treatment (1% w/V in DMPU, 120 °C for 1 – 2 h); b) zoom on the high RV region of subfigure a), with secondary product peaks marked (compare Fig. 6a in the main text).

The results of MALDI-TOF-MS are summarized in Figure S 22 and Table S 3, and full mass spectra are depicted in Figure S 23 to Figure S 31. Main ions directly attributable or closely related to the macromonomers corresponding to the repeating units of the respective DPs were detected for all DPs of $g < 6$. For the two high g DPs (which, it should be noted, are of low structural perfection) no distinct peaks were found. For PG5^{NHAlloc} and PG5^{NHCbz}, regular mass patterns are apparent, the origins of which are unclear, though they may be related to the potential greater photoreactivity of the unsaturated protecting groups Alloc and Cbz.

Table S 3: Interpretation of mass spectra depicted in Figure S 22.

Starting Polymer	Main ion found (m/z)	Macromonomer (expected m/z for M ⁺)	Allocated species (expected m/z)
PG3 ^{NHBoc} ₅₀₀	2775.22	2624.40	(M+DMPU+Na) ⁺ (2774.49); also found: (M+DMPU+K) ⁺
PG4 ^{NHBoc} ₅₀₀	5550.01	5426.88	(M+DMPU) ⁺ (5555.98) (also found: M ⁺ /(M+H) ⁺)
PG5 ^{NHBoc} ₅₀₀	11163.27	11032.84	(M+DMPU) ⁺ (11160.93)
PG5 ^{NHAlloc} ₅₀₀	11008.69	10519.83	Possibly: M-DCTB reaction product, + n·DMPU (10619.94 + n·128.09)
PG5 ^{NHCbz} ₅₀₀	12278.66	12120.34	Possibly: (M+DMPU+Na) ⁺ (12271.42); unexplained pattern with $\Delta m/z \approx 420$
PG5 ^{CO₂Me} ₅₀₀	9230.90	9206.98	(M+Na) ⁺ (9229.92); also found: M ⁺ /(M+H) ⁺ , (M+K) ⁺
PG5 ^{CO₂tBu} ₅₀₀	10676.81	10552.49	(M+DMPU) ⁺ (10680.58)
PG6 ^{NHBoc} ₅₀₀	N/A	22245	N/A
PG7 ^{NHBoc} ₅₀₀	N/A	44670	N/A

For ¹H-NMR spectroscopy, a sample of PG5^{NHBoc}₅₀₀ was treated with DMPU, heated to 80 °C for 1 h, then precipitated into Et₂O. The precipitate was dissolved in little methylene chloride, evaporated to dryness and then dissolved in DMSO-*d*₆. ¹H-NMR spectra (Figure S 32) 1) displayed far sharper peaks than the original DP, indicating shorter relaxation times and therefore more open structures and 2) showed signals in the olefinic spectral region, which is usually empty for DPs.

The mass and ¹H-NMR spectroscopic observations agree with previous results obtained for the degradation of PG5^{NHBoc}₅₀₀ under the influence of TFA.¹¹

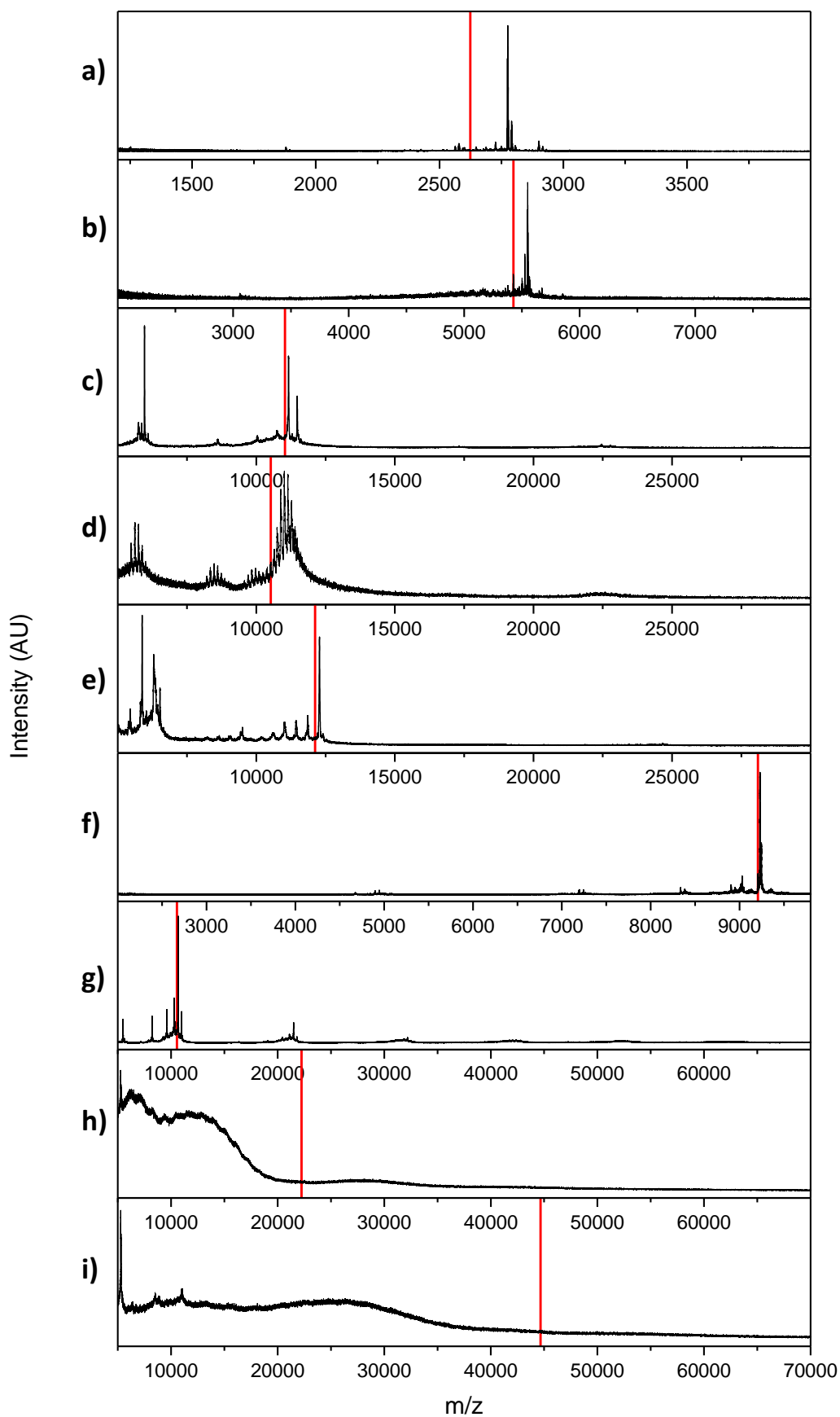


Figure S 22: MALDI-TOF-MS of DPs after heating (DMPU, 120 °C, 1 - 2 h); red lines: expected m/z (M^+); a) $PG3_{500}^{NHBoc}$, b) $PG4_{500}^{NHBoc}$, c) $PG5_{500}^{NHBoc}$, d) $PG5_{500}^{NHAlloc}$, e) $PG5_{500}^{NHCbz}$, f) $PG5_{500}^{CO_2Me}$, g) $PG5_{500}^{CO_2tBu}$, h) $PG6_{500}^{NHBoc}$, i) $PG7_{500}^{NHBoc}$.

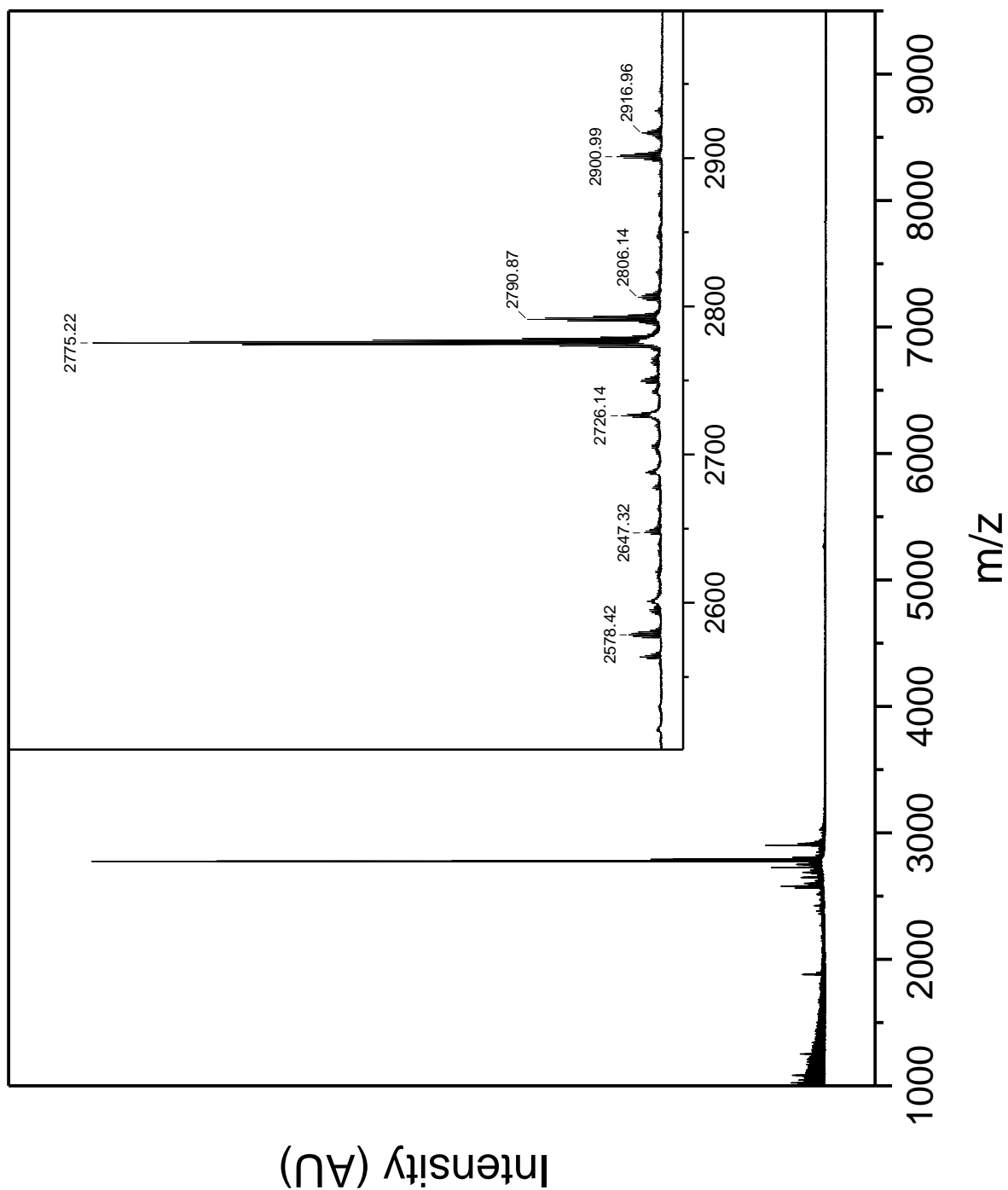


Figure S 23: MALDI-TOF mass spectrum of the products of heat treatment (DMPU, 2 h at 120 °C) of PG3₅₀₀^{NH₂Boc}.

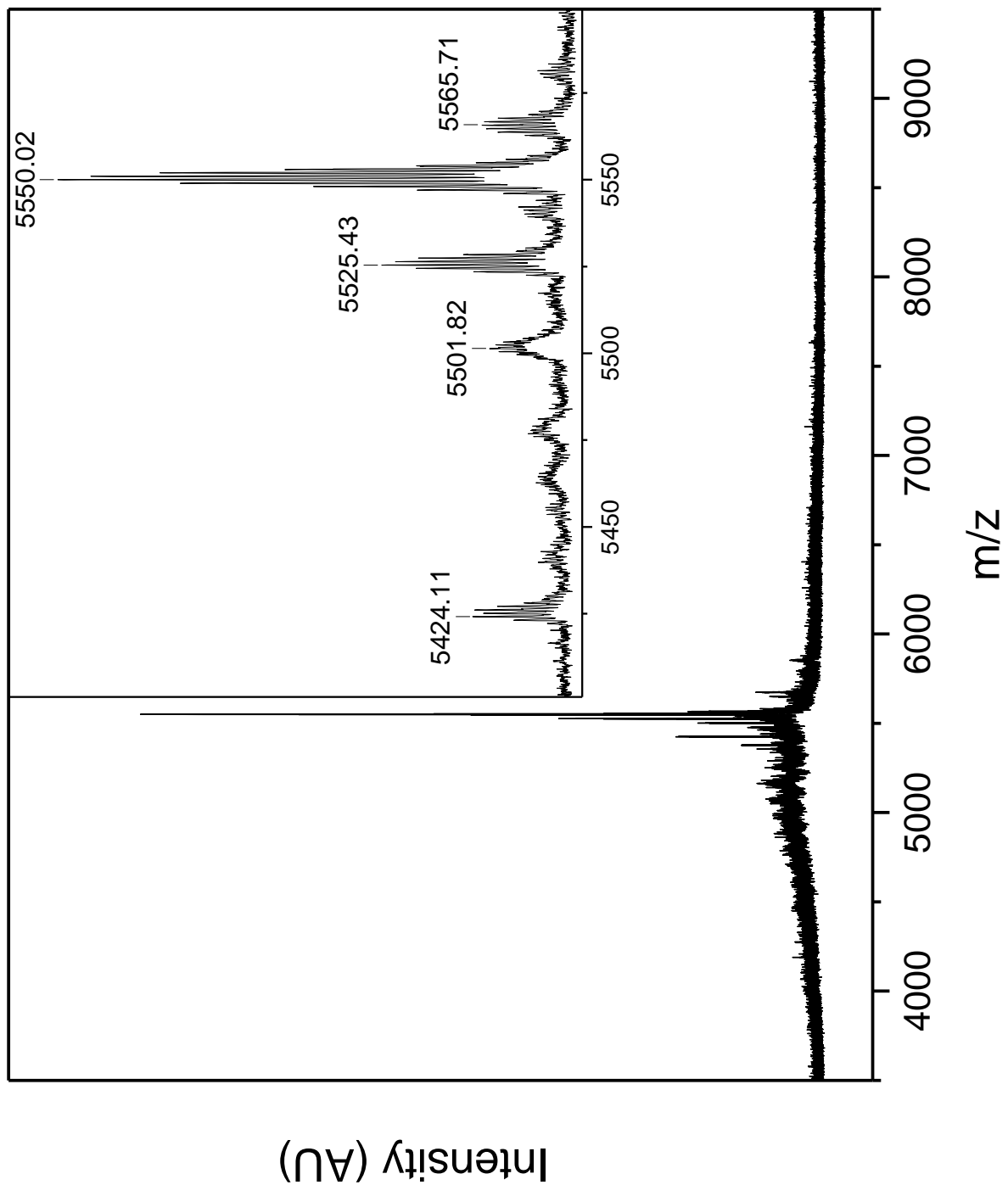


Figure S 24: MALDI-TOF mass spectrum of the products of heat treatment (DMPU, 2 h at 120 °C) of PG4^{NH₅₀₀Boc}.

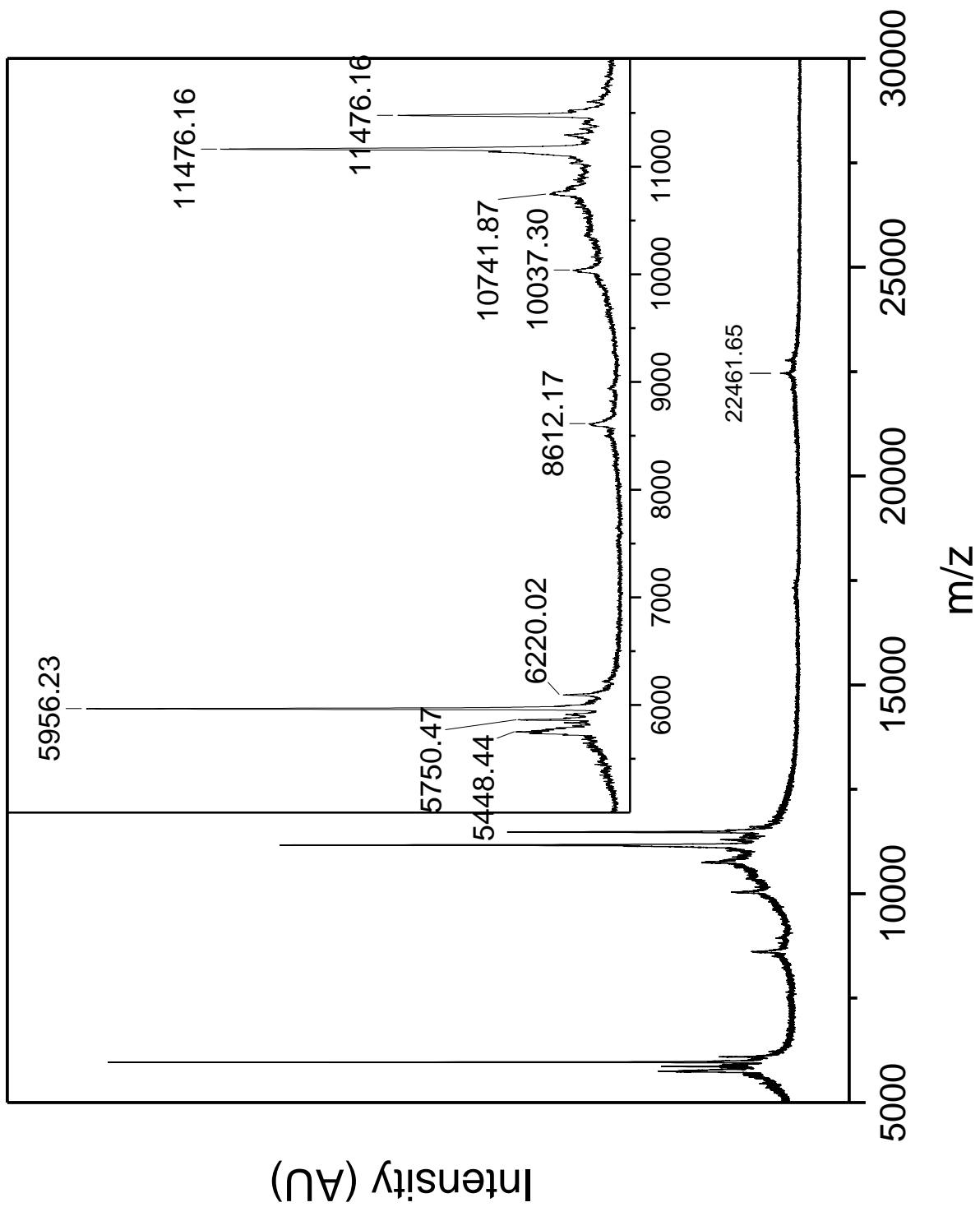


Figure S 25: MALDI-TOF mass spectrum of the products of heat treatment (DMPU, 2 h at 120 °C) of PG5₅₀₀^{NH^{Boc}}.

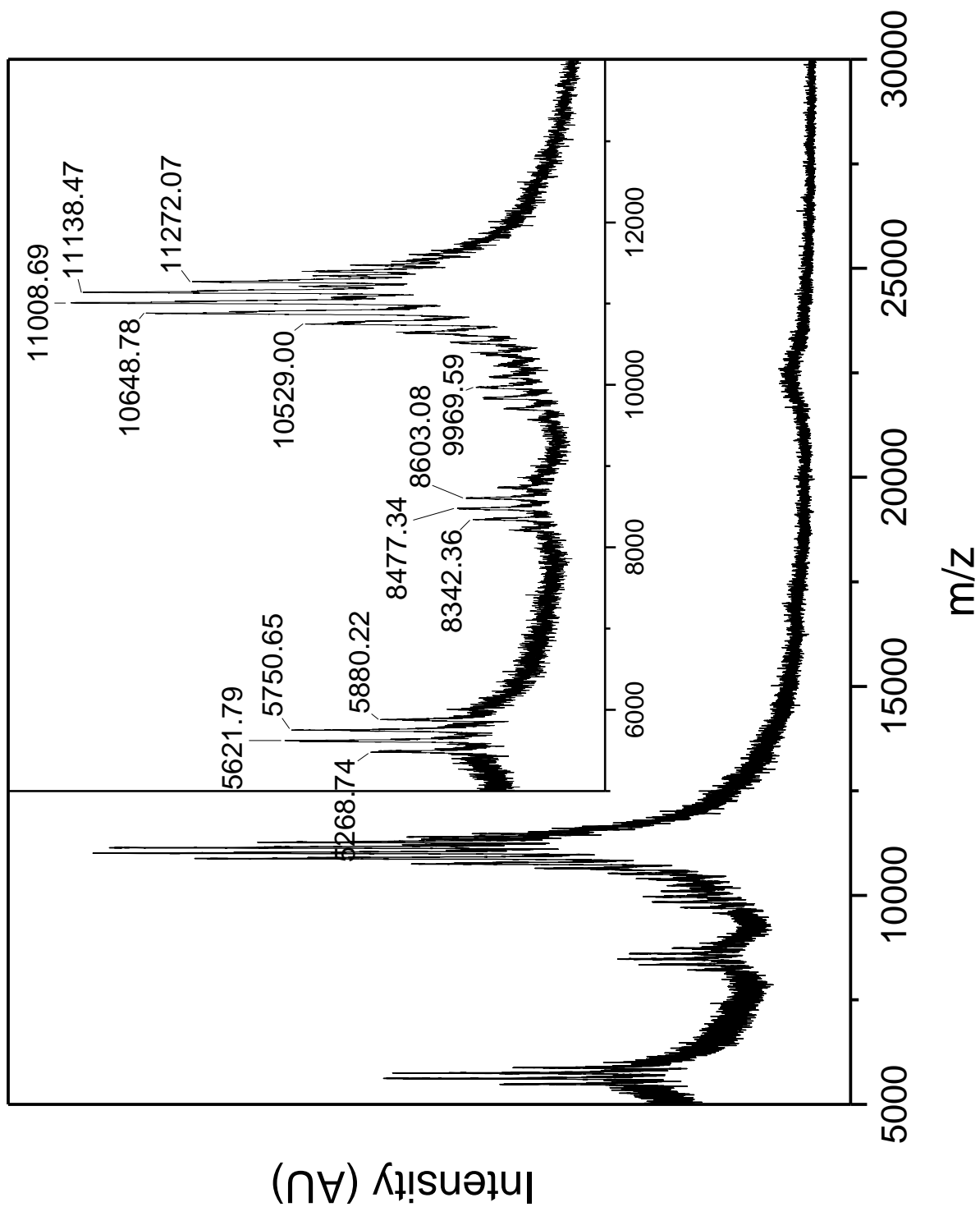


Figure S 26: MALDI-TOF mass spectrum of the products of heat treatment (DMPU, 2 h at 120 °C) of PG5^{NHAlloc}₅₀₀.

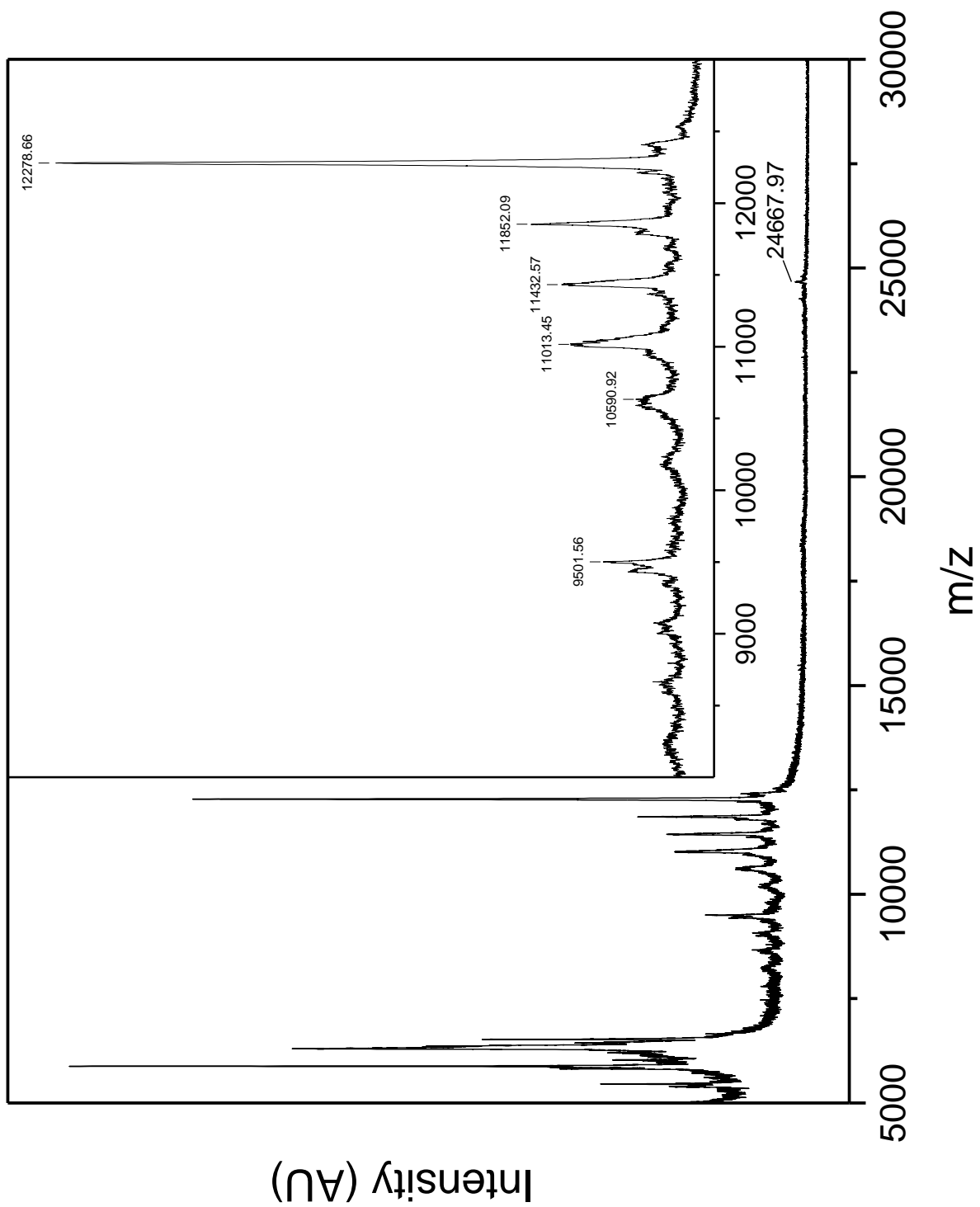


Figure S 27: MALDI-TOF mass spectrum of the products of heat treatment (DMPU, 2 h at 120 °C) of $PG5_{500}^{NH^{C}bz}$.

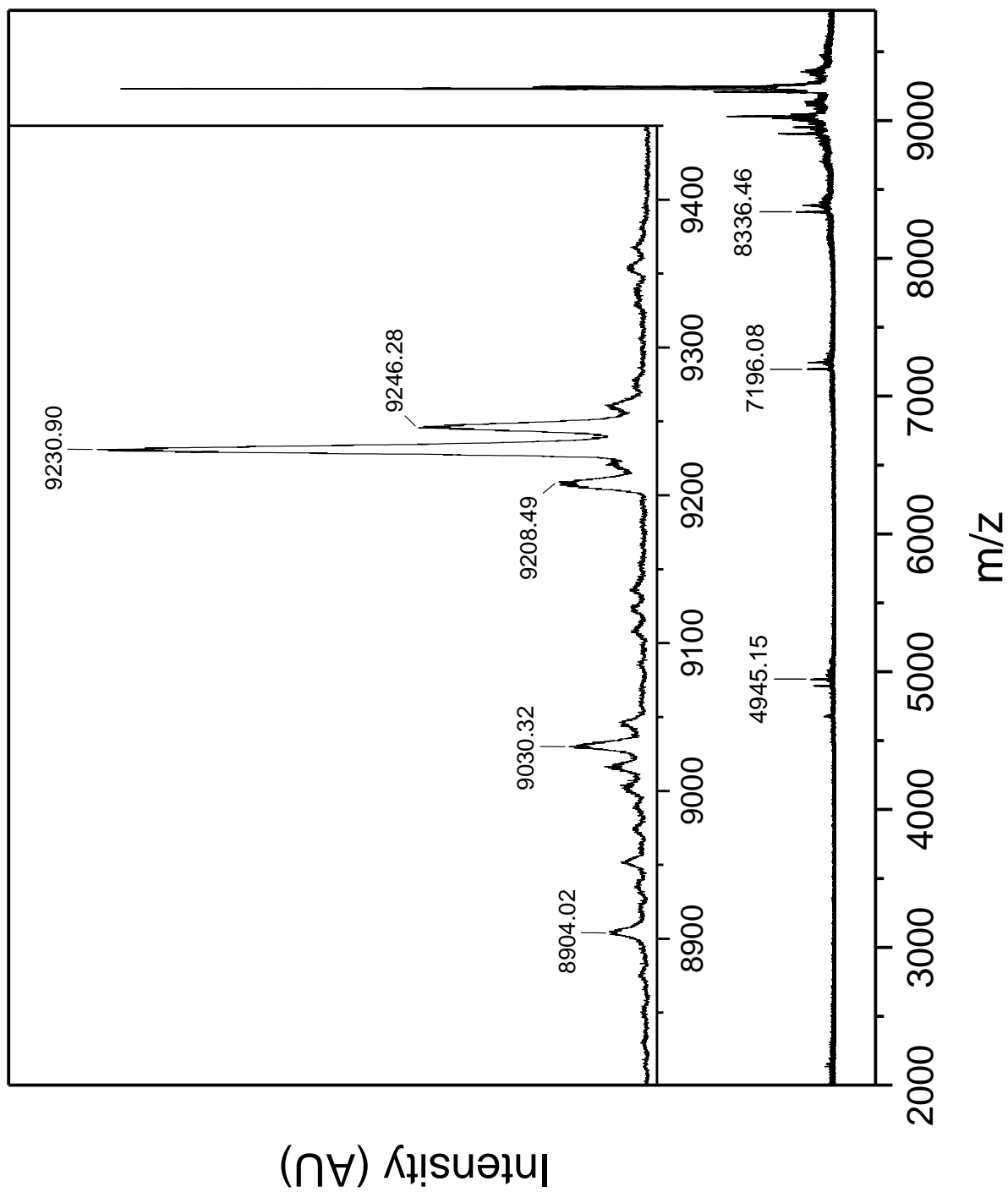


Figure S 28: MALDI-TOF mass spectrum of the products of heat treatment (DMPU, 2 h at 120 °C) of $PG5_{500}^{CO_2Me}$.

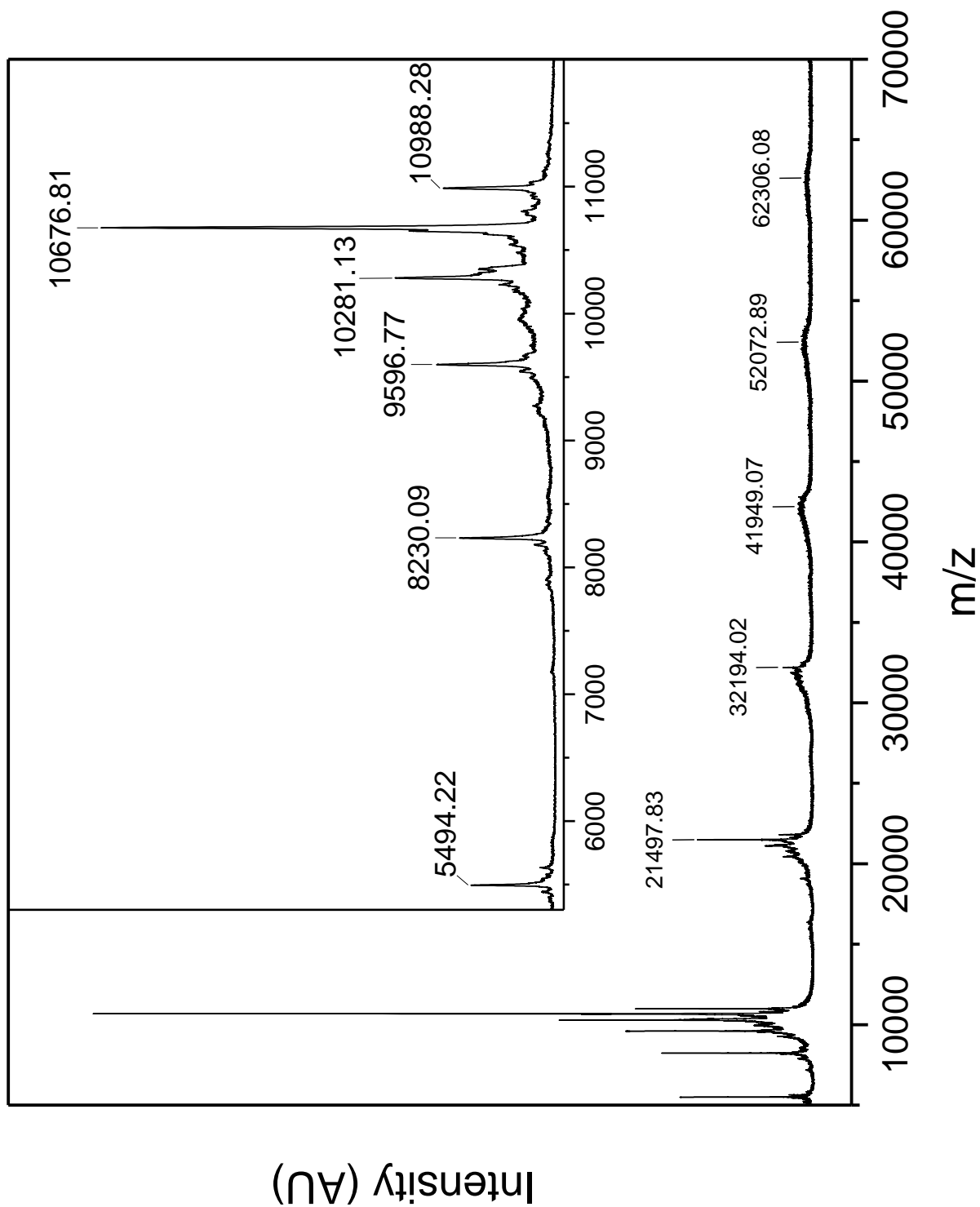


Figure S 29: MALDI-TOF mass spectrum of the products of heat treatment (DMPU, 2 h at 120 °C) of PG5₅₀₀^{CO₂tBu}.

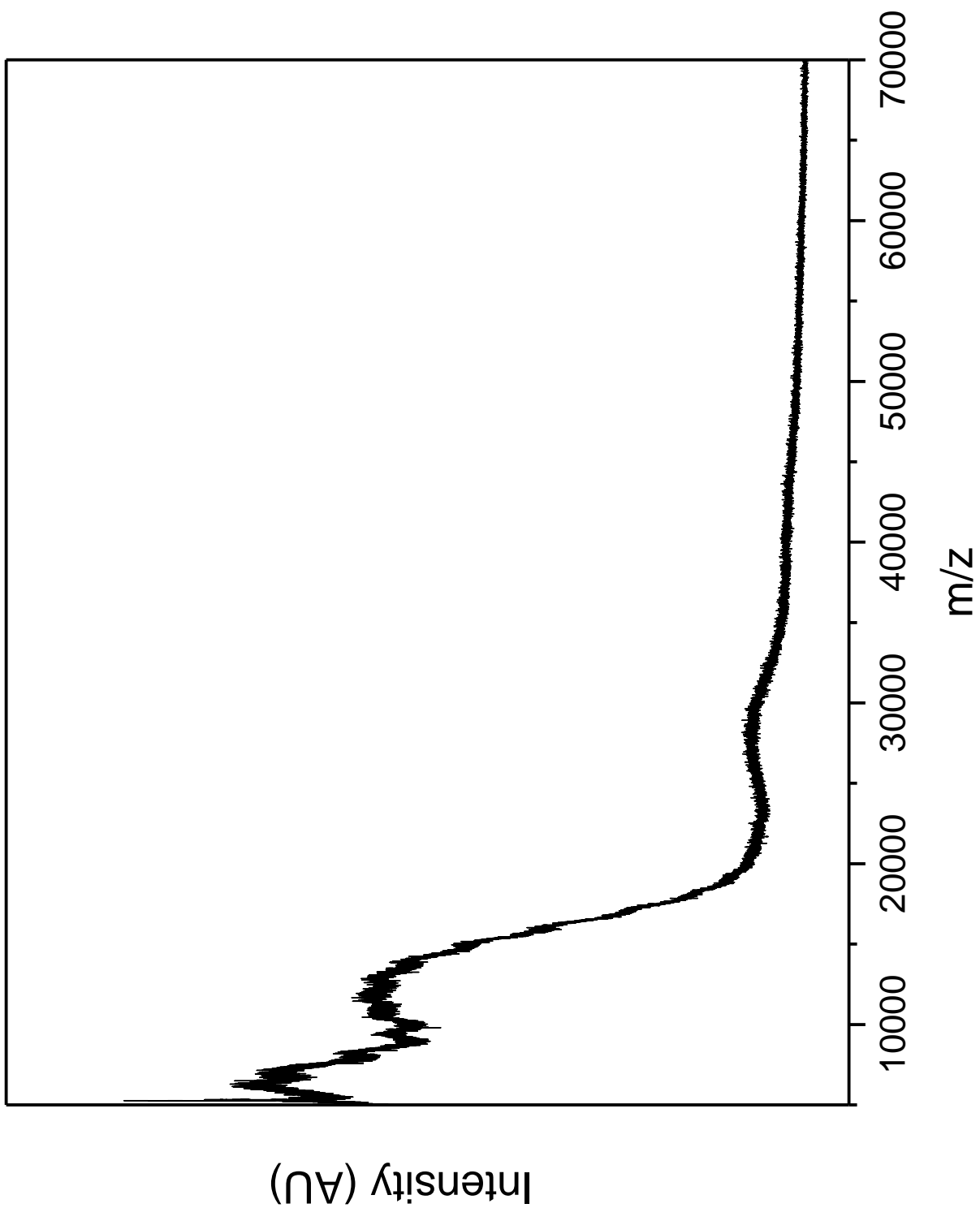


Figure S 30: MALDI-TOF mass spectrum of the products of heat treatment (DMPU, 2 h at 120 °C) of PG6^{NH₂Boc}₅₀₀.

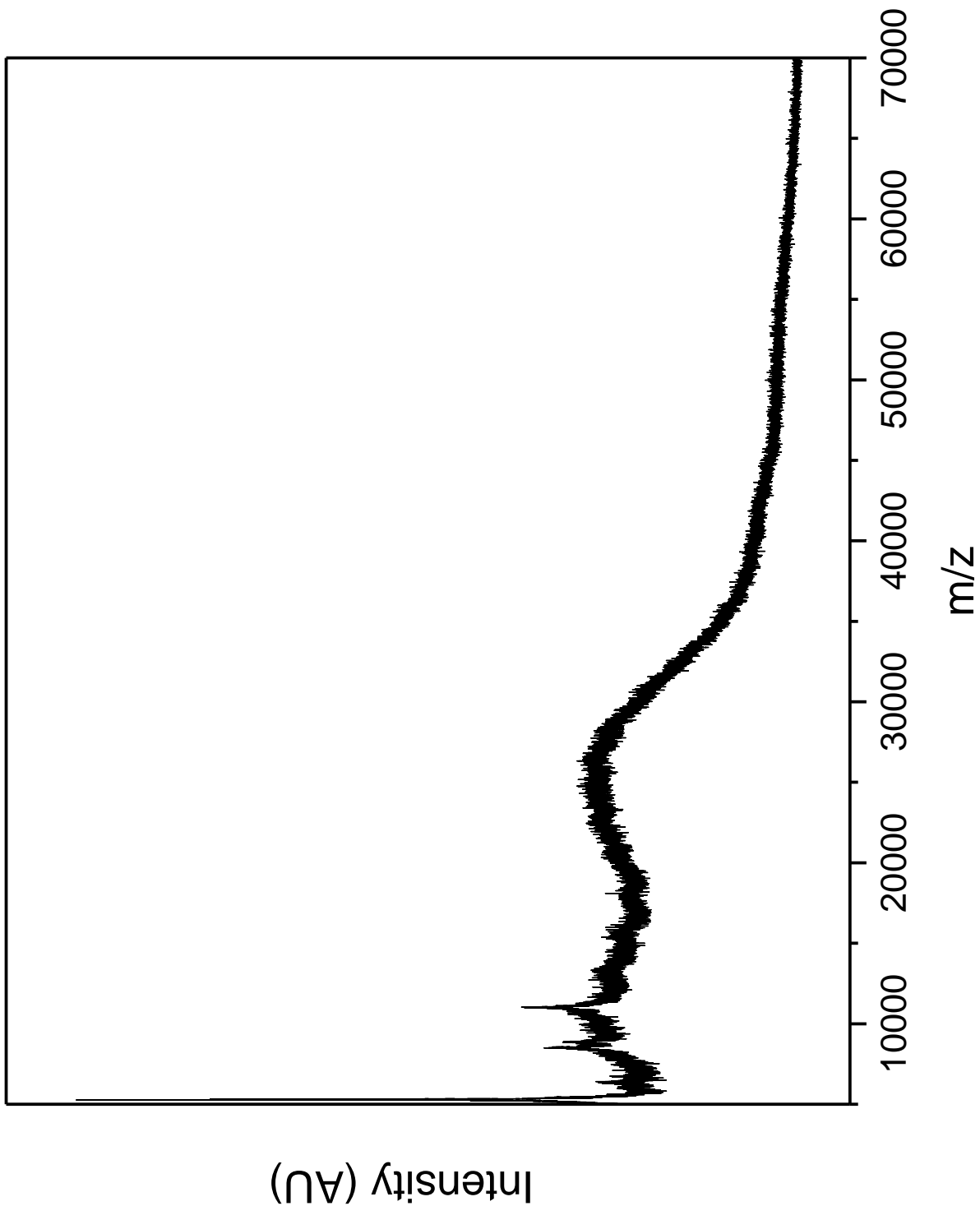


Figure S 31: MALDI-TOF mass spectrum of the products of heat treatment (DMPU, 2 h at 120 °C) of PG7₅₀₀^{NH^{Boc}}.

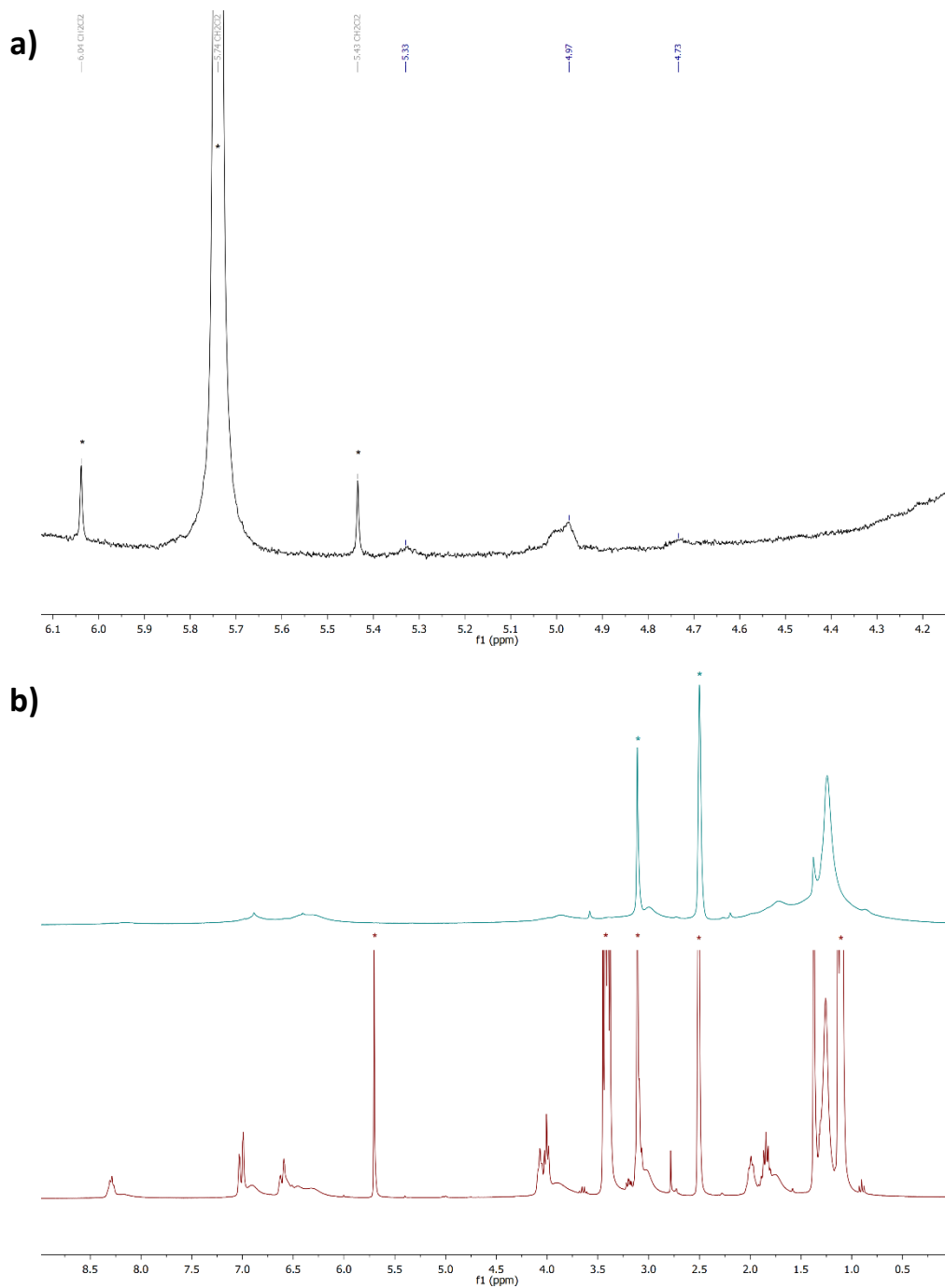


Figure S 32: a) Olefinic region of the $^1\text{H-NMR}$ spectrum of $\text{PG5}_{500}^{\text{NHBOC}}$ scission products (DMPU, 80 °C, 1 h; 300 MHz, 310 K, DMSO-d_6 ; b) comparison between the $^1\text{H-NMR}$ spectra of $\text{PG5}_{500}^{\text{NHBOC}}$ (top, 300 MHz, 343 K, DMSO-d_6 , top) and scission products (bottom); solvent peaks (CH_2Cl_2 , Et_2O , DMSO , H_2O) are marked with asterisks.

4.9 Prolonged heating of $g \neq 5$ DPs

While prolonged heating did not substantially affect the outcome of scission experiments with $g = 5$ DPs at a given set of conditions (see main text, Fig. 5c), this may change for $g \neq 5$ DPs, for which much harsher conditions (better solvents and/or higher temperatures) are required to induce any degradation, and where hence scission might be slower than for the $g = 5$ homologs. In order to probe the influence of prolonged heating, DPs of $g = 3, 4, 6, 7$ (low structural perfection where applicable) were subjected to harsh degradation conditions (DMPU, 120 °C) for up to 72 h. The products were investigated by GPC as shown in Figure S 33.

For the two $g < 5$ DPs (Figure S 33a,b), only small changes – shifts of the main polymeric peaks to slightly higher RV and slight increases of the relative concentration of the small-molecules scission products identified as the corresponding macromonomers (see subsection 4.8) – were observed. For the $g > 5$ DPs on the other hand, substantial shifts of polymer peak RV were observed, and indeed for both DPs degradation overall was more severe than it was after 2 h under otherwise identical conditions (see Figure S 21a). For $\text{PG6}_{500}^{\text{NHBOc}}$ (Figure S 33c), both the oligomeric fraction peak RV and the relative concentration of the small molecule fraction appear to *decrease* with increased reaction time. This and the accompanying discoloration of the reaction mixture indicate that under the applied conditions (no special precautions to eliminate oxygen or moisture), additional side reactions take place. This may also apply to the degradation of $\text{PG7}_{500}^{\text{NHBOc}}$ (Figure S 33d), where the relative concentration of small-molecule products decreases after 24 h, though overall the polymer degradation is far less severe than it is for $\text{PG6}_{500}^{\text{NHBOc}}$.

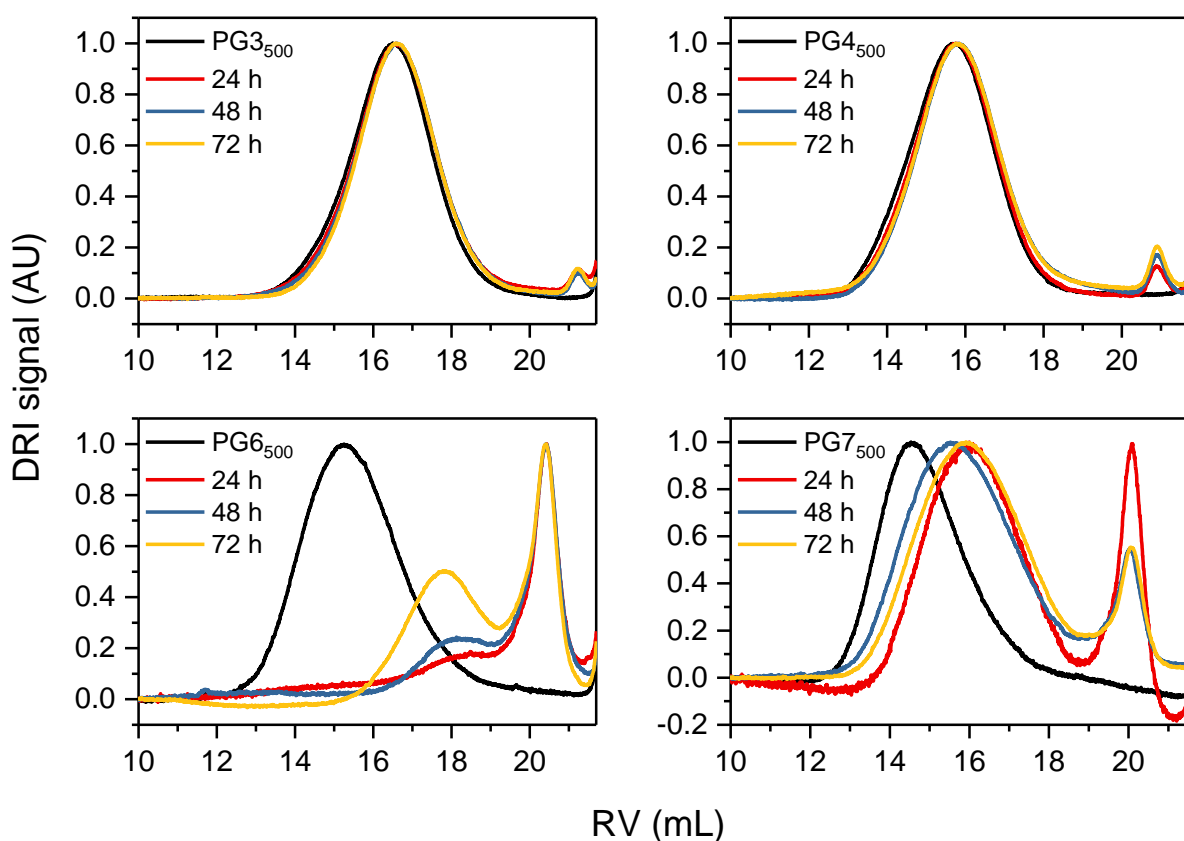


Figure S 33: Prolonged “hot solvent” treatment of $g \neq 5$ DPs. The starting materials (1 % w/V of a) $\text{PG3}_{500}^{\text{NHBOc}}$; b) $\text{PG4}_{500}^{\text{NHBOc}}$; c) $\text{PG6}_{500}^{\text{NHBOc}}$ of low structural perfection; d) $\text{PG7}_{500}^{\text{NHBOc}}$ of low structural perfection) were dissolved in DMPU and then kept at 120 °C. Samples were removed for analysis by GPC after 24 h, 48 h, and 72 h.

5. Molecular dynamics simulation

5.1 Methods

The conformation previously reported¹⁵ for a PG5^{NHBoc} polymer chain with $N = 100$ repeat units, PG5₁₀₀^{NHBoc}, in vacuum was used as starting point for this study. The desolvated environment of this model, which involved 160902 explicit atoms, led us to start simulations in a completely un-swelled state. For the NVT-MD simulation in DMPU solution the DP chain was placed in the center of an orthorhombic simulation box of $296 \times 196 \times 153 \text{ \AA}^3$ filled with explicit solvent molecules (procedure described below). DMPU was represented by using an all-atom model.

The energy was calculated using the AMBER force-field,¹⁶ all the bonding and van der Waals parameters required for the DPs under study being taken from our previous studies, which successfully modelled the structure and properties of PG1-PG6.^{15,17–20} All the bonding and van der Waals parameters required for DMPU molecules were taken from Generalized AMBER force-field (GAFF).²¹ Atomic charges were adjusted using the Restrained Electrostatic Potential (RESP) strategy.²² The resulting electrostatic parameters are displayed in Figure S 34.

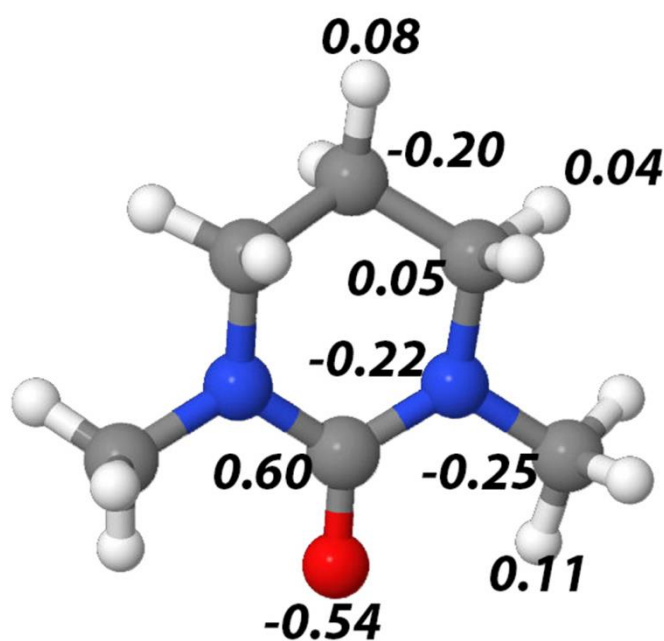


Figure S 34: Atomic charges of DMPU.

Initially, the orthorhombic simulation box was filled with DMPU solvent molecules. After 100 ns of NPT-MD at 298 K, the density was 1.04 g cm^{-3} , which is in excellent agreement with the experimental density (1.06 g cm^{-3}). After this, the PG5₁₀₀^{NHBoc} chain was placed in the middle of the equilibrated solvent box upon eliminating those solvent molecules which exhibit overlap with the DP. A total of 35319 solvent molecules remained in the box (741699 explicit solvent atoms) and, therefore, the whole simulated system contained 902601 explicit atoms. Then, the solvent alone was thermally relaxed by three consecutive runs while the DP was kept frozen: 10 ns of NVT-MD at 500 K was used to re-distribute the solvent in the box. Second, 7.5 ns of isothermal relaxation at 298 K was run. Finally,

the DP was set free and all atoms of the system were submitted to 25 ns of NVT-MD at 298 K (thermal equilibration). The temperature was controlled by a weak coupling method, the Berendsen thermostat²³ with a time constant for heat-bath coupling of 1 ps. The end of the thermal relaxation simulation was taken as the starting point of the production trajectory (80 ns) at 298 K, which was run in duplicate.

Atom-pair distance cut-offs were applied at 12 Å to compute van der Waals and electrostatic interactions. Bond lengths involving hydrogen atoms were constrained using the SHAKE algorithm with a numerical integration step of 2 fs.²⁴

5.2 Additional results

As visible in Fig. 9a, the productive simulation results not only in an elongation of the DP backbone, but also in a significant overall contraction of the DP branchwork. This is evident from both the development of the average radius of the DP which was determined considering that the radial probability distribution profile is proportional to the radial density.¹⁷ Thus, the radius decreases from 51.6 Å to 46.8 Å after a productive trajectory of 80 ns, which corresponds to a narrowing of ~9% (Figure S 35).

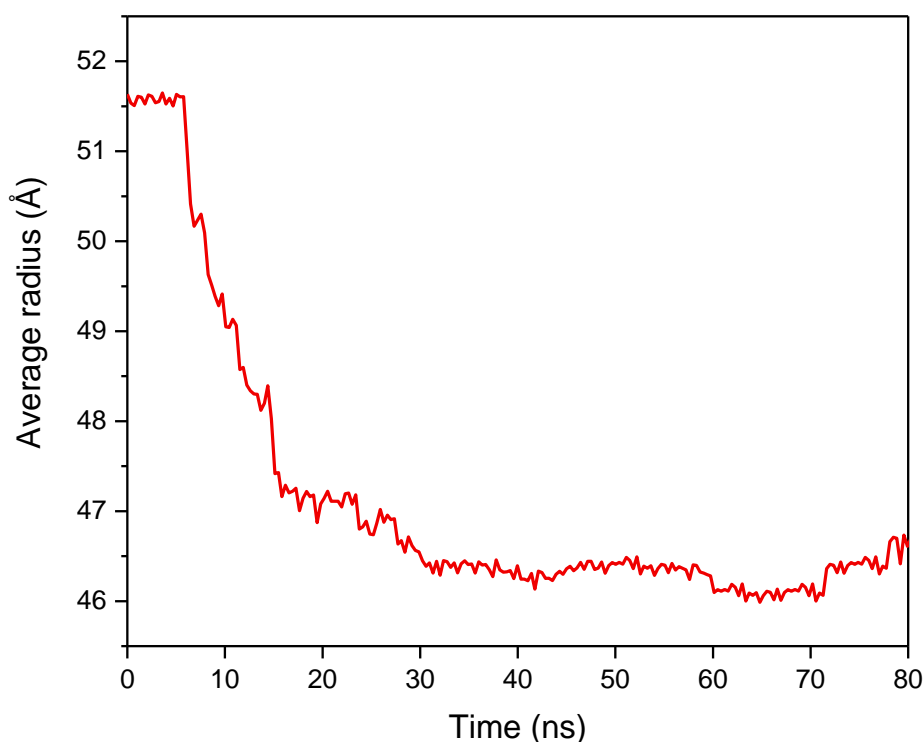


Figure S 35: Evolution of the average radius over the course of simulation.

Radial density profiles calculated for the DP and the solvent are compared in Figure S 36. They allow to explain the elongation of the polymer backbone and the reduction of the DP radius: At the beginning of the MD production run, the density of the polymer backbone, $\sim 0.8 \text{ g cm}^{-3}$, drops to $\sim 0.3 \text{ g/cm}^3$ at neighboring regions, evidencing the presence of a very porous region surrounding the backbone (Figure S 36a).¹⁵ Further out, the density increases to $\sim 1.1 \text{ g cm}^{-3}$ and remains constant until the progressive decreasing associated with the external layer of the DP cylinder starts at $r \approx 40 \text{ Å}$.

Initially, the DMPU density (Figure S 36b) shows a peak with $\sim 0.4 \text{ g cm}^{-3}$ in the region close to the backbone that rapidly drops to $\sim 0.1 \text{ g cm}^{-3}$, indicating that a few solvent molecules penetrated into the porous region of the DP during the equilibration run previous to the production trajectory. Throughout the DP branchwork the density of DMPU is null until $r \approx 40 \text{ \AA}$, reflecting that the solvent does not penetrate into the dense intermediate and external layer of the DP.

After 80 ns of productive run, the shapes of the two profiles are changed significantly: The porous region close to the DP backbone becomes much denser and the drop at the external layer starts at $r \approx 32 \text{ \AA}$, indicating that the whole DP becomes more compact. The DMPU density as a function of the radial distance from the backbone follows the opposite trends: DMPU molecules enter inside the DP, not only at the periphery but also at the region close to the backbone. After 80 ns the DMPU density is higher than 0.1 g cm^{-3} at around $r = 35 \text{ \AA}$, which represents a shortening of $\sim 7 \text{ \AA}$ with respect to the starting structure. This significant peripheral swelling compensates for the reduction of the DP radius and explains the elongation of the backbone. Besides, the entrance of solvent molecules at the region close to the backbone is expected to induce strain phenomena at the main chain, which could allow to understand the experimentally observed main chain scission. The swelling at both the region close to the backbone and the periphery is illustrated in Figure 8b (main text), which displays the position of the DMPU molecules in the cross section of the $\text{PGg}_{100}^{\text{NHBoc}}$ model.

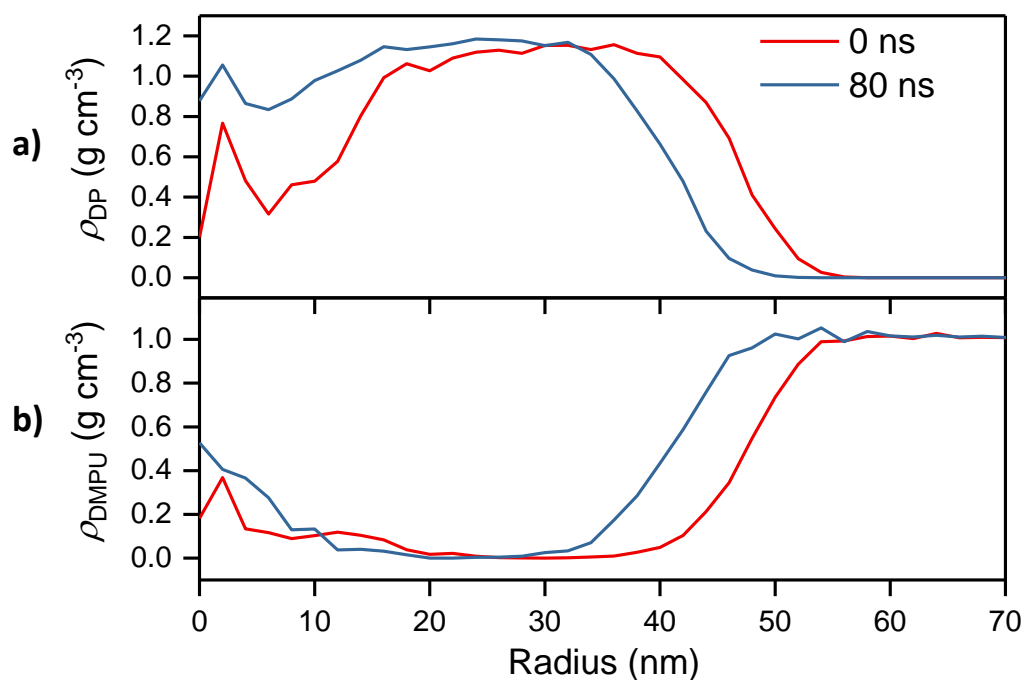


Figure S 36: Densities of a) the DP branchwork and b) DMPU at the beginning and end of the productive MS simulation.

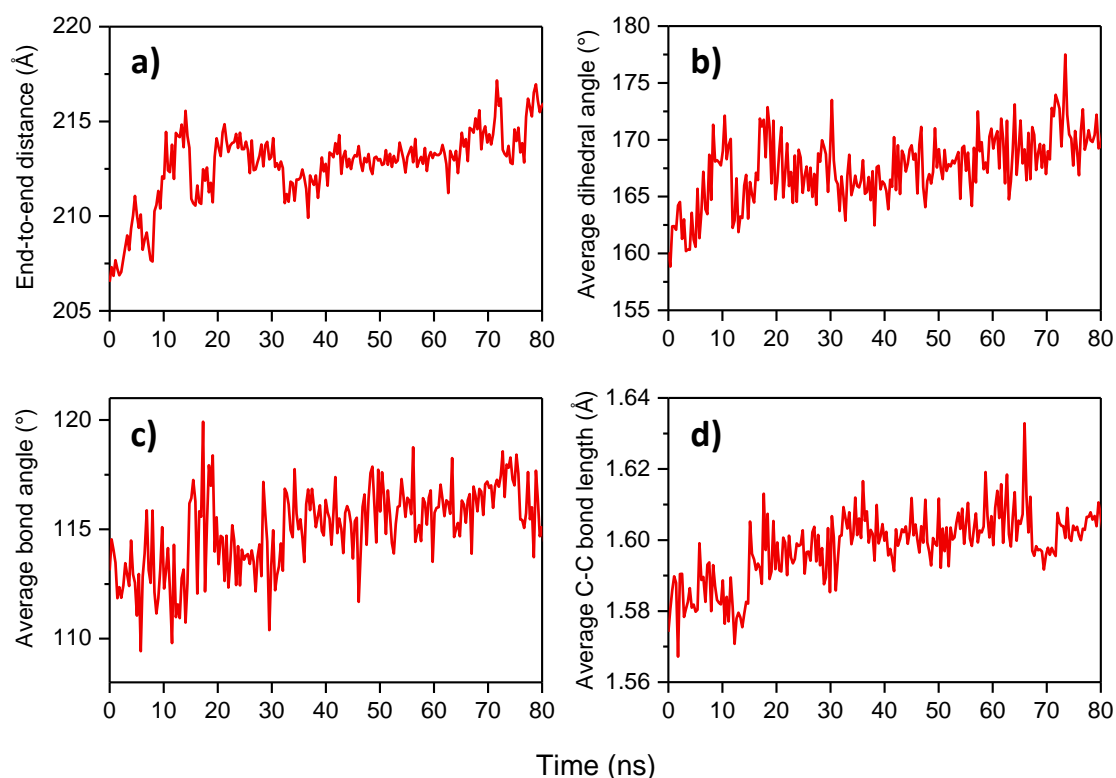


Figure S 37: Evolution of DP backbone parameters during the productive MD run: a) end-to-end distance; b) average backbone dihedral angle; c) average backbone bond angle; d) average backbone bond length (all averages over the entire chain; compare Fig. 8c)

To estimate the forces acting on backbone bonds as a consequence of swelling, the force constant parameter and stretching force-field expression extracted from the GAFF force-field were applied to all backbone bonds of length r and values were averaged according to the probabilities given by the distribution function $g(r)$ during the last 15 ns of the simulation run (Figure S 38a). Interestingly, only few bonds experience substantial tension, apparently in two regimes, evident as overlapping peaks at $2.7 \text{ nN} \pm 0.3 \text{ nN}$ and $2.9 \text{ nN} \pm 0.2 \text{ nN}$. Meanwhile, the majority of backbone bonds experience little or no strain ($F \approx 0 \text{ nN}$, $r \approx 1.54 \text{ \AA}$). As the force profile along the backbone of a representative snapshot shown in Figure S 38b shows, the forces are concentrated in the middle of the short simulated DP segment.

These results suggest that scission – as is the case *e.g.* in sonochemically induced polymer degradation^{25–27} – occurs in a chain-centered fashion, *i.e.* within a narrow distance of the middle of the polymer chain. However, it is uncertain whether this would hold for much longer chains, where multiple loci along one chain might experience sufficient tension, or where there might be a broad plateau of force distribution wherever geometry is locally cylindrical, *i.e.* past the chain ends. The kinetics of swelling and bond scission events are also relevant in this discussion, but they are currently still unexplored.

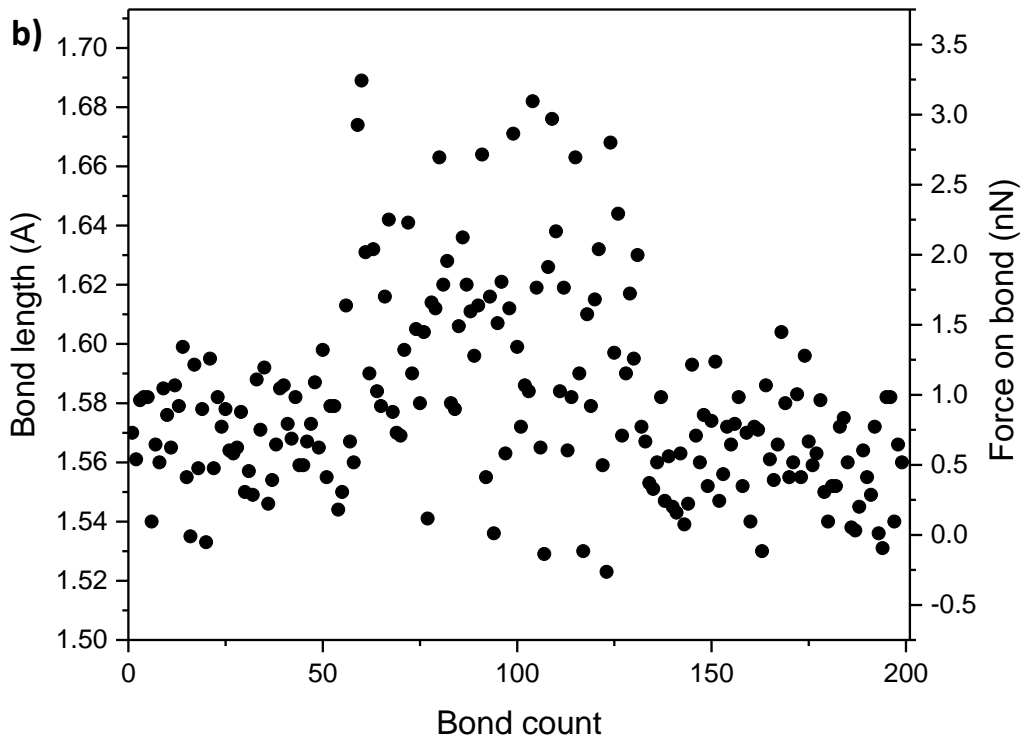
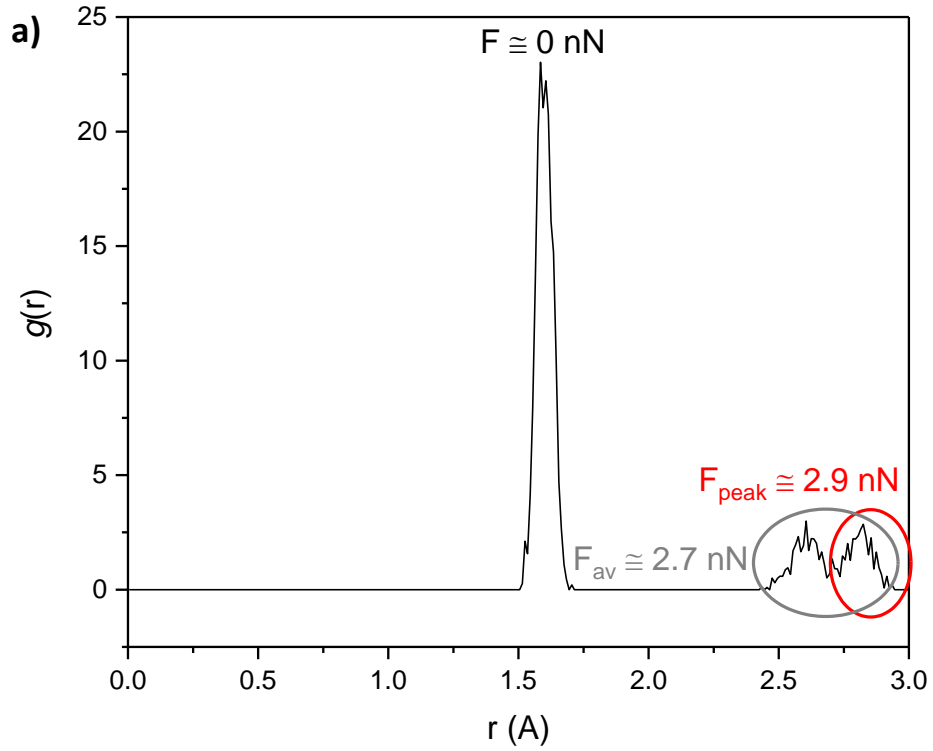


Figure S 38: a) Probability distribution of bond lengths averaged during the last 15 ns (65 ns – 80 ns) of the simulation trajectory, with the force regimes corresponding to the three peaks marked; b) bond lengths/tension forces of a representative snapshot.

6. EPR spectroscopy

For the initial experiment shown in Figure S 39a, PG5₅₀₀^{NHBoc} (ca. 10 mg) was added to a quartz EPR tube which was flushed briefly with dry nitrogen. DMPU (0.5 mL, purged with nitrogen) was added. The contents were shaken briefly, then inserted into the pre-heated thermostat in the EPR spectrometer. The sample was maintained at 353 K for 5 min, then quenched by plunging into liquid nitrogen. The thermostat was cooled to 200 K, then the sample was inserted and left to equilibrate before measurement. Further cycles of heating/cooling were performed to discern whether radicals accumulate, but no significant changes were found, indicating that the present low concentration of radicals with a Landé g -factor of $g_j \approx 2.01$ (Figure S 39a) was transient. After ca. 20 min of total time spent at 80 °C, the sample was cooled to RT and the solution was diluted to ca. 1 mg mL⁻¹ in preparation for GPC (DMF, containing 1 mL L⁻¹ toluene and 1 g L⁻¹ LiBr; Figure 9c, main text).

For radical trapping with DMPO, the sample and all precursor solutions were prepared in a nitrogen-filled glove box (< 4 ppm O₂): DMPO (352 mg; ABCR, 97 %) was dissolved in dry DMPU (ca. 2 mL, degassed thoroughly in the). A sample of this solution was added to an EPR tube and the DMPO solution (ca 1 mL) was added to PG5₅₀₀^{NHBoc} (ca. 50 mg). The resulting mixture was shaken and added to another EPR tube. The two sample tubes were tightly stoppered and wrapped in parafilm before exiting the glove box. The reference solution containing only DMPO was heated to 353 K for 5 min using the thermostat of the EPR spectrometer and then measured after vitrification by cooling to 200 K directly in the spectrometer. The sample solution containing PG5₅₀₀^{NHBoc} as well as the radical trap was treated similarly, however with two additional periods of heating to 80 °C as indicated in Figure S 39b; rather than showing further accumulation of trapped radicals, the EPR spectra recorded after prolonged heating show a lower radical concentration. In agreement with other results, this indicates that main-chain scission occurs on a time scale of a few minutes, as apparently the rate of radical formation drops below that of adduct decomposition for longer heating times. A kinetic analysis of such data is however not possible without very significant effort: The thermal stability of DMPO itself is unknown, as is the stability of the radical adducts. Furthermore, the likely present multiple species are not spectroscopically distinguishable, as the solid state spectra show strong line broadening. Additionally, the decrease in intensity after further heating in Figure S 39b is not even across the entire spectrum, suggesting that some of the multiple adducts present are less stable than others. After EPR measurement, the sample was cooled to RT and precipitated into Et₂O/hexane (1:1). The solid obtained was reprecipitated from little DCM, then dried in vacuum to afford a glassy solid which was subjected to GPC (Figure 8d, main text) and MALDI-TOF-MS (Figure S 40). Neither method showed evidence of macromonomer, further supporting the proposed homolytic mechanism.

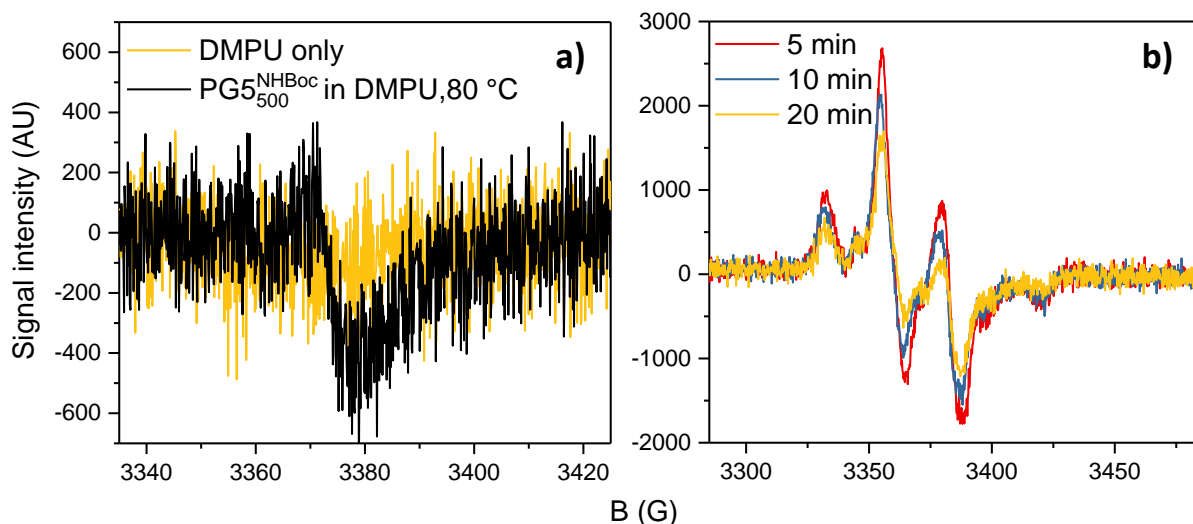


Figure S 39: a) Preliminary EPR experiment in absence of radical quencher (ca. 5 % in DMPU, heated to 80 °C for 5 min; spectrum measured at X-band, 200 K, 20 accumulated scans). The Landé g-factor of the weak signal is $g_j \approx 2.01$ b) Stability of quenched radicals: $PG5_{500}^{NHBOc}$ and DMPO heated in DMPU to 80 °C for the indicated total time before cooling to conduct solid-state CW-EPR measurements (X-band, 200 K, single scan).

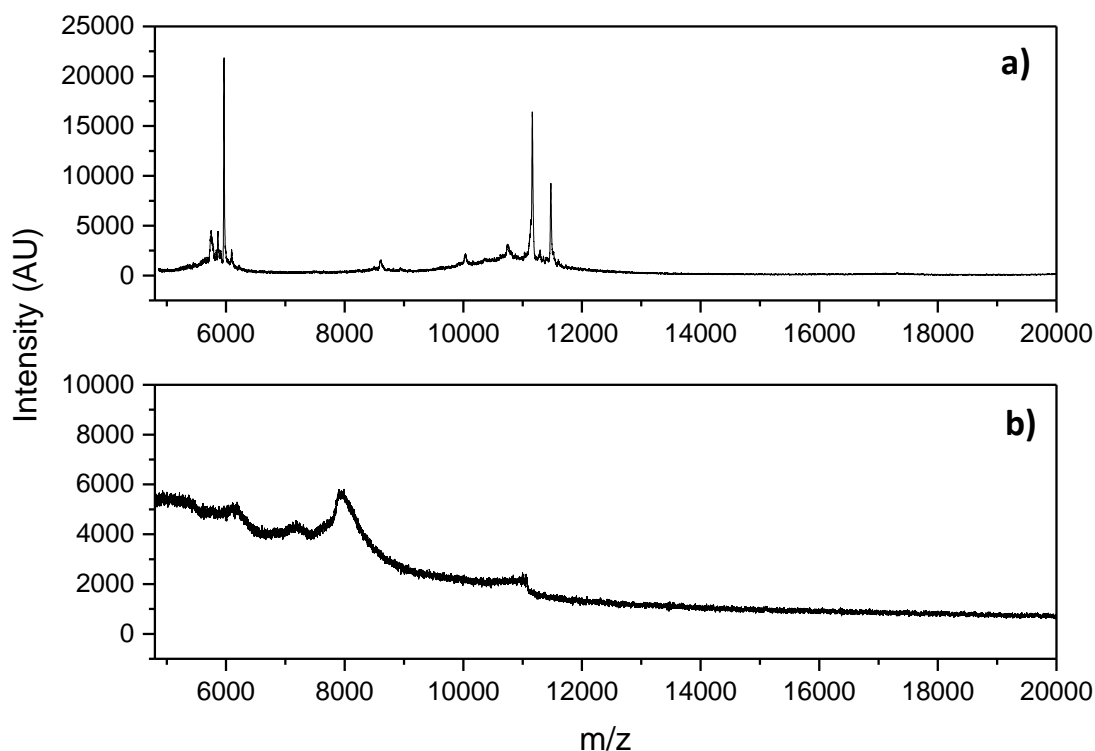


Figure S 40: Comparison of MALDI-TOF mass spectra of $PG5_{500}^{NHBOc}$ heated to 80 °C in DMPU a) without scavenger (see Figure S 25) and b) in presence of DMPO.

The EPR signal in Figure 9b (main text) was simulated by a manual deconvolution approach. To that end, the signal was first integrated and baseline-corrected (Figure S 41a). The spectrum was then simulated by Gaussian curves, assuming $A_H \approx A_N$, *i.e.* a simple quartet of peaks (Figure S 41b).

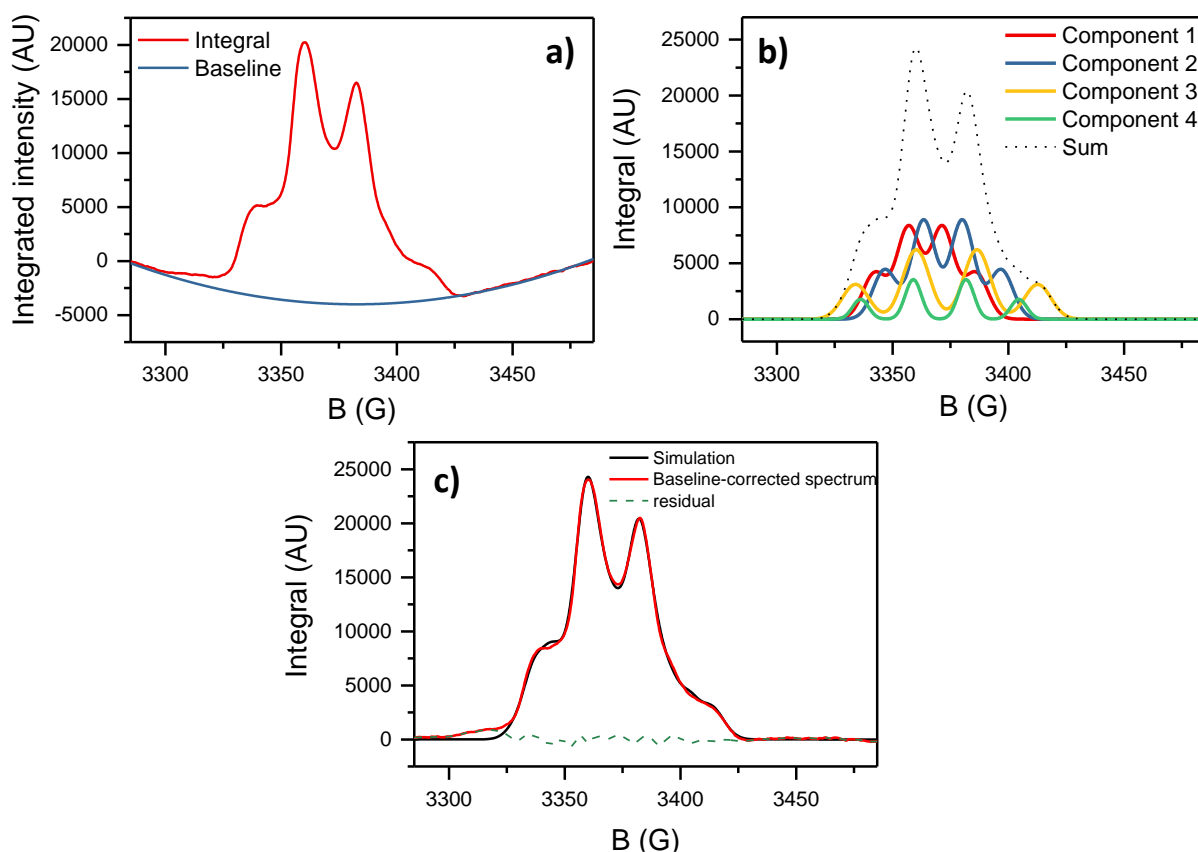


Figure S 41: a) Baseline correction of the integrated, background-corrected EPR signal; b) deconvolution of the integral into four Gauss-broadened quadruplets (see Table S 4); c) overlay of the corrected integrated spectrum with the simulated spectrum; the residual is indicated by the green dashed line.

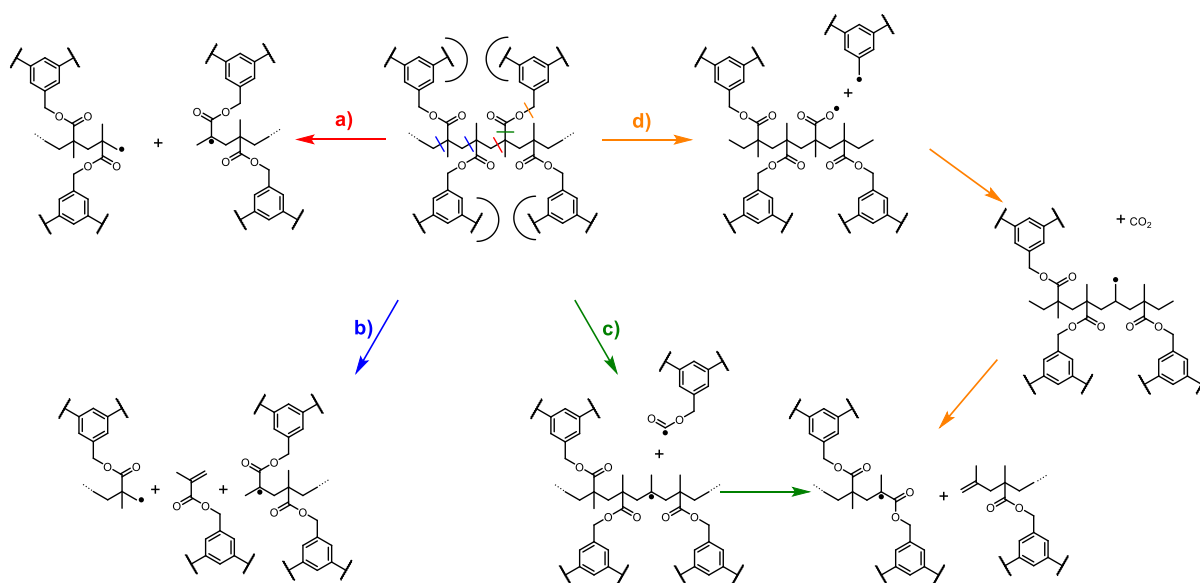
Table S 4: Parameters for the deconvolution components shown in Figure S 41b; ^{a)} It is assumed here that $A_N \approx A_H = A$, resulting in a symmetric 1:2:2:1 line split centered around B_{center} ; ^{b)} k is a dimensionless line broadening parameter for the Gaussian curve of the form $I(B) = I_0 e^{-\frac{k}{2}(B-B_0)^2}$.

	B_{center} (G)	A (G) ^{a)}	k ^{b)}	Peak intensity I_0 (AU)
Component 1	3364.2	14.6	0.0191	8174.3
Component 2	3371.8	16.7	0.019	8839.3
Component 3	3373.3	26.2	0.0151	6212.5
Component 4	3370.3	22.8	0.0411	3540.9

7. Discussion of possible backbone scission mechanisms

From the results obtained by EPR spectroscopy (Fig. 9 in the main text), it is clear that a homolytic reaction of some sort is the main pathway of DP degradation. This is then followed by the generation of macromonomer, *i.e.* likely some depropagation of active radical chain ends.

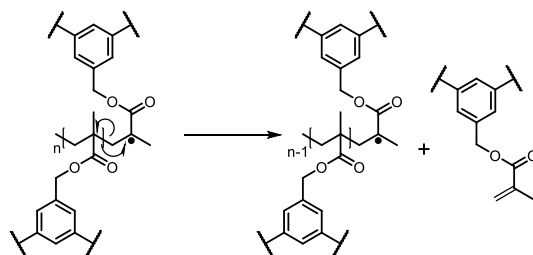
The precise mechanism of the initial backbone scission remains elusive and can only be speculated on, as the structures of the radical species generated in DP main-chain scission remain unclear. This is further complicated by the lack of good reference investigations: Even for simple structures such as PMMA, precise scission mechanisms have been the matter of some debate. For the thermal decomposition of this simple plastic, a number of mechanistic pathways has been suggested, analogies to which are shown in Scheme S 5. These include the simple, direct homolysis of a backbone C-C bond (Scheme S 5a),²⁸ an initial quasi-concerted fragmentation of the backbone directly affording one unit of macromonomer as shown in Scheme S 5b,²⁹ or side-chain homolysis (Scheme S 5c,d).³⁰



Scheme S 5: Some potential radical pathways for initial backbone scission: a) “standard” homolytic pathway;²⁸ b) alternative initiation model obtained from reactive MD simulations;²⁹ c), d) side-chain initiated scission processes.³⁰

The experimental evidence shown in Fig. 9 of the main text and in subsection 4.9 of the SI make it seem unlikely that degradation proceeds by a pathway involving a primary homolysis of a bond in the side chain, as shown in Scheme S 5c,d: First, there is no evidence of species derived *e.g.* from the dendritic tolyl radicals eventually produced in side-chain scission (though admittedly subsequent depolymerization may simply produce much larger quantities of macromonomer such as to mask the presence of such species in MALDI-TOF-MS). Second, and more strikingly, chain scission does proceed in the presence of the radical trapping agent DMPO, but produces only inconsequential amounts of small-molecule fragments as indicated by both GPC (Fig. 9c) and MALDI-TOF-MS (Figure S 40b). In the case of side chain-first homolysis, some small-molecule fraction would be expected, and more importantly scission would likely be quenched as DMPO reacts with backbone radicals. This suggests that, rather than side-chain scission or three-part fragmentation such as in Scheme S 5b (which would also produce a macromonomer fraction), the straightforward homolysis of a single C-C bond along the backbone is the likeliest mechanistic course. This notion is further supported by data from the sonochemical literature, in which sol

A second question is the origin of macromonomer likely expelled from radical chain ends: Tertiary radicals likely undergo straightforward depropagation (Scheme S 6), but the fate of primary radicals – which would also be generated *e.g.* in the process shown in Scheme S 5a – is less certain.^{31,32}



Scheme S 6: Depropagation mechanism of tertiary macroradicals formed in the initial scission process.

8. NMR Spectra

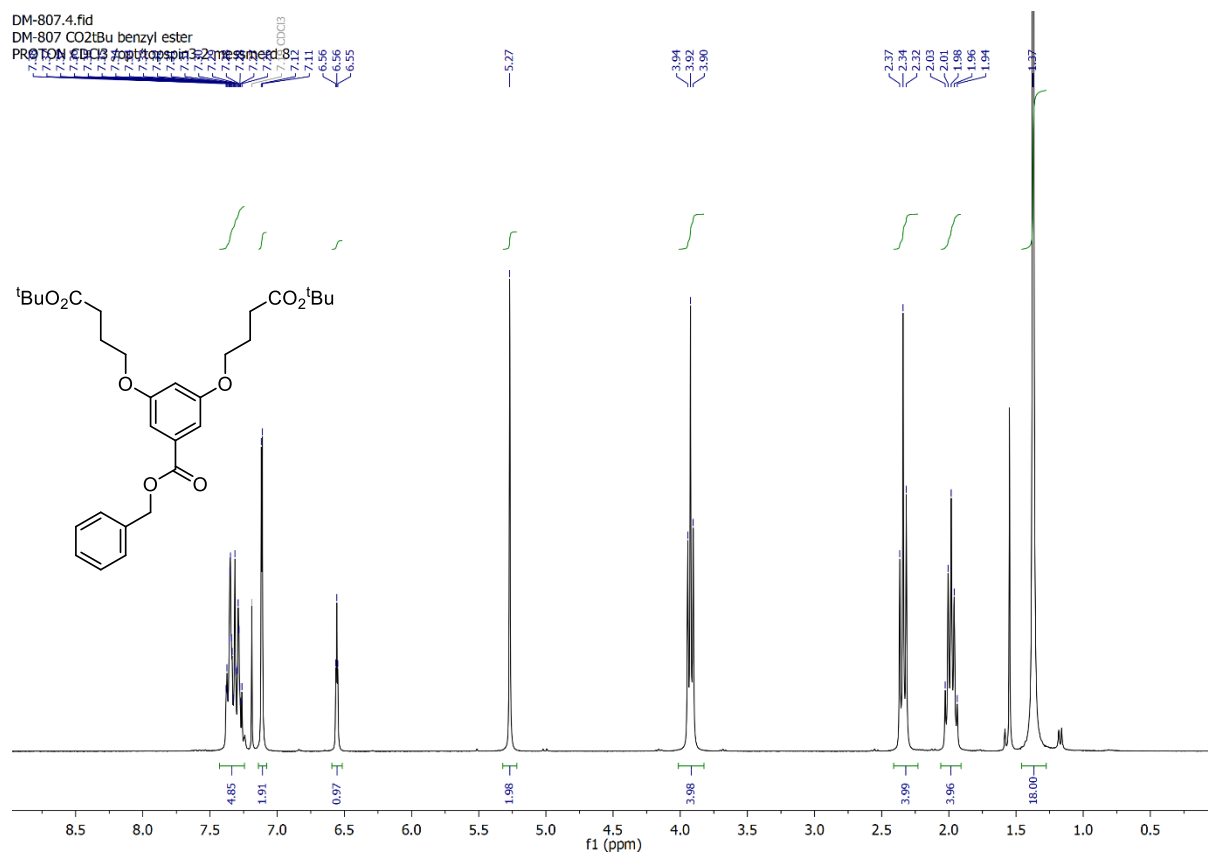
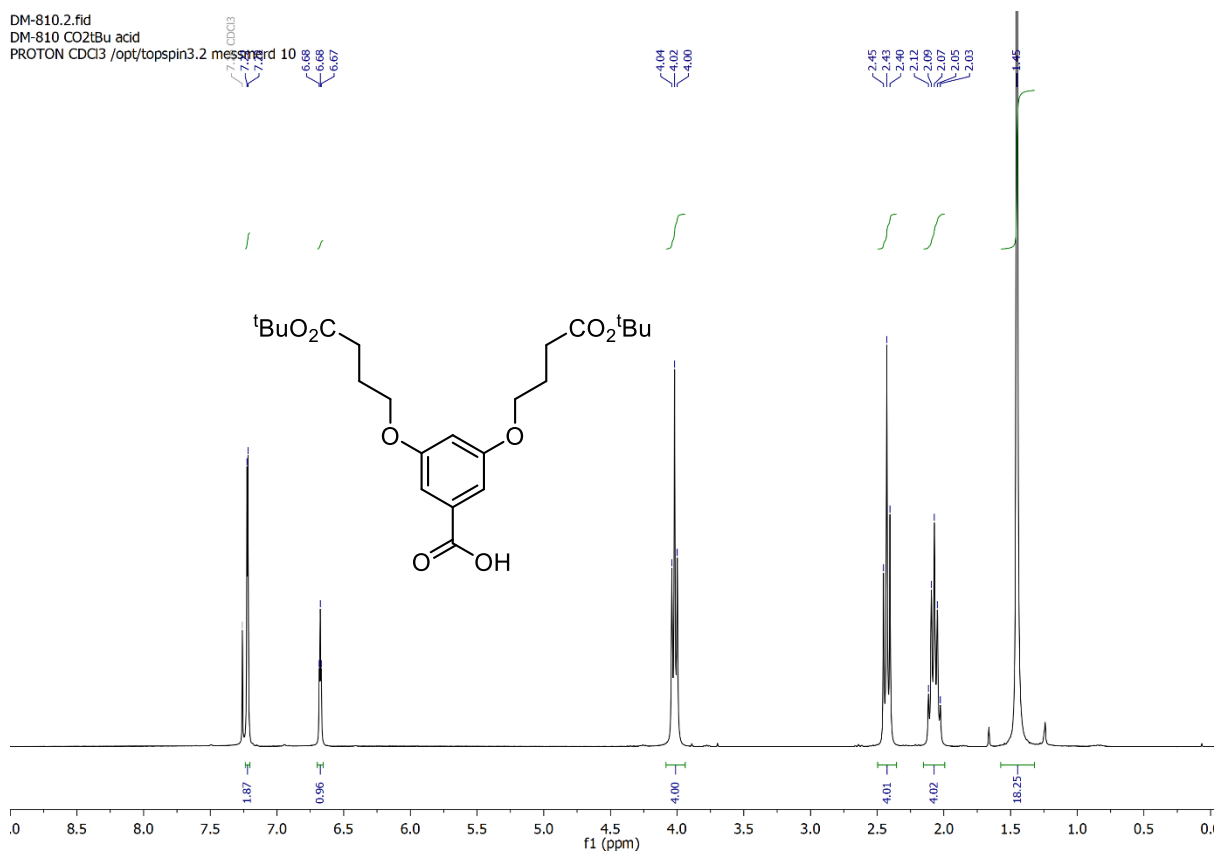
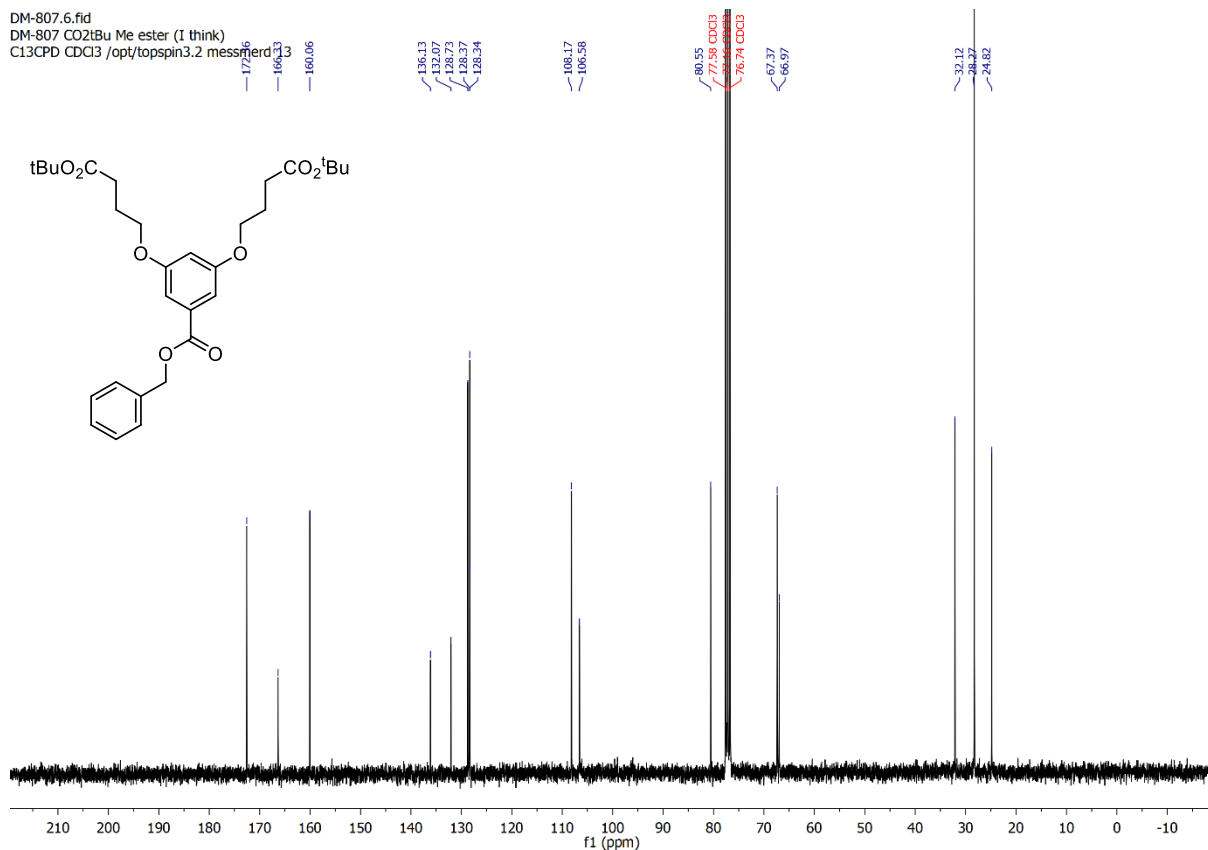
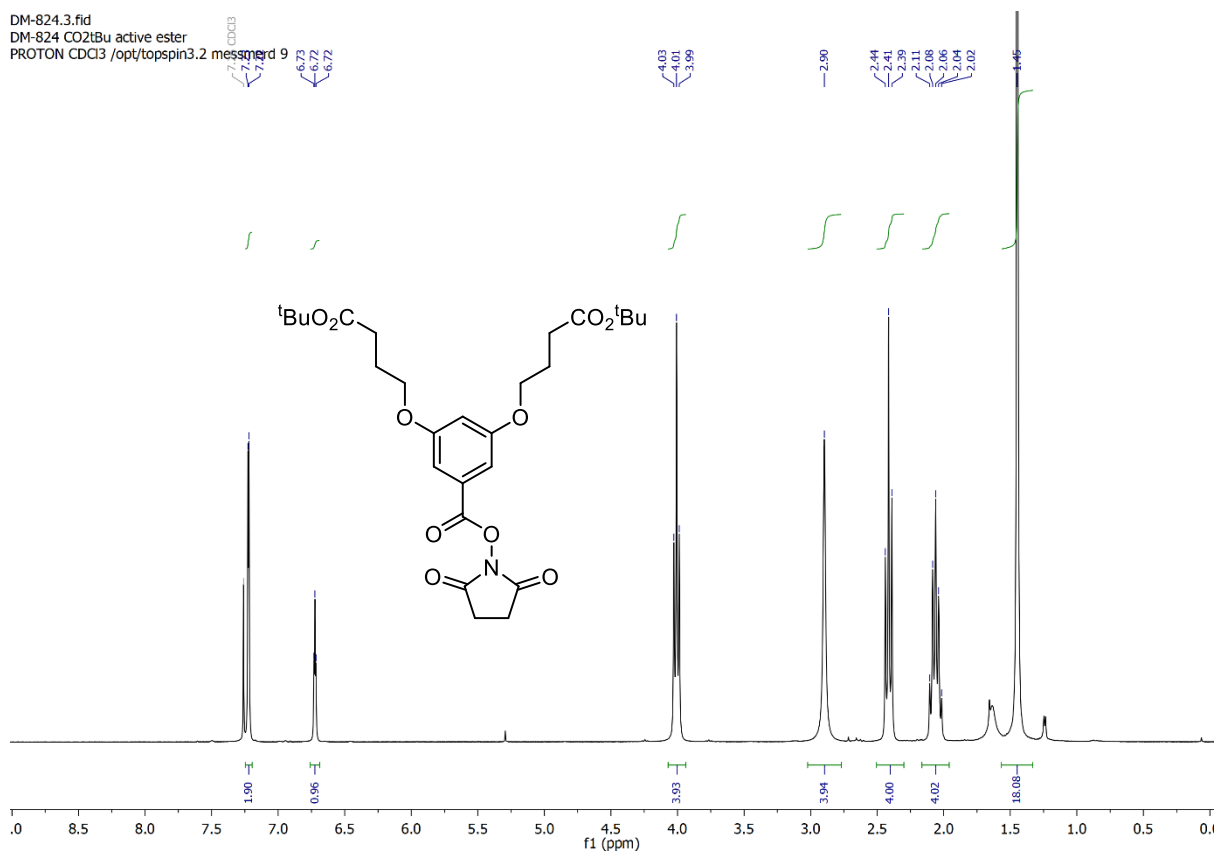
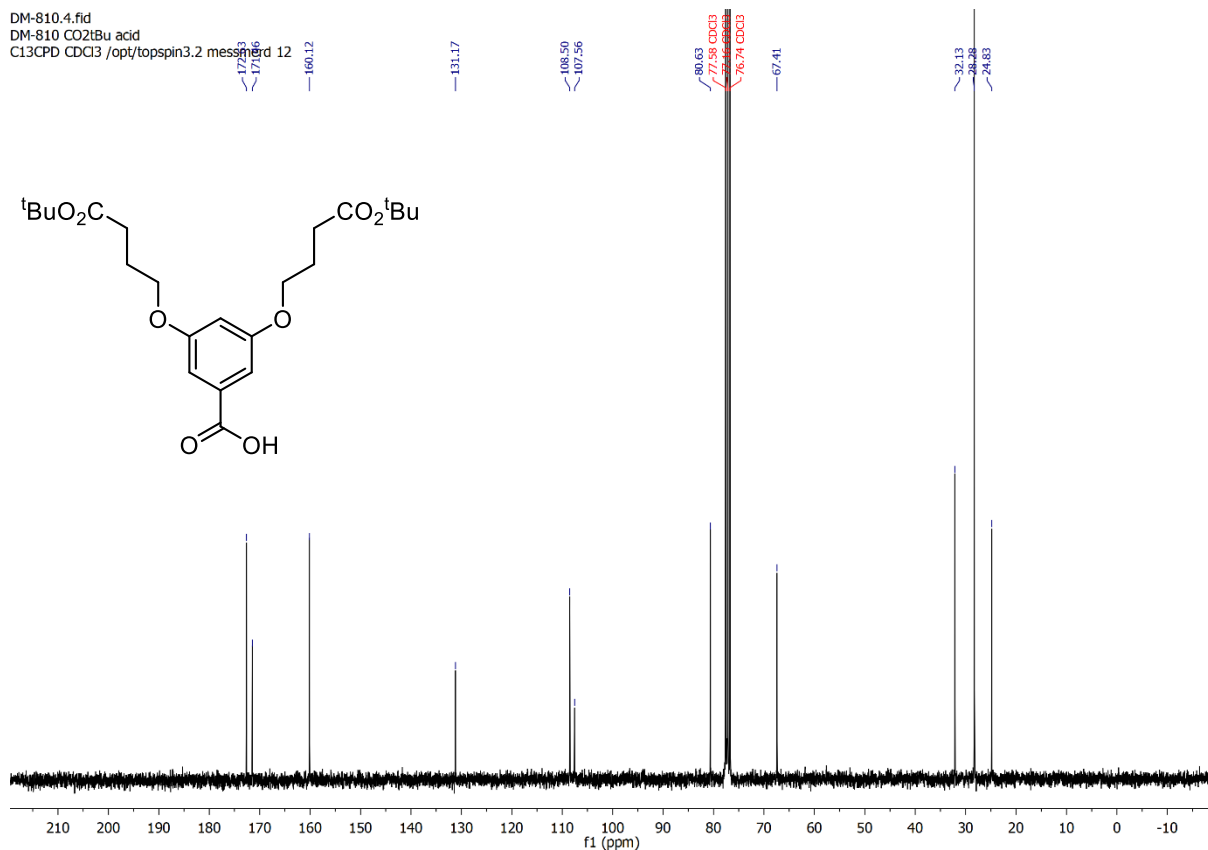
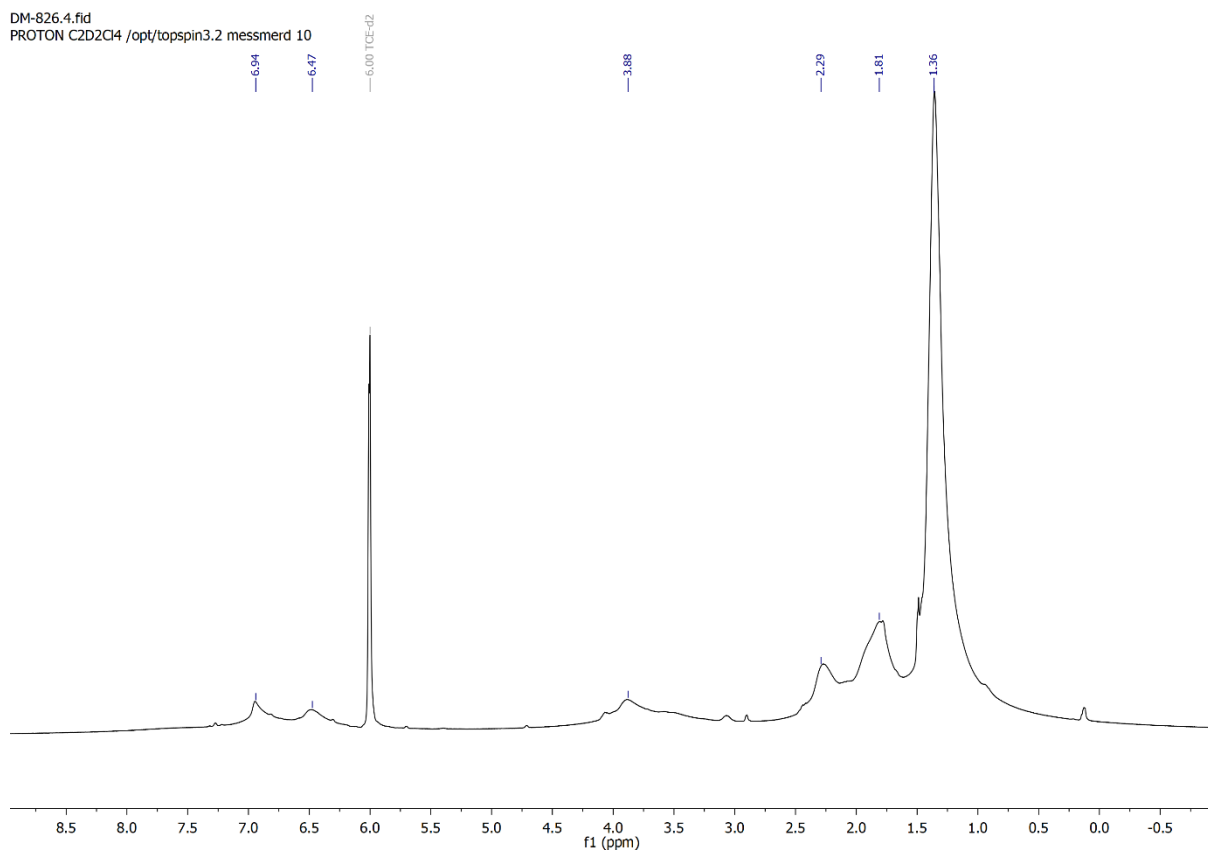
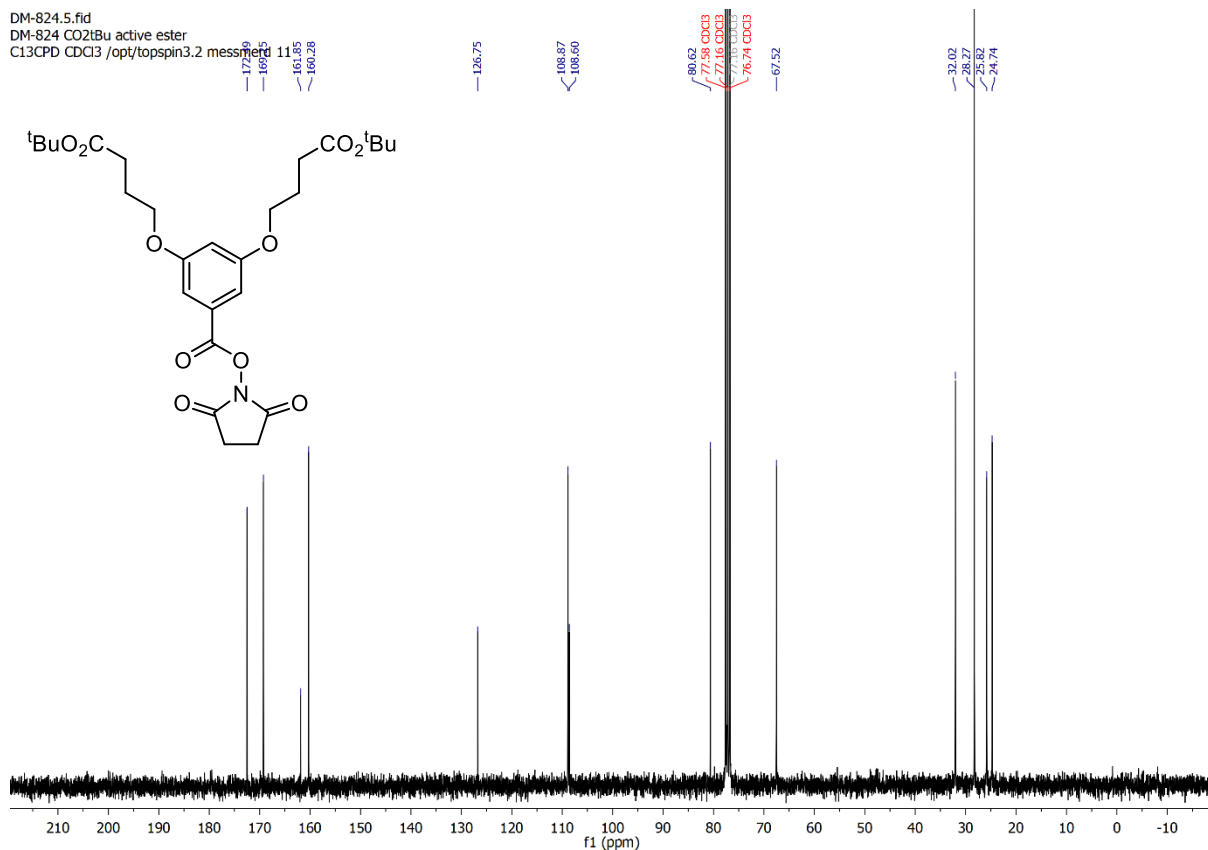


Figure S 42: ¹H-NMR spectrum of S5.







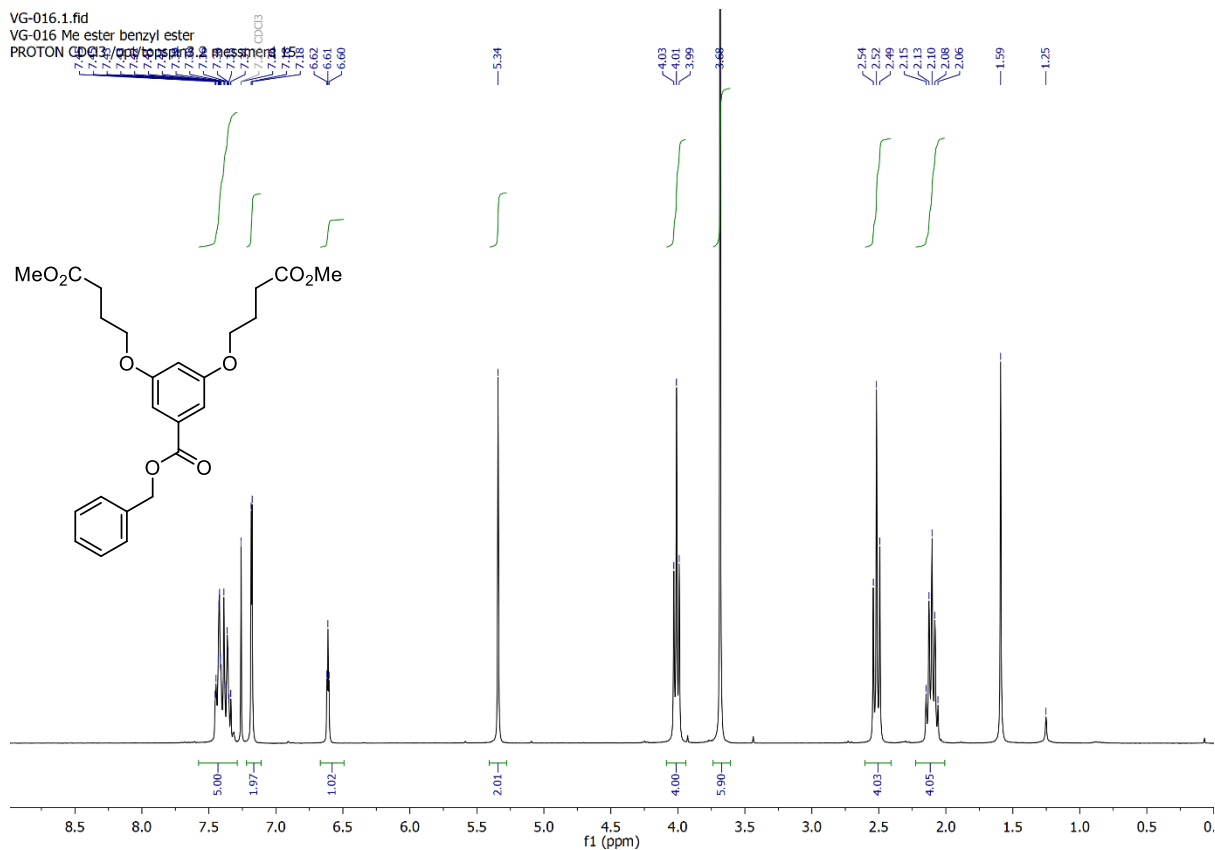


Figure S 49: $^1\text{H-NMR}$ spectrum of **S7**.

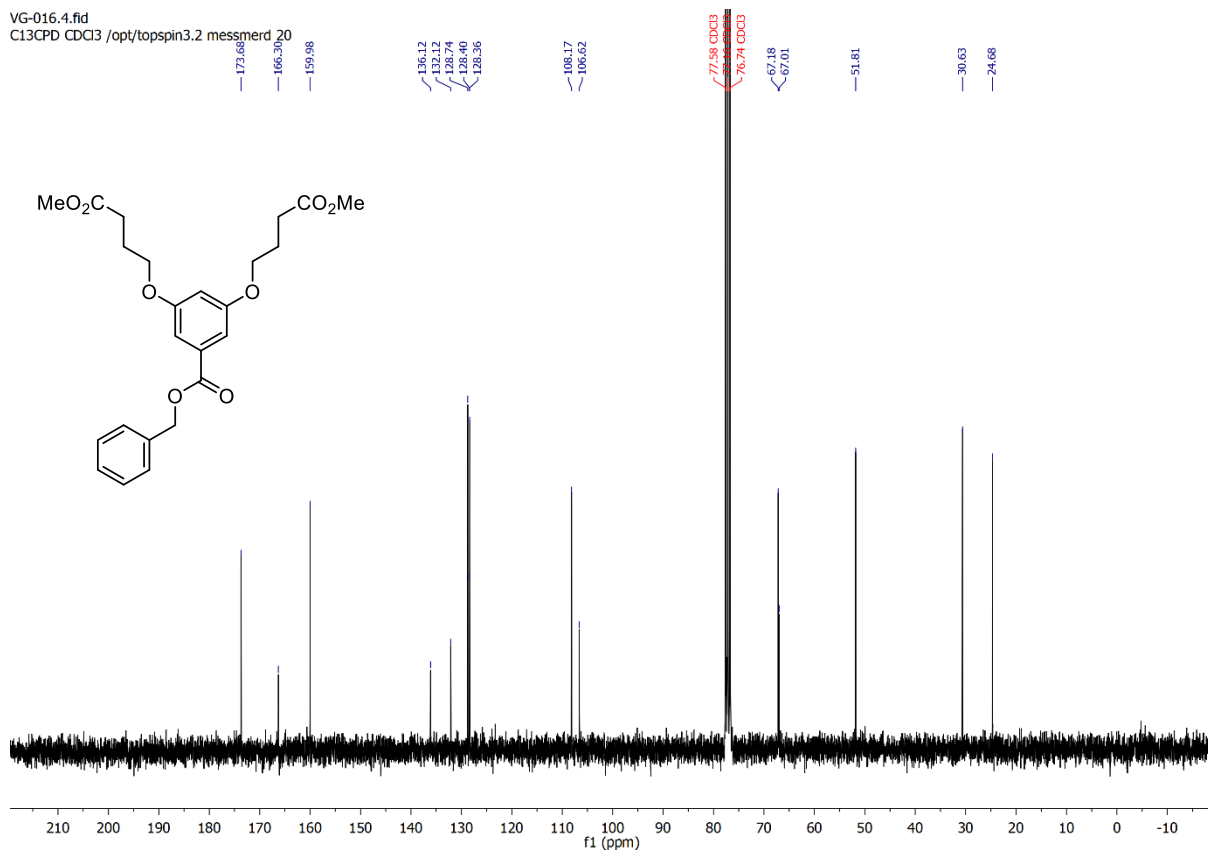


Figure S 50: $^{13}\text{C-NMR}$ spectrum of **S7**.

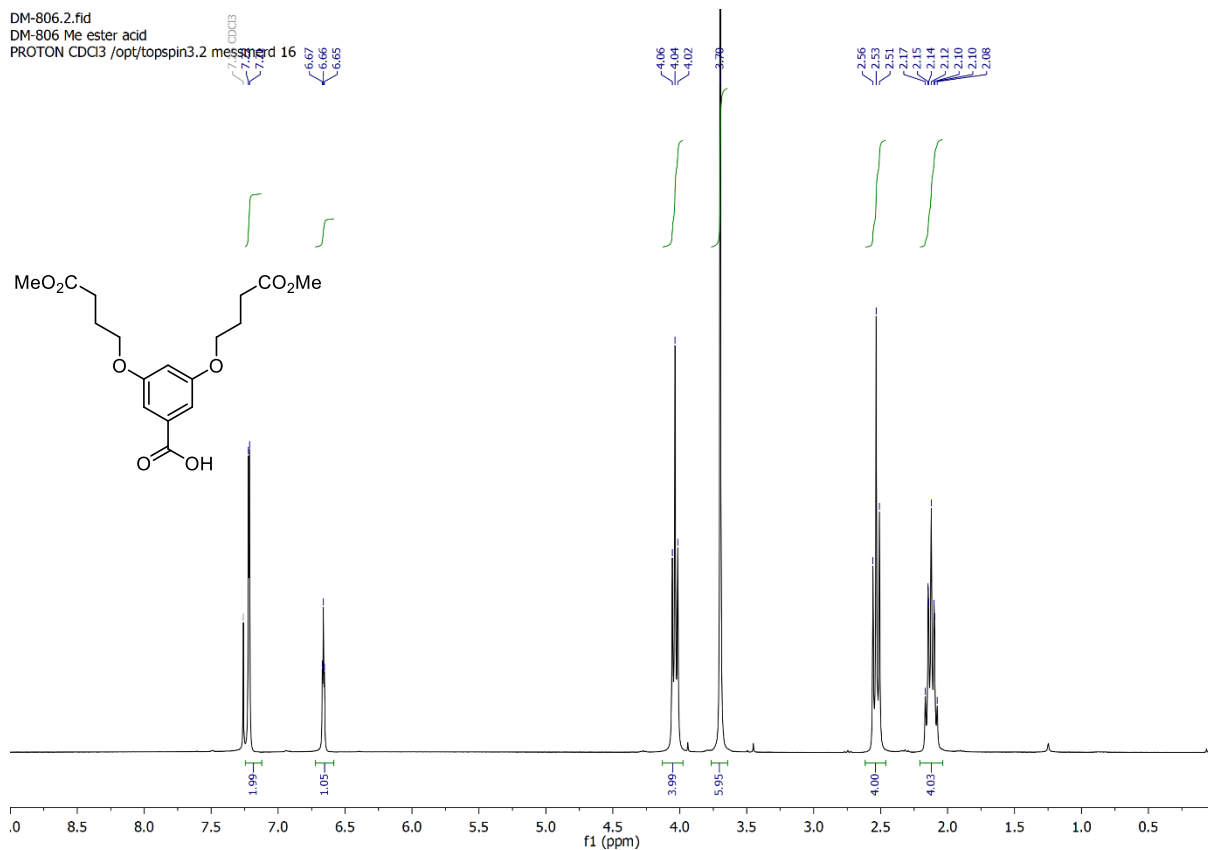


Figure S 51: $^1\text{H-NMR}$ spectrum of **58**.

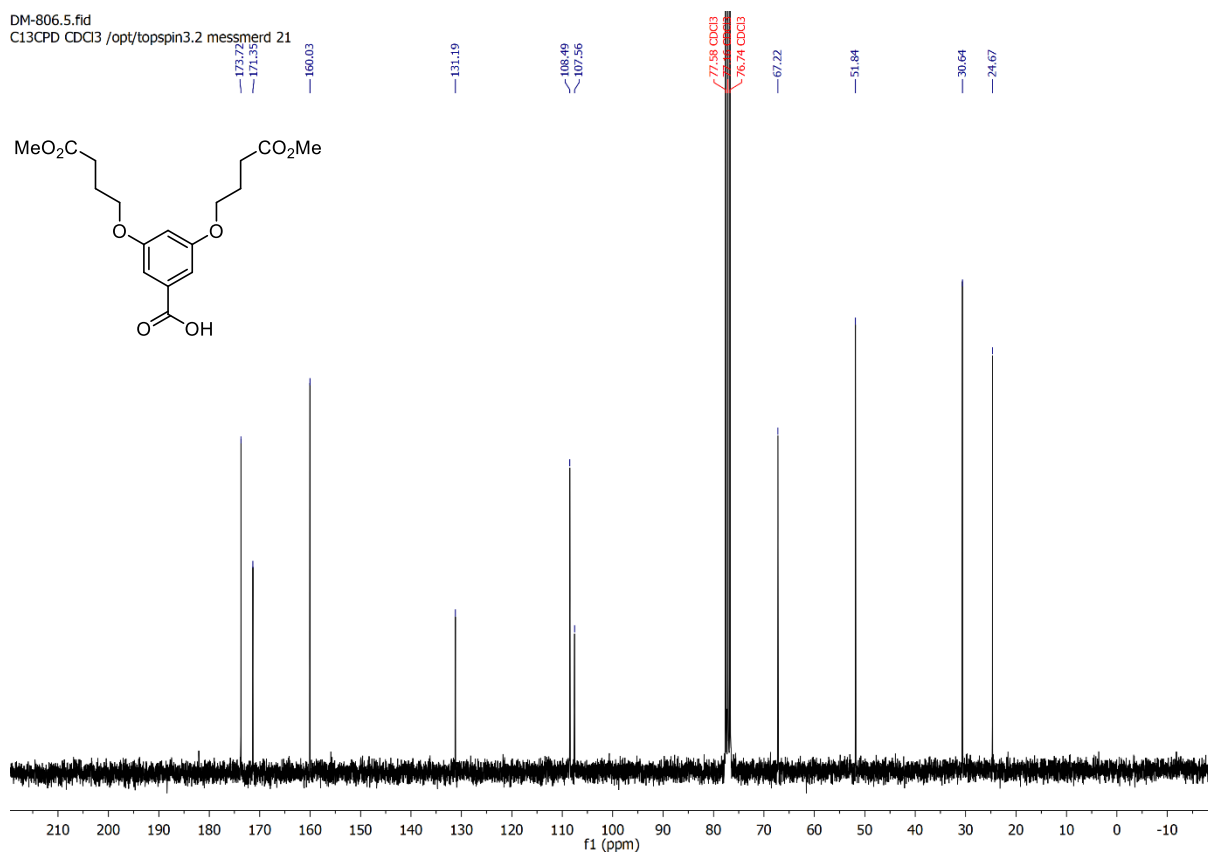


Figure S 52: $^{13}\text{C-NMR}$ spectrum of **58**.

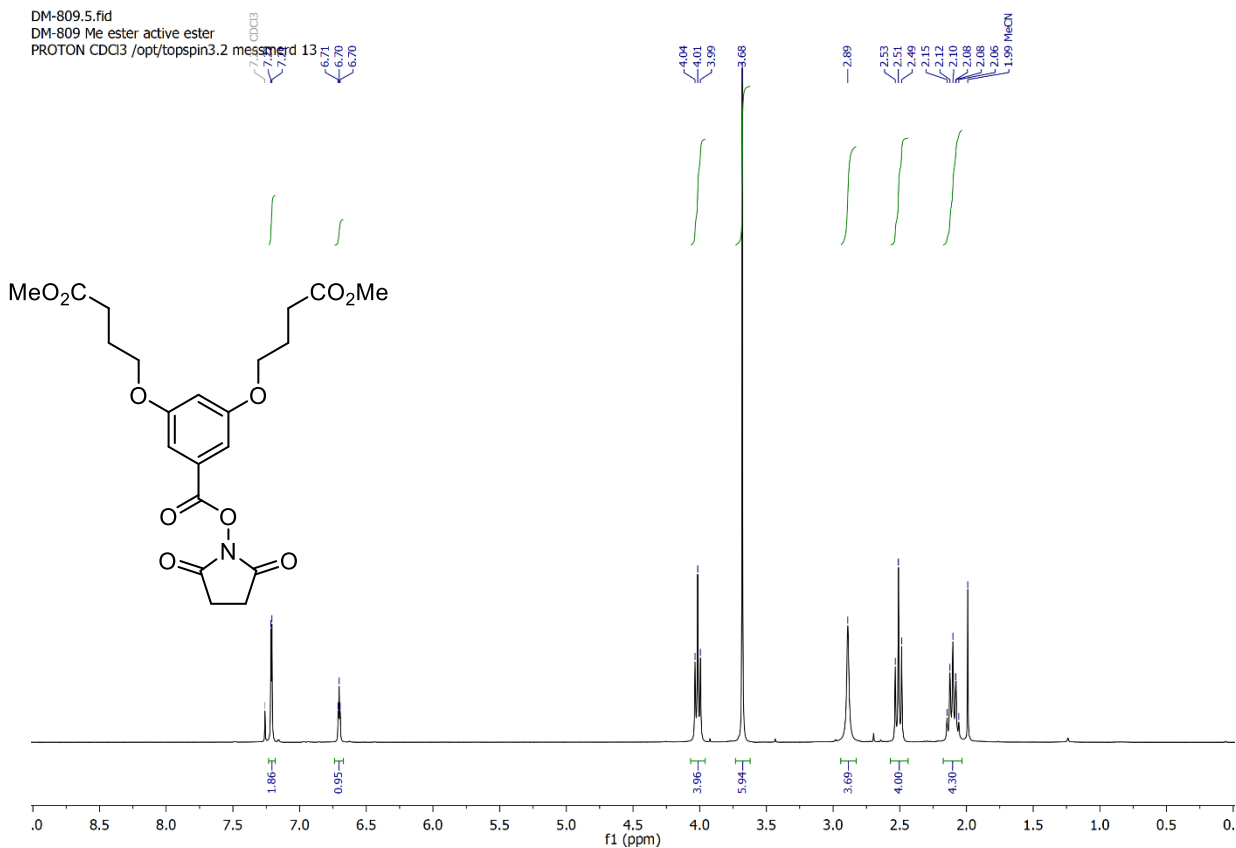


Figure S 53: ¹H-NMR spectrum of **S3**.

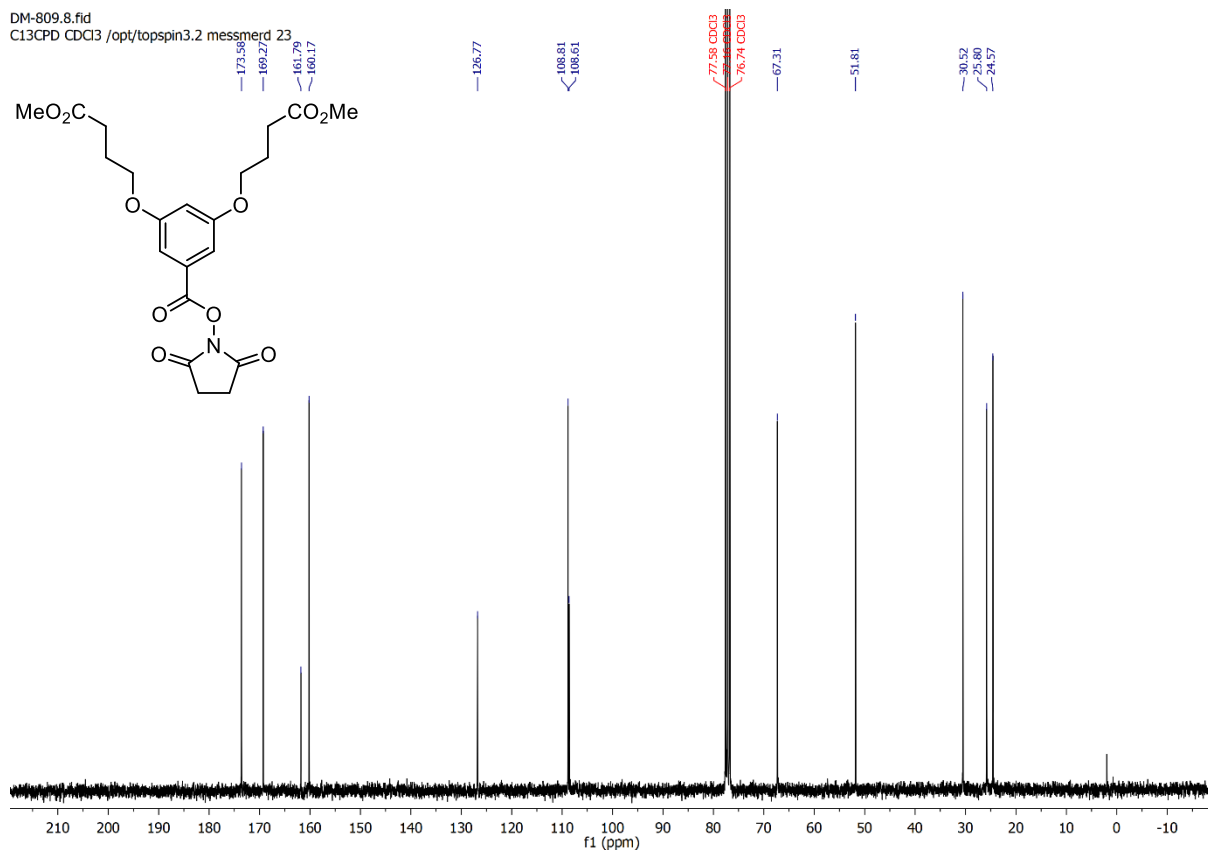


Figure S 54: ¹³C-NMR spectrum of **S3**.

DM-916.1.fid
DM-916 PG5 Me ester
PROTON DMSO /opt/topspin3.2 messmerd 26

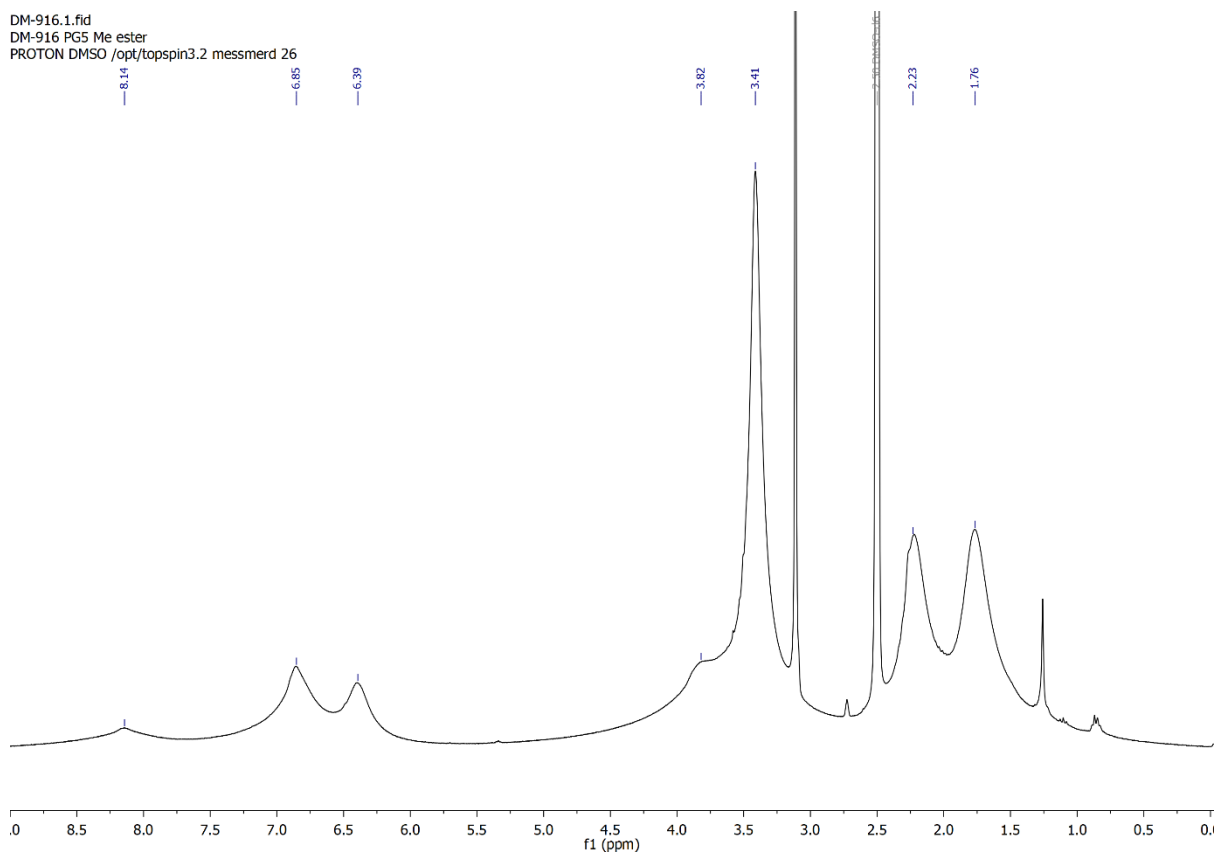


Figure S 55: $^1\text{H-NMR}$ spectrum of $\text{PG5}_{500}^{\text{CO}_2\text{Me}}$ (**8**).

DM-953.1.fid
PROTON DMSO /opt/topspin3.2 messmerd 32

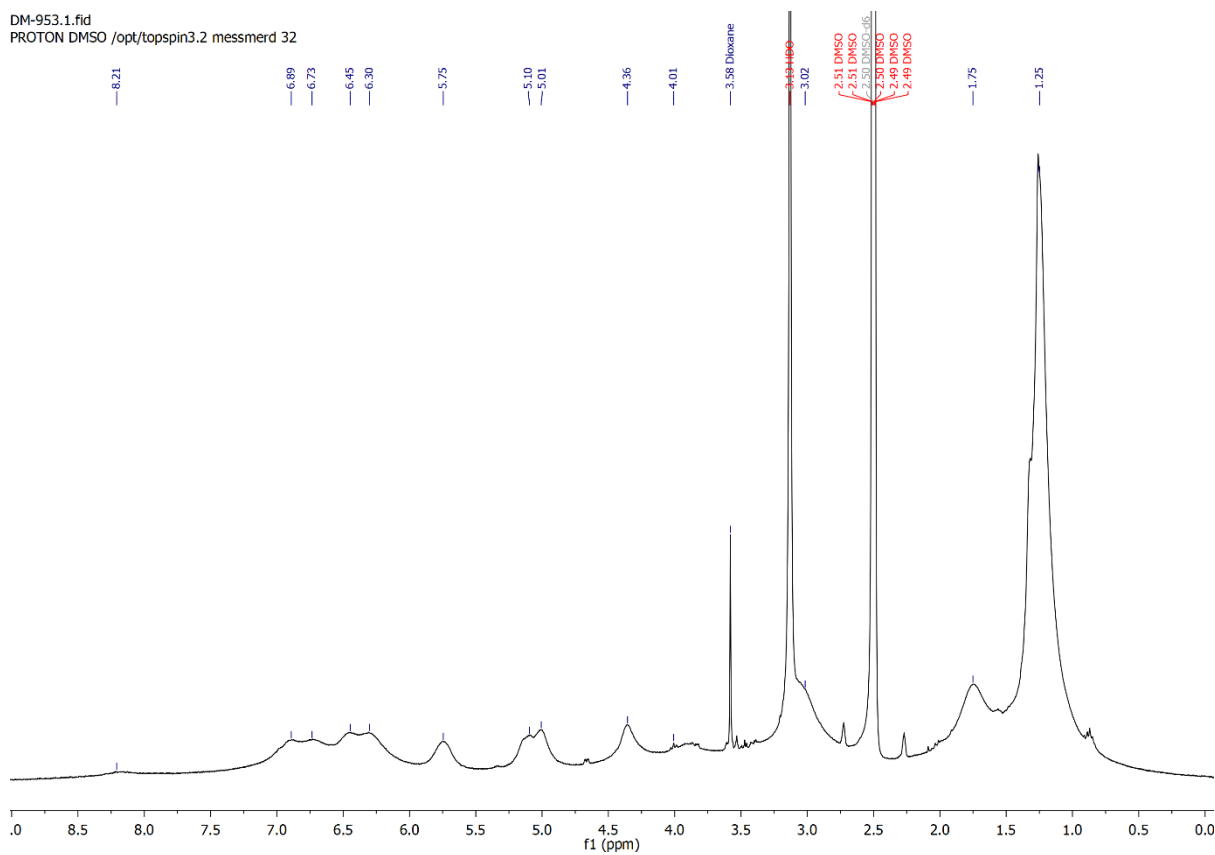


Figure S 56: $^1\text{H-NMR}$ spectrum of $\text{PG5}_{500}^{\text{Alloc}36}$ (**S9**).

DM-954.1.fid
PROTON DMSO /opt/topspin3.2 messmerd 33

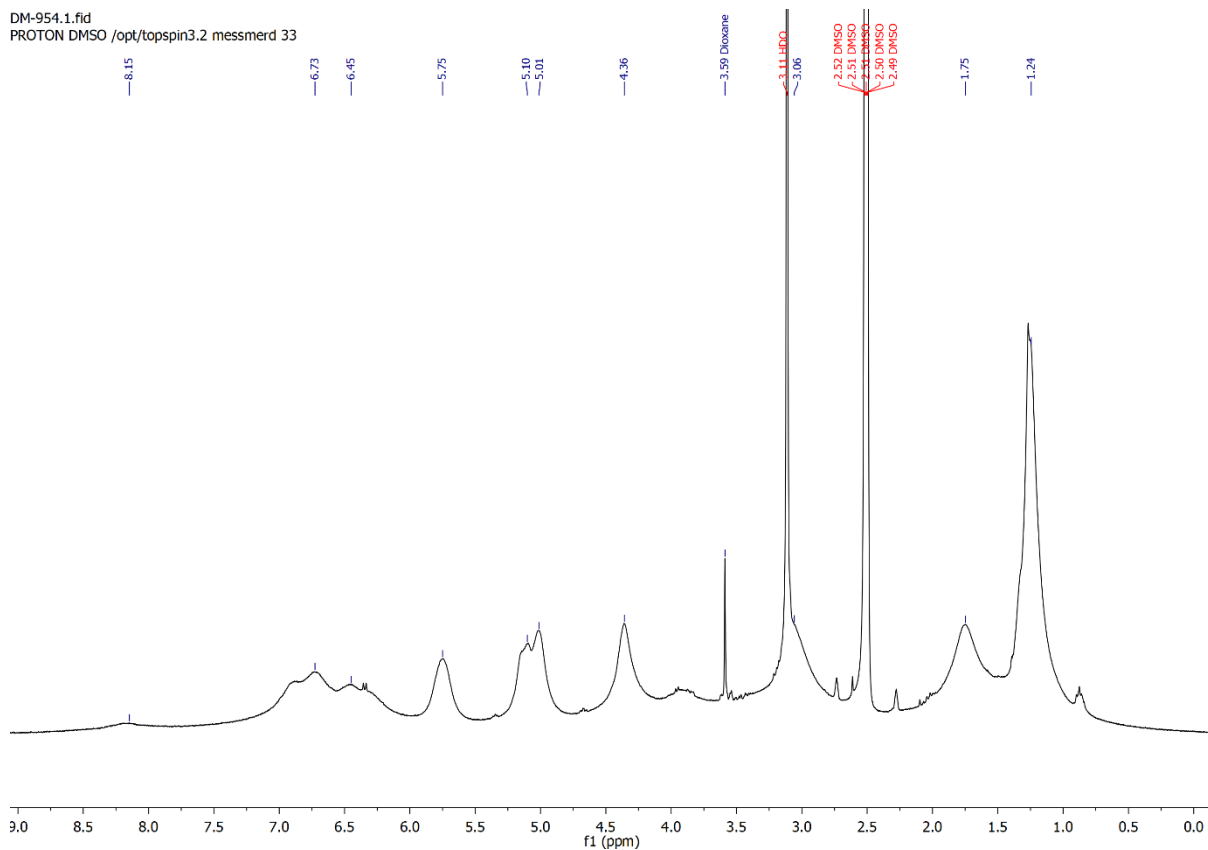


Figure S 57: ¹H-NMR spectrum of PG5^{Alloc57} (S10).

DM-955.1.fid
PROTON DMSO /opt/topspin3.2 messmerd 34

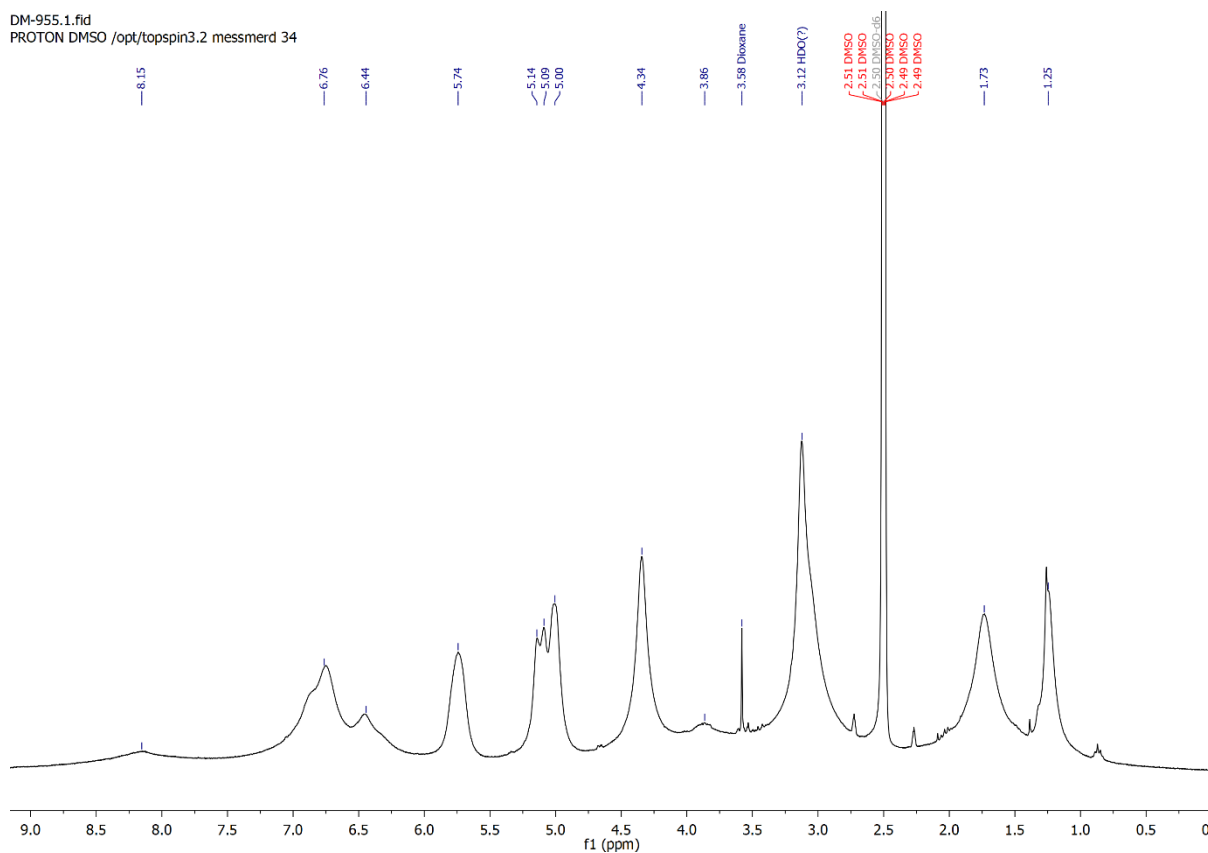


Figure S 58: ¹H-NMR spectrum of PG5^{Alloc80} (S11).

VG-010.1.fid
PROTON DMSO /opt/topspin3.2 messmerd 18

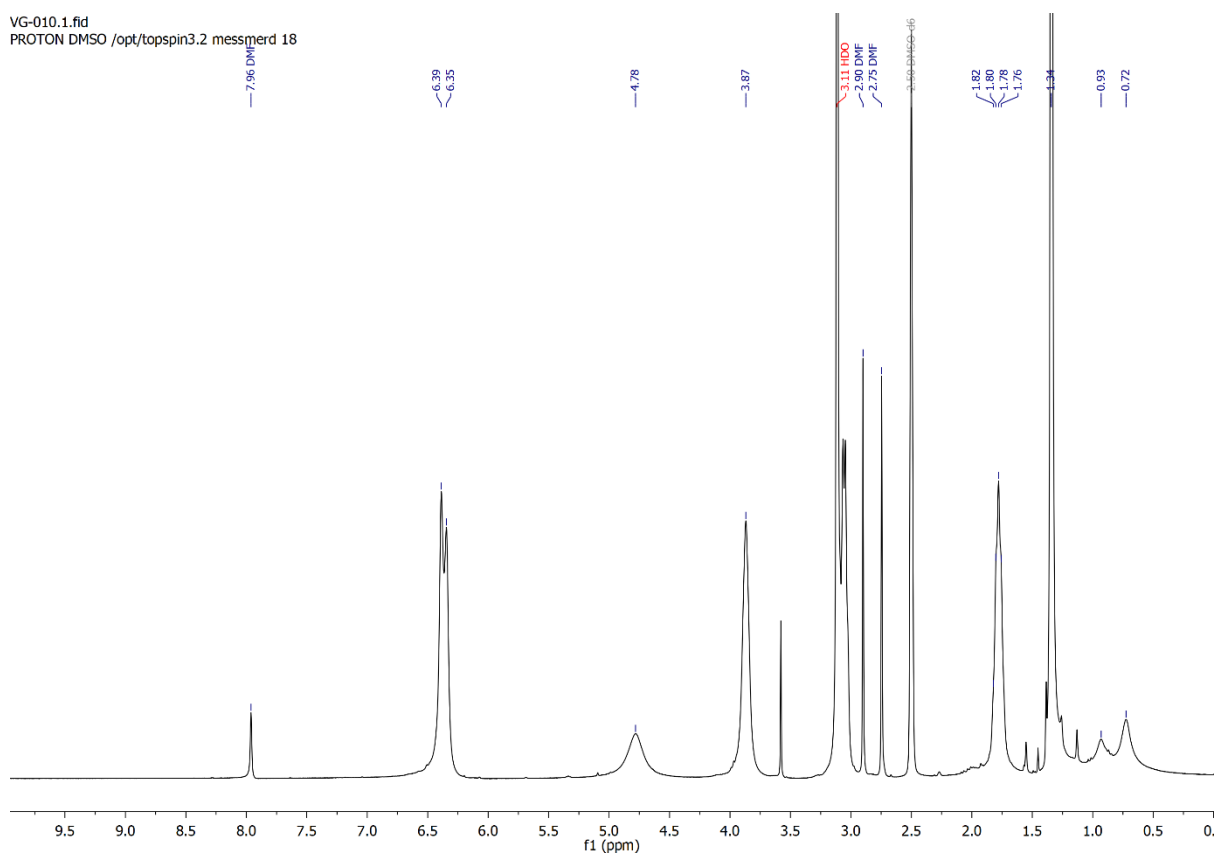


Figure S 59: $^1\text{H-NMR}$ spectrum of $\text{PG1}^{\text{NHBOC}}_{10'000}$ (S12).

DM-848.1.fid
DM-848 PG2 > 10000
PROTON DMSO /opt/topspin3.2 messmerd 44

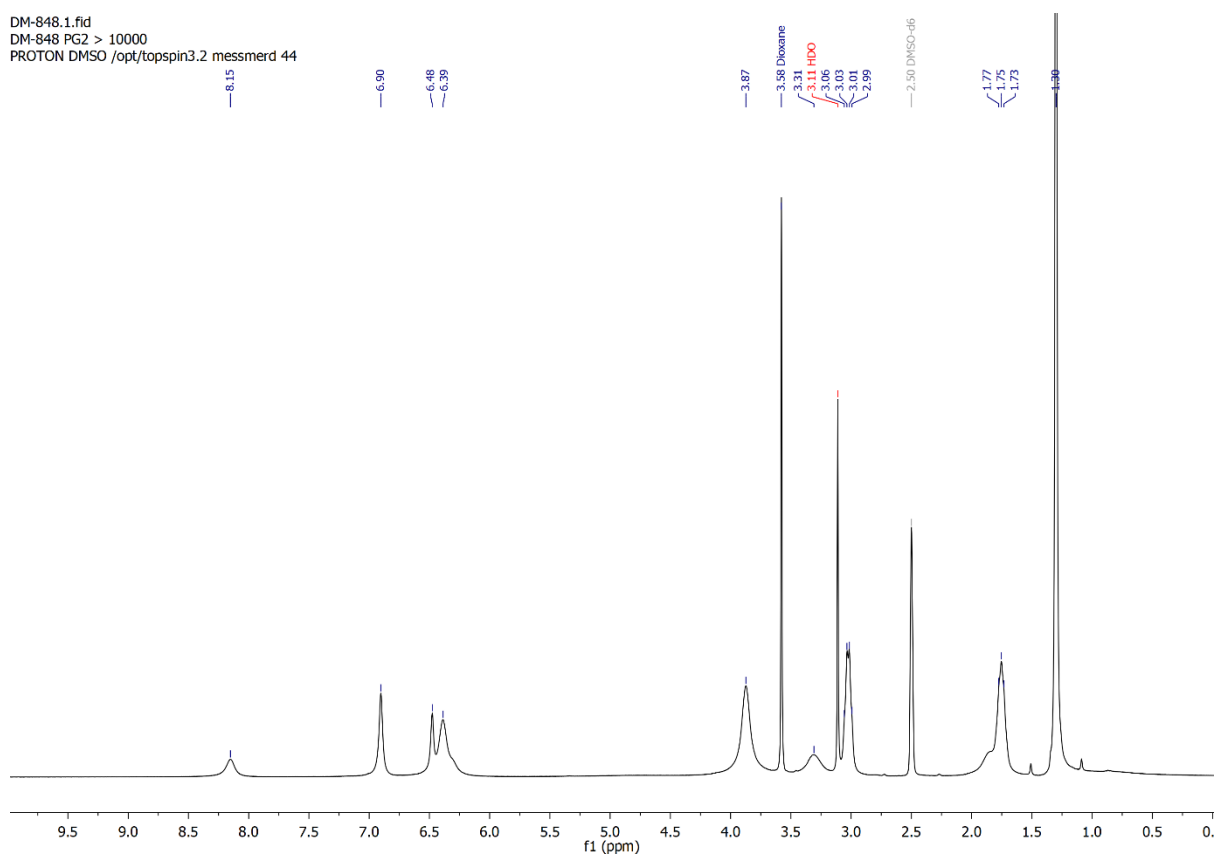


Figure S 60: $^1\text{H-NMR}$ spectrum of $\text{PG2}^{\text{NHBOC}}_{10'000}$ (S13).

DM-869.2.fid
PROTON DMSO /opt/topspin3.2 messmerd 19

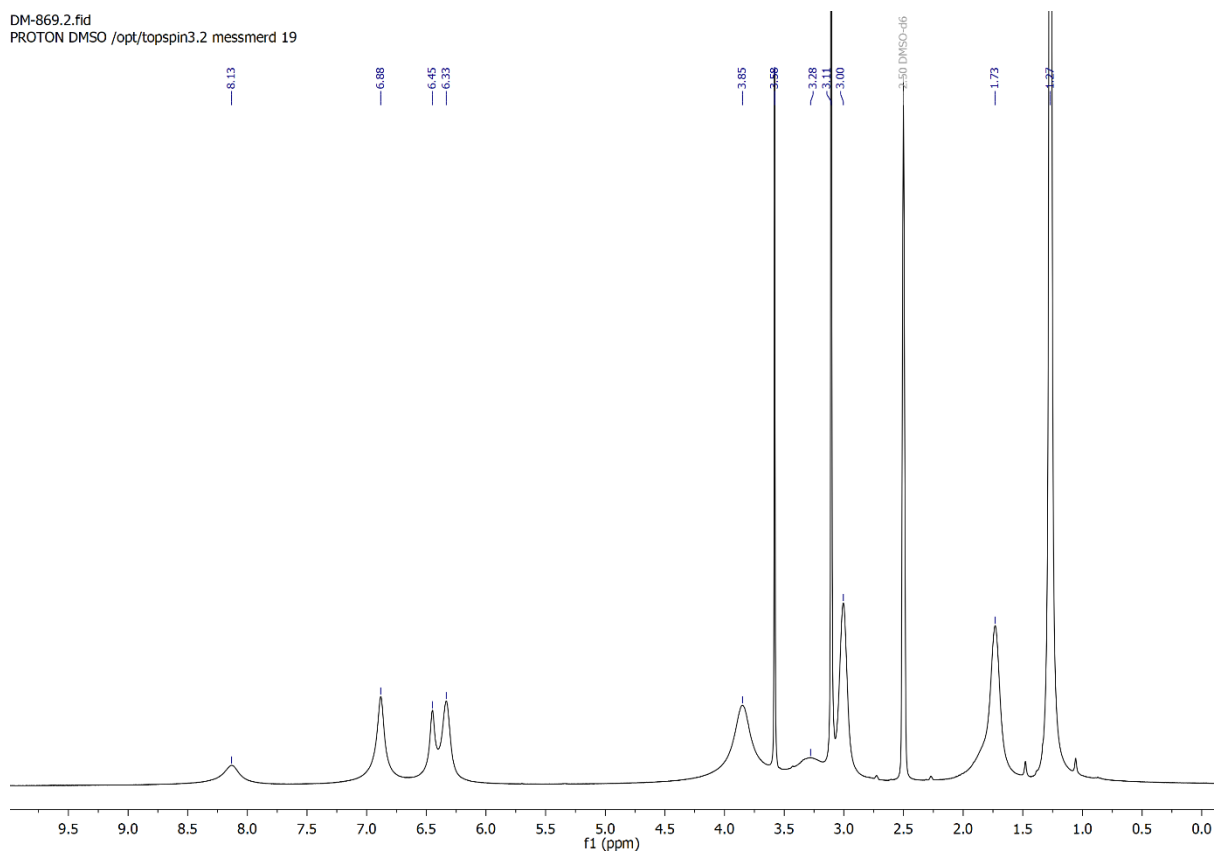


Figure S 61: ¹H-NMR spectrum of PG3^{NHBOC}_{10'000} (S14).

DM-892.1.fid
DM-892 PG4 long
PROTON DMSO /opt/topspin3.2 messmerd 48

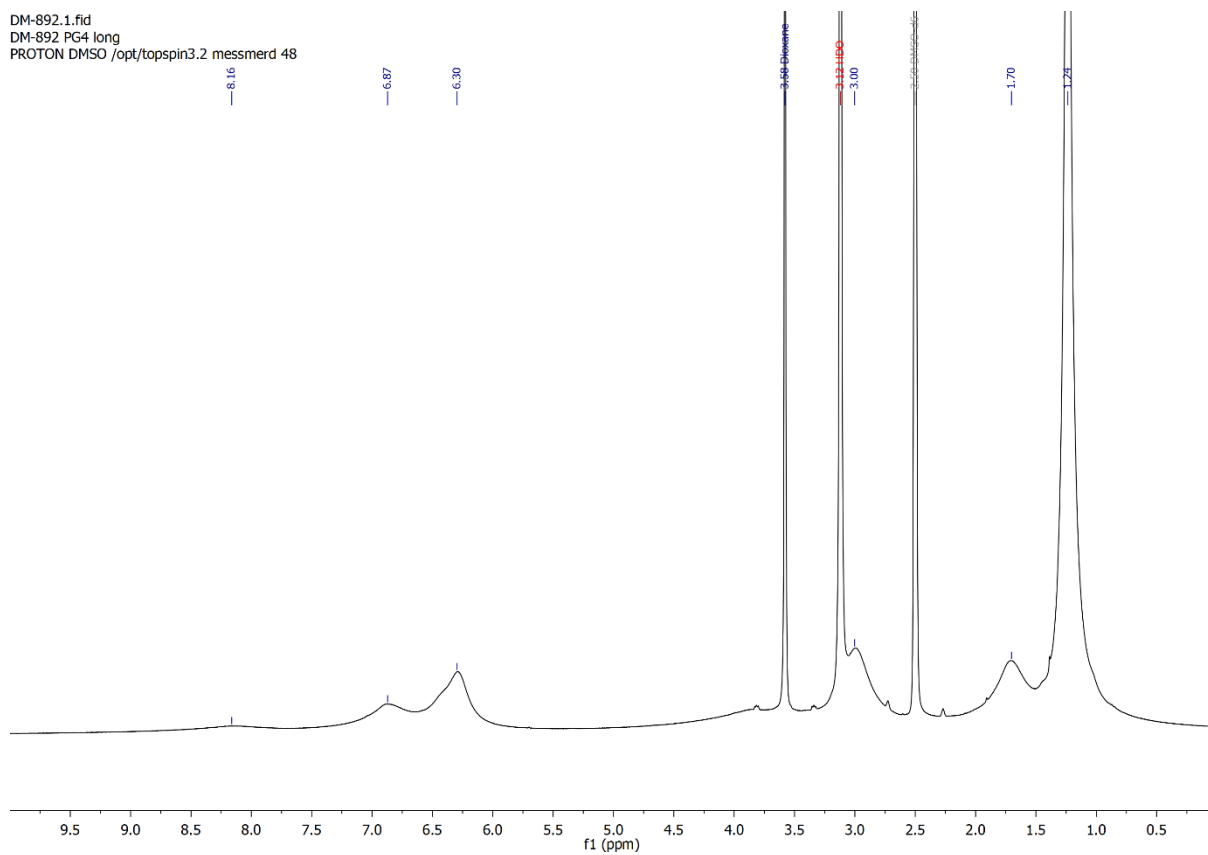


Figure S 62: ¹H-NMR spectrum of PG4^{NHBOC}_{10'000} (S15).

DM-924.1.fid
DM-924 lyophilizate
PROTON DMSO /opt/topspin3.2 messmerd 8

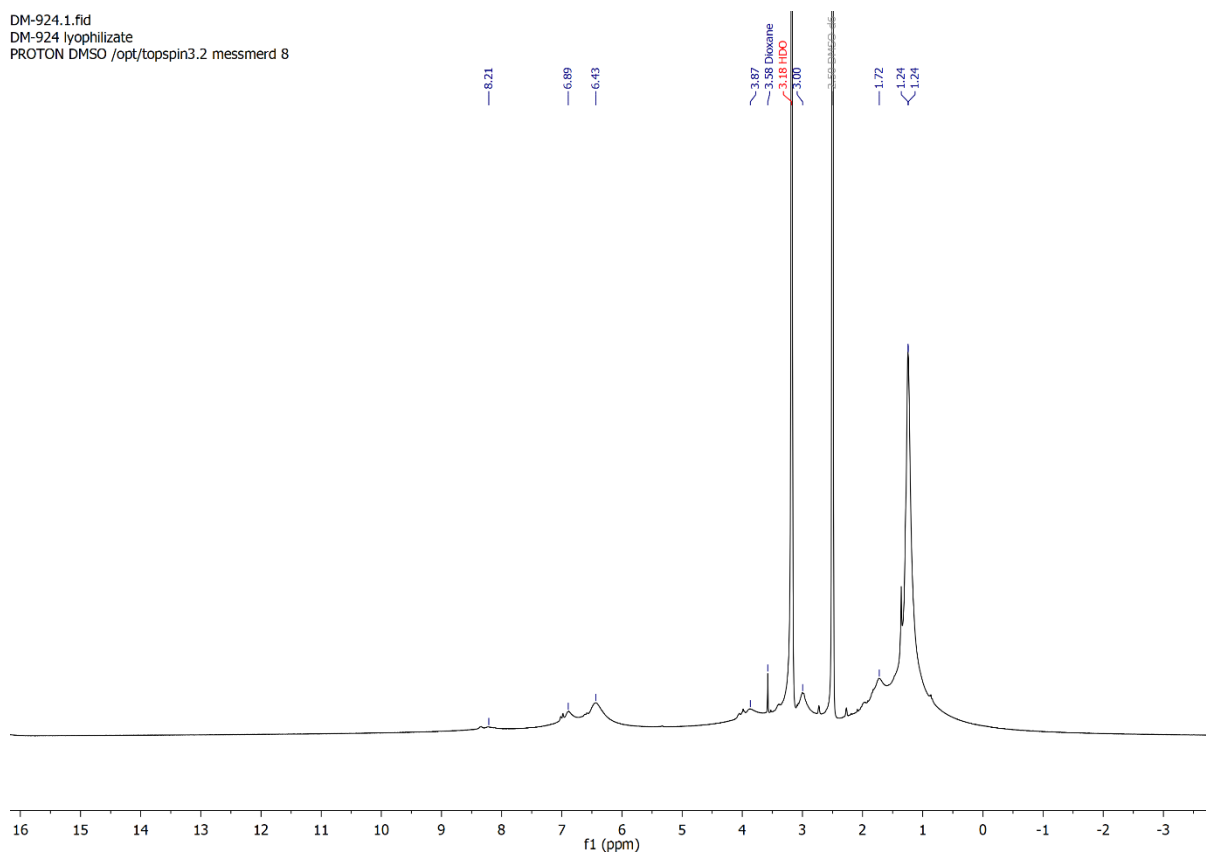


Figure S 63: $^1\text{H-NMR}$ spectrum of $\text{PG5}^{\text{NHBOC}}_{\text{5'000}}$ (2).

DM-931.1.fid
DM-931 lyo
PROTON DMSO /opt/topspin3.2 messmerd 9

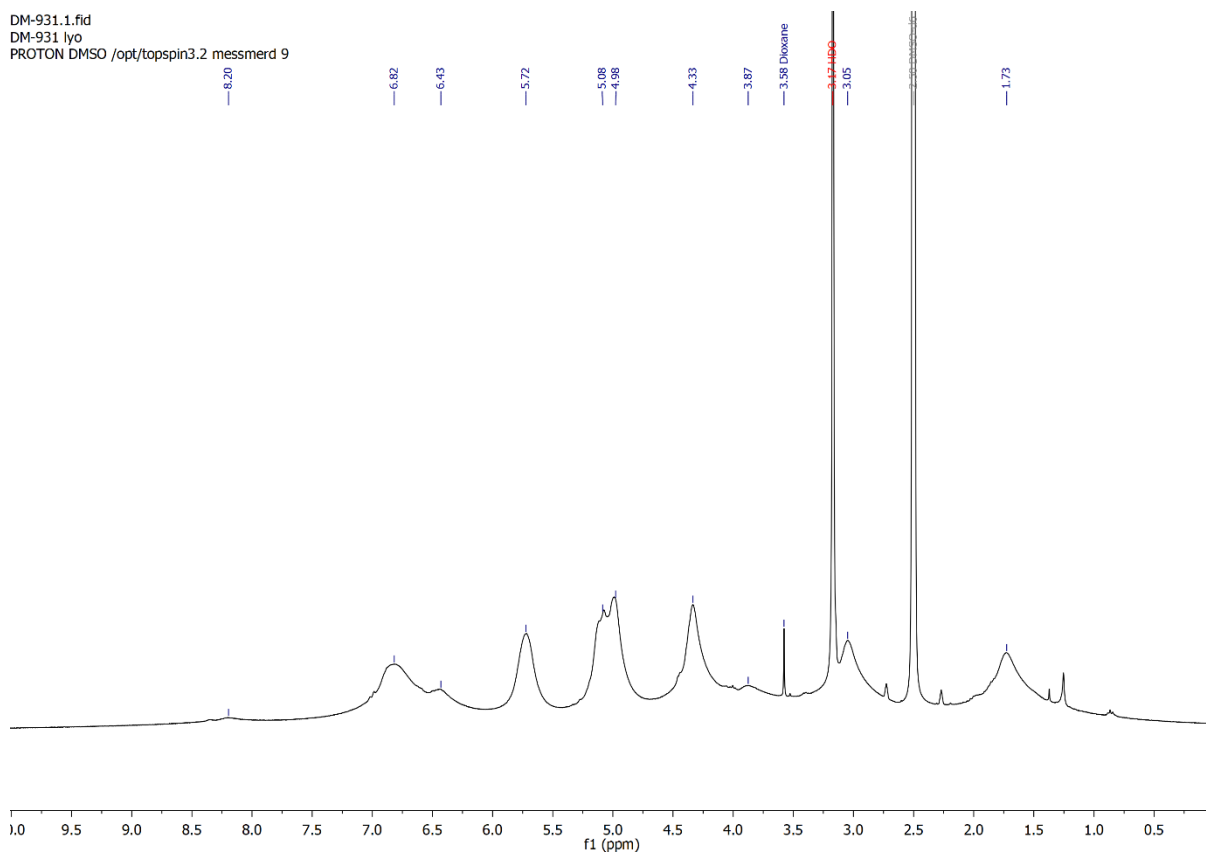


Figure S 64: $^1\text{H-NMR}$ spectrum of $\text{PG5}^{\text{NHAlloc}}_{\text{10'000}}$ (4).

Bibliography

- (1) Usov, I.; Mezzenga, R. FiberApp: An Open-Source Software for Tracking and Analyzing Polymers, Filaments, Biomacromolecules, and Fibrous Objects. *Macromolecules* **2015**, *48* (5), 1269–1280.
- (2) Schindelin, J.; Arganda-Carreras, I.; Frise, E.; Kaynig, V.; Longair, M.; Pietzsch, T.; Preibisch, S.; Rueden, C.; Saalfeld, S.; Schmid, B.; et al. Fiji: An Open-Source Platform for Biological-Image Analysis. *Nat. Methods* **2012**, *9* (7), 676–682.
- (3) Thompson, S.; Hamilton, A. D. Amphiphilic α -Helix Mimetics Based on a Benzoylurea Scaffold. *Org. Biomol. Chem.* **2012**, *10* (30), 5780.
- (4) Patel, R. N.; Goswami, A.; Chu, L.; Donovan, M. J.; Nanduri, V.; Goldberg, S.; Johnston, R.; Siva, P. J.; Nielsen, B.; Fan, J.; et al. Enantioselective Microbial Reduction of Substituted Acetophenones. *Tetrahedron: Asymmetry* **2004**, *15* (8), 1247–1258.
- (5) Wolfe, S.; Wilson, M.-C.; Cheng, M.-H.; Shustov, G. V.; Akuche, C. I. Cyclic Hydroxamates, Especially Multiply Substituted [1,2]Oxazinan-3-Ones. *Can. J. Chem.* **2003**, *81* (8), 937–960.
- (6) Messmer, D.; Kröger, M.; Schlüter, A. D. Pushing Synthesis towards the Maximum Generation Range of Dendritic Macromolecules. *Macromolecules* **2018**, *51* (14), 5420–5429.
- (7) Canilho, N.; Kasemi, E.; Mezzenga, R.; Schlüter, A. D. Liquid-Crystalline Polymers from Cationic Dendronized Polymer-Anionic Lipid Complexes. *J. Am. Chem. Soc.* **2006**, *128* (43), 13998–13999.
- (8) Yu, H.; Schlüter, A. D.; Zhang, B. Synthesis of High Generation Dendronized Polymers and Quantification of Their Structure Perfection. *Macromolecules* **2014**, *47* (13), 4127–4135.
- (9) Shu, L.; Gössl, I.; Rabe, J. P.; Schlüter, A. D. Quantitative Aspects of the Dendronization of Dendronized Linear Polystyrenes. *Macromol. Chem. Phys.* **2002**, No. 203, 2540–2550.
- (10) Zhang, B.; Yu, H.; Schlüter, A. D.; Halperin, A.; Kröger, M. Synthetic Regimes Due to Packing Constraints in Dendritic Molecules Confirmed by Labelling Experiments. *Nat. Commun.* **2013**, *4*, 1993.
- (11) Yu, H.; Schlüter, A. D.; Zhang, B. Main-Chain Scission of a Charged Fifth-Generation Dendronized Polymer. *Helv. Chim. Acta* **2012**, *95* (12), 2399–2410.
- (12) Van Der Hoff, B. M. E.; Glynn, P. A. R. Ultrasonation of Polystyrene in Solution. *J. Macromol. Sci. - Chem.* **1974**, *8* (2), 429–449.
- (13) Van Der Hoff, B. M. E.; Gall, C. E. A Method for Following Changes in Molecular Weight Distributions of Polymers on Degradation: Development and Comparison with Ultrasonic Degradation Experiments. *J. Macromol. Sci. - Chem.* **1978**, *A11* (9), 1739–1758.
- (14) Van Der Hoff, B. M. E.; Glynn, P. A. R. The Rate of Degradation by Ultrasonation of Polystyrene in Solution. *J. Macromol. Sci. Part A - Chem.* **1974**, *8* (2), 429–449.
- (15) Bertran, O.; Zhang, B.; Schlüter, A. D.; Kröger, M.; Alemán, C. Computer Simulation of Fifth Generation Dendronized Polymers: Impact of Charge on Internal Organization. *J. Phys. Chem. B* **2013**, *117* (19), 6007–6017.
- (16) Cornell, W. D.; Cieplak, P.; Bayly, C. I.; Gould, I. R.; Merz, K. M.; Ferguson, D. M.; Spellmeyer, D. C.; Fox, T.; Caldwell, J. W.; Kollman, P. A. A Second Generation Force Field for the

- Simulation of Proteins, Nucleic Acids, and Organic Molecules. *J. Am. Chem. Soc.* **1995**, *117* (19), 5179–5197.
- (17) Bertran, O.; Zhang, B.; Schlüter, A. D.; Halperin, A.; Kröger, M.; Alemán, C.; Spellmeyer, D. C.; Fox, T.; Caldwell, J. W.; Kollman, P. A.; et al. Computer Simulation of Dendronized Polymers: Organization and Characterization at the Atomistic Level. *RSC Adv.* **2013**, *3* (1), 126–140.
- (18) Pasquino, R.; Zhang, B.; Sigel, R.; Yu, H.; Ottiger, M.; Bertran, O.; Aleman, || C; Schlü, # A D; Vlassopoulos, D. Linear Viscoelastic Response of Dendronized Polymers. *Macromolecules* **2012**, *45*, 8813–8823.
- (19) Gstrein, C.; Zhang, B.; Abdel-Rahman, M. A.; Bertran, O.; Alemán, C.; Wegner, G.; Schlüter, A. D.; Halperin, A.; Schlüter, A. D.; Talmon, Y.; et al. Solvatochromism of Dye-Labeled Dendronized Polymers of Generation Numbers 1–4: Comparison to Dendrimers. *Chem. Sci.* **2016**, *7* (7), 4644–4652.
- (20) Bertran, O.; Zhang, B.; Schlüter, A. D.; Kröger, M.; Alemán, C. Modeling Nanosized Single Molecule Objects: Dendronized Polymers Adsorbed onto Mica. *J. Phys. Chem. C* **2015**, *119* (7), 3746–3753.
- (21) Wang, J.; Wolf, R. M.; Caldwell, J. W.; Kollman, P. A.; Case, D. A. Development and Testing of a General Amber Force Field. *J. Comput. Chem.* **2004**, *25* (9), 1157–1174.
- (22) Cieplak, P.; Cornell, W. D.; Bayly, C.; Kollman, P. A. Application of the Multimolecule and Multiconformational RESP Methodology to Biopolymers: Charge Derivation for DNA, RNA, and Proteins. *J. Comput. Chem.* **2018**, *16* (11), 1357–1377.
- (23) Berendsen, H. J. C.; Postma, J. P. M.; van Gunsteren, W. F.; DiNola, A.; Haak, J. R. Molecular Dynamics with Coupling to an External Bath. *J. Chem. Phys.* **1984**, *81* (8), 3684–3690.
- (24) Ryckaert, J.-P.; Ciccotti, G.; Berendsen, H. J. . Numerical Integration of the Cartesian Equations of Motion of a System with Constraints: Molecular Dynamics of n-Alkanes. *J. Comput. Phys.* **1977**, *23* (3), 327–341.
- (25) Peterson, G. I.; Bang, K.-T.; Choi, T.-L. Mechanochemical Degradation of Denpols: Synthesis and Ultrasound-Induced Chain Scission of Polyphenylene-Based Dendronized Polymers. *J. Am. Chem. Soc.* **2018**, *140*, 8599–8608.
- (26) Gooberman, G. Ultrasonic Degradation of Polystyrene. Part 1. A Proposed Mechanism for Degradation. *J. Polym. Sci.* **1960**, *42* (139), 25–33.
- (27) Chakraborty, J.; Sarkar, J.; Kumar, R.; Madras, G. Ultrasonic Degradation of Polybutadiene and Isotactic Polypropylene. *Polym. Degrad. Stab.* **2004**, *85*, 555–558.
- (28) Inaba, A.; Kashiwagi, T.; Brown, J. E. Effects of Initial Molecular Weight on Thermal Degradation of Poly(Methyl Methacrylate): Part 1—Model 1. *Polym. Degrad. Stab.* **1988**, *21* (1), 1–20.
- (29) Stoliarov, S. I.; Westmoreland, P. R.; Nyden, M. R.; Forney, G. P. A Reactive Molecular Dynamics Model of Thermal Decomposition in Polymers: I. Poly(Methyl Methacrylate). *Polymer* **2003**, *44* (3), 883–894.
- (30) Manring, L. E. Thermal Degradation of Poly(Methyl Methacrylate). 4. Random Side-Group Scission. *Macromolecules* **1991**, *24*, 3304–3309.
- (31) Kashiwagi, T.; Inabi, A.; Hamins, A. Behavior of Primary Radicals during Thermal Degradation of Poly(Methyl Methacrylate). *Polym. Degrad. Stab.* **1989**, *26* (2), 161–184.

- (32) Wilkie, C. A. TGA/FTIR: An Extremely Useful Technique for Studying Polymer Degradation. *Polym. Degrad. Stab.* **1999**, *66* (3), 301–306.